

**WELD POOL PENETRATION MEASUREMENT USING
ULTRASOUND WITH THERMAL GRADIENT CORRECTION FACTORS**

John M. Anderton

B.S., Portland State University 1986

M.S., Oregon Graduate Institute 1995

A thesis presented to the faculty of the
Oregon Graduate Institute of Science and Technology
in partial fulfillment of the requirements for the degree
Doctor of Philosophy in
Materials Science and Engineering

September 1997

The dissertation "Weld Pool Penetration Measurement Using
Ultrasound With Thermal Gradient Correction Factors" by John Anderton has been
examined and approved by the following Examination Committee:

David Atteridge
Thesis Advisor, Professor

William Wood
Professor

Lemmy Meekisho
Associate Professor

Dr. Steve R. Doctor
Pacific Northwest Research Laboratories

Acknowledgments

I appreciate the help and support of everyone that made this dissertation possible. I would especially like to thank the members of my committee, Bill Wood who provided consistent support over the years, Dave Atteridge for editing and being there to listen, Steve Doctor for giving me a forum for my work and driving out of his way and Lemmy Meekisho for his consistent hardware and software support.

Special thanks to Bob Turpin for always knowing where everything is and knowing the right way to do anything with the tools at hand, Milt Scholl for getting my thesis printed, Margaret Ziomek-Moroz for her help in getting me admitted to the department, and Doug Davis for his incredible patience.

I could not have completed this without all of my teachers including Jack Devletian, Tony Bell, Dr. Yasrebi, Paul Clayton as well as students and support staff who know where it is and how to do it or did it for me without an account number including Jack McCarthy, Kristen Terry, Roxanne Metzker, Nancy Biskey, Andy Villeneuve, Jerry Boehme, Andy Huffstutter, Ken Burns, Jeff Schilling, Julius Dalzell and all the librarians.

Thanks to all my fellow students through the years who have always been a support including Francie, Jim, Kevin, Wade, Gary, Dave, and Dave, Mia and Xiaoyan.

And finally a special thank you to Susan Hunter and Ismoon and Jonquil Hunter-Morton who have been my family the last several years and put up with my being a student and my attempts at being a parent.

TABLE OF CONTENTS

Acknowledgments	iii
Table of Contents	iv
List of Figures.....	v
List of Tables.....	vii
Abstract.....	viii
1. Introduction.....	1
2. Electroslag Surfacing.....	5
3. Acoustic Measurement Techniques and Theory.....	8
4. Finite Element Analysis.....	17
5. Previous Research.....	23
6. Experimental Theory.....	31
7. Experimental Procedure.....	36
8. Results and Discussion	
8.1. Time of Flight vs. Temperature.....	45
8.2. Thermocouple Measurements.....	55
8.3. Finite Element Model.....	58
8.4. Ultrasonic Test on Weld Pool.....	62
8.5. Destructive Testing.....	67
8.6. Calculation of Liquid/Solid Interface.....	70
8.7. Refraction.....	72
8.8. Frequency Response at Temperature.....	74
9. Conclusion.....	77
10. Future Work.....	79
11. Appendix	
11.1. Vision Based Electroslag Surfacing Bead Following and Overlap System..	80
11.2. Software Code	99
12. References.....	109

List of Figures

1. ESS Process	6
2. Electroslag Weld Head... ..	6
3. Spark Generation Circuit	10
4. Wave Modes	12
5. Interatomic Force and Distance	14
6. Finite Element	18
7. Finite Difference Grid... ..	19
8. Finite Element Convection Node	21
9. Top Side Ultrasonic Testing... ..	26
10. Topside Ultrasonic Testing... ..	28
11. Differential TOF Measurement... ..	30
12. Time of Flight Measurements	32
13. Determination of Weld Pool Depth... ..	35
14. Measurement of Thermal Gradients... ..	37
15. Transducer, Weld Head and Substrate Orientation... ..	38
16. Water Couple... ..	39
17. FEA Model... ..	41
18. Configuration for Measuring Time of Flight at Temperature... ..	42
19. Extensometer Link... ..	47
20. Peak Analysis... ..	48
21. Elongation and Time of Flight in Ductile Iron... ..	50
22. Speed of Ultrasound at Temperature in Ductile Iron... ..	51
23. Photo of Nitrided Ductile Iron Substrate... ..	52
24. Adjusted Time of Flight vs. Temperature... ..	53
25. Curve Fit to Ultrasound Data... ..	54
26. Thermocouple Data from Top of Substrate	55
27. Thermocouple Data from Middle of Substrate... ..	55
28. Thermocouple Data from Bottom of Substrate	56
29. Thermocouples Data at 37.5 mm.	57

30. Domain of the FEA Model...	58
31. Finite Element Model Thermal Data Compared with Thermocouple Data...	59
32. FEA Model versus Thermocouple Data for Top of Substrate...	60
33. Comparison of FEA Temperature Gradients and Fit Curve...	61
34. Ultrasonic Paths During Cladding...	63
35. Ultrasonic Reflection Peaks...	64
36. Ultrasonic Data Peaks...	65
37. White Iron Interface Between Cladding and Substrate 40X...	67
38. Cross Section of FEDI430...	68
39. White Iron Mixed Zone Profile...	68
40. Calculation of Reflector Position ...	69
41. Reflector Position in Relation to Mixed Zone Boundaries...	70
42. Snell's Law...	71
43. Thermal Profiles and Gradients from Finite Element Analysis.....	72
44. Ultrasonic Flight Path Due to Thermal Gradients ...	73
45. Imaginary Portion of Fourier Transform...	74
46. Real Portion of Fourier Transform ...	75
A1. Fully Connected Neural Network...	83
A2. Hyperbolic Tangent...	84
A3. Captured Image of Bead ...	87
A4. Data Flow ...	88
A5. Bead Overlap Determination ...	89
A6. Vision System...	90
A7. Captured Image of Laser Illuminated Profile ...	90
A8. Head tracking position ...	93
A9. Measured Bead Profiles vs. Profiles Predicted by Neural Network. ...	95

List of Tables

1.Example Values	63
AI. Experimental Parameters	91

Abstract

WELD POOL PENETRATION MEASUREMENT USING ULTRASOUND WITH THERMAL GRADIENT CORRECTION FACTORS

John Anderton

Supervising Professor: David Atteridge

Weld penetration is critical to final weld performance. There are many techniques for determining surface parameters of weld pools but the transient nature of the pools, high temperatures and intense electromagnetic energy make direct measurement of the penetration of weld pools difficult.

In order to determine weld pool penetration ultrasonically from below the weld pool it is necessary to compensate for the variation in the time of flight of the ultrasound wave due to temperature gradients. This requires both a precise understanding of the location and magnitude of the temperature gradients and the time of flight of ultrasound at the range of temperatures seen in the gradients. Given this information it is possible to develop a correction factor to an ultrasonic time of flight reading that accurately represents the actual penetration of a weld pool.

This research examines the electroslag surfacing (ESS) processing of AISI 1005 low carbon steel clad onto a ductile iron substrate. The high temperature cladding on low temperature substrate provides a deep weld penetration. Ultrasonic time of flight measurements were made from a piezoelectric transducer on the backside of the substrate to the solid/liquid interface of the weld pool during welding.

The speed of ultrasound over a range of temperatures was determined from furnace heated ductile iron substrates. The sample was stepped and contact piezoelectric methods used to determine time of flight. A finite element model was developed and analyzed to predict thermal gradients in the substrate around the weld pool. The model was correlated to thermocouple data of substrate heating during welding. The predicted thermal gradients and speed/temperature curves are combined with the time of flight measurement to determine the location of the solid/liquid weld interface.

An automated seam tracking system for ESS was also developed. This system utilizes a line laser at right angles to the view of a CCD camera which illuminates the relief of the existing bead for the camera. Optimas software was used to locate the edge of the bead and determine the correct location for the weld head to overlap the existing bead.

Chapter 1

Introduction

Welding is one of our most important and most utilized manufacturing processes. It is the primary method for permanently joining metals into a single unit and has been used since the discovery of metals. Welding is a process of permanently joining two metals through the appropriate combinations of temperature, pressure and metallurgical conditions. Some processes involve only the application of extreme pressures to form a metallurgical bond. In fusion processes heat is applied in order to locally melt both pieces and allow them to reform as a single unit. The quality of the bonding between the pieces is directly related to the attributes of the molten pool formed.

Since welding began methods have been devised to test the strength of the bond between the metals. This usually involves applying stress to the bond in the critical directions. This method is limited in that it can give a minimum value to the weld strength but can only give an absolute value of the weld strength by testing the bond to failure. Another method for assessing weld quality is by cross sectioning the weld and visually inspecting it which is also a destructive test. There are a range of post-process nondestructive test methods for determining weld quality such as ultrasonic testing and xray inspection but these are all post process methods which do not allow real time modification of the weld process. A preferred method of weld testing would be to assess the weld during fabrication which would assure weld acceptance. Many parameters have been studied as indicators of weld qualities, weld pool temperature, pool surface dimensions, and heat input among others. One of the most difficult to measure and most critical is the weld penetration because the depth of the bond formed is critical to the

strength. The high temperature of the molten metal and short life of the pool at any point during processing makes any direct measure of weld pool penetration challenging.

Practically there is not a way to put a ruler into the pool to the bottom of the pool and measure the depth. A method is needed to measure the distance to the pool through the substrate. Many nondestructive evaluation techniques have been developed which could be used. Electromagnetic waves are a possible carrier, microwaves are used but have limited penetration. Eddy currents are subject to the changing magnetic properties of the substrate at high temperatures. Real time radiographic inspection forms a two dimensional image of the substrate and can be used to identify weld defects during welding¹ but the x-ray generation equipment and shielding required make it difficult to use and as a through transmission technique it isn't effective in determining weld penetration. Magabsorption, acoustic emission, neutron thermography, and x-ray tomography are possible techniques but are very complex, expensive or not optimized to this application.

Electromechanical waves are better able to penetrate metals without appreciable attenuation. Ultrasonic waves are widely used to determine structures internal to metal substrates because they reflect from any interface with a difference in acoustic impedance. Since the weld pool will have a difference in impedance between the molten metal and solid metal an ultrasonic signal should be reflected from it and the distance to the interface can be determined by the time of flight of the signal and a knowledge of the speed of the signal through the material. Ultrasonic methods have features which make it attractive. It can be implemented without a great deal of equipment, results are immediately available, it is low cost and not hazardous.

A major difficulty with ultrasonic testing is that the speed of the signal varies with the temperature of the substrate and since the welding process varies the temperature from ambient to molten temperatures, the variations in speed are complex and broad. The temperature gradients also refract the signal which increases the path length. If it were possible to know the temperature and gradients at several points along the ultrasound propagation path and the speed of ultrasound at these temperatures it would be possible to accurately determine the distance to the solid/liquid interface.

Beyond measuring the penetration it is possible to take a series of time of flight measurements and using deconvolution techniques obtain a two dimensional cross section image of the weld pool. This would allow determining not only the depth of the penetration but also the shape of the solid/liquid interface. A cross section shape determination would be very valuable in understanding the mechanics of the solidification process.

While ultrasonic determination of penetration should be applicable to any welding process that generates a pool of liquid metal to form a bond, a specific test process for development is required. The development process, besides being required to have a molten weld pool, should have a wide, flat bottomed pool and a sharp liquid/solid interface rather than a thick mushy zone in order to return a stronger signal. The mushy zone is the area of partial solidification of the molten metal. A sharp delineation between the solid and liquid will more effectively reflect the ultrasonic wave at one point and produce a short duration reflected signal. With a mushy zone the signal is reflected weakly from several depths producing a wider less intense pulse. A process with controllable penetration would allow adjustment of the primary variable to test the accuracy of the system.

All of the work done in this field have used GTAW and GMAW systems. These have the advantage that they are directly applicable to industry since GTAW and GMAW are the most widely used welding techniques. The weld pools generated can be adjusted, which is an advantage, but tend to be narrow with a round bottom which will return a weak signal. Electroslag surfacing (ESS) while not strictly a joining process has several advantages over GTAW as a development tool. The weld pool is much larger with a flat bottom which gives a more intense return signal. The penetration tends to be low but by selecting proper substrate and cladding materials it can be increased. Power input is high and at 7 inches/minute welding rate, the thermal gradients are steep making a thin mushy zone and a sharper return signal.

Predicting the thermal gradients in the substrate in order to correct for the change in ultrasonic speed can be done with a finite element (FE) program. A FE program is dependent on good boundary conditions such as heat flow at boundaries and temperature

constraints and this application is well posed for this requirement. The top temperature will be held to the melting temperature over a finite area and the bottom surface will be cooled with a water jet holding its temperature below 100°C over a finite area. There is negligible natural air convection on the top due to the powdered flux load and there will be negligible radiated heat losses. The convection cooling from the forced jet can be accurately quantified using some assumptions. The test of accuracy for this simulation is its correlation to measured thermocouple values attached to a substrate during welding.

The last tool required is the speed of ultrasound at temperature in the selected substrate material. This is determined by heating a substrate to a set temperature and measuring the difference in time of flight between two points. The concept is straight forward but controlling all variables is complex. This is a difficult procedure due to the high temperatures involved, the sensitivity of piezoelectrics to temperature and the attenuation of ultrasound at high temperatures. Noncontact methods such as laser ultrasound generation and interferometers have been developed for these measurements and have many advantages but cost make them unusable for this project. Contact methods are not the preferred technique but with care and fast measurements they are more than adequate and can be used without damaging the equipment.

These three variables of time of flight, temperature at each point along the flight path and velocity at temperature are substituted into one equation to determine the path length to the solid/liquid interface. This research will describe the development of a weld penetration measurement system using electrosag surfacing. All of the methods used will be technologies which are applicable to field or industrial uses.

Chapter 2

Electroslag Surfacing

Electroslag Surfacing was developed in Europe in the early 70's. It became popular in Europe and Japan but did not see industrial use in the United States until it was introduced by Oregon Graduate Institute (OGI) in 1986. OGI developed electroslag surfacing from 1987 to 1990 bringing the technology to local industry and finding new applications. From 1990 to 1995 OGI researched applications for the US Navy primarily for application and repair of bearing surfaces on ship propulsion shafts. This resulted in a comprehensive report on Inconel-625 for single and multilayer surfacing applications and 70%Cu-30%Ni alloy for single layer surfacing applications on low alloy steel. ²

Until recently Submerged Arc Surfacing (SAS) was the primary process for high deposition rate surfacing but ESS can produce substantially greater deposition rate with less dilution and less impurity inclusion content.³ ESS provides a manufacturing process with higher productivity and quality and lower cost.

ESS is an arcless process. The energy to melt the admetal comes from resistive heating as the strip admetal passes through a flux layer and into a pool of molten flux and then admetal. Power levels on the order of 600 amps and 27 volts are passed through the admetal strip to ground through the electroconductive flux. The flux melts from resistive heating at 2300°C and the heat from this molten pool melts both substrate and the admetal strip forming a molten metal pool below the flux pool which floats on top of it. The substrate is electrically ground. Flux and admetal are continuously supplied as the cladding process moves across the substrate surface as illustrated in Fig. 1.

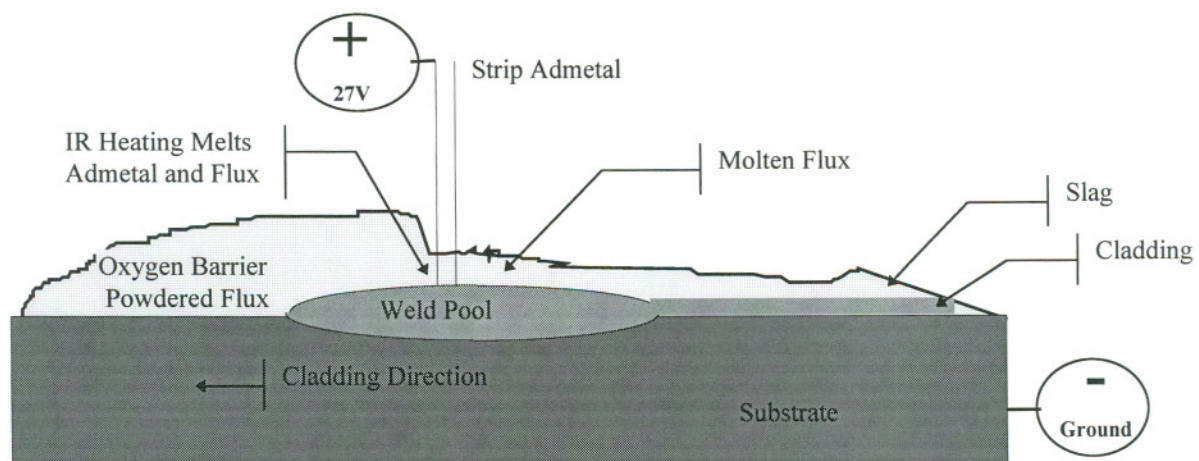


Fig. 1. ESS Process

ESS processing can be implemented at a modest cost and with little training. Standard power supplies in most welding shops can be used for the process. The main capital outlay is for a weld head that feeds strip admatal and conducts electricity through the strip and for consumable raw materials such as flux and strip. Weld heads as shown in Figure 2 typically cost \$5000.

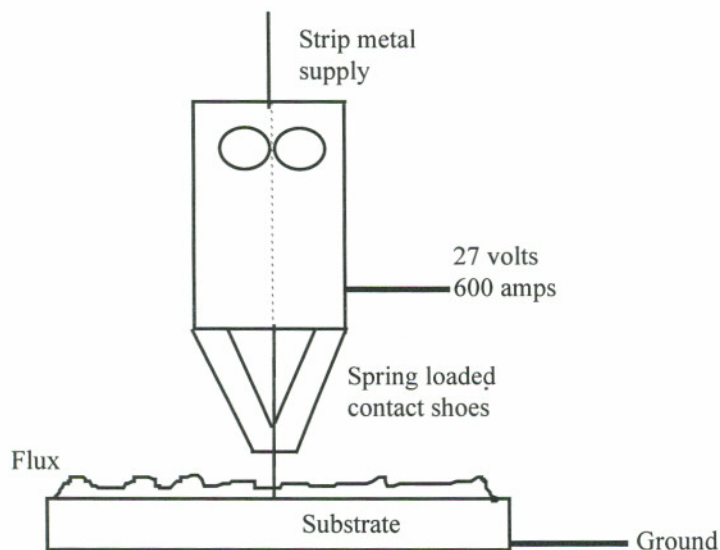


Fig. 2. Electroslag Weld Head

A range of different materials can be combined with the ESS process. The two processes studied under the Navy contract at OGI are Inconel 625 and Copper-Nickel on

steel substrates. These were examined for use as bearing surfaces on new and refurbished propulsion shafts on naval vessels. Bearing surfaces are subject to high temperatures, high pressures and corrosive sea water. Bearing surfaces on large shafts are machined shrink fit or interference fit collars pressed on to a mild steel shaft. The collars must be precisely machined for a proper fit and can cost up to \$150,000/sleeve. The problem with this application is in the corrosion that can occur when contaminants get into the interface between the collar and shaft and cause galvanic corrosion between the dissimilar materials. Inspection for the corrosion can only be done by visual inspection after removing the collar and requires a new collar. ESS can provide an equivalent bearing surface without an interface subject to contamination and corrosion resulting in a lower maintenance cost.

Penetration control is critical to overlay quality and performance in this process. Excessive penetration increases dilution of the overlay and inadequate penetration reduces bond quality and indicates contamination of the weld. A moderate level of penetration is desired which gives a good bond but minimizes the dilution of the admetal. A good level of penetration for Inconel 625 on steel is 0.5 mm which gives a 6% - 8% dilution of substrate to the admetal.⁴

The ability to accurately locate the liquid/solid interface provides a method to control dilution in the admetal. All penetration information at present is derived from destructive testing of a small number of samples. Penetration determination from ultrasonic testing would provide a tool for real time modification of weld parameters to control penetration depth.

Chapter 3

Acoustic Measurement Techniques and Theory

This experiment will use ultrasonic techniques to locate the liquid/solid interface. It is a good technology for this application due to its low cost, comparative ease of implementation, accuracy and sensitivity. The time of flight values will be corrected using the finite element model of the thermal gradients and the temperature velocity curves to give an accurate location of the liquid/solid interface.

Ultrasonic testing (UT) is a nondestructive material evaluation technique. It is a widely used method of material evaluation and has found a wide range of applications including defect detection, defining bond characteristics, grain size, elastic constants, thickness measurements and three dimensional imaging. More techniques are continually being developed. UT has the advantages of superior penetration, high accuracy, speed and high sensitivity to small discontinuities.

A UT system usually consists of an ultrasonic signal generator, a couplant fluid to carry the generated elastic wave to the material, a signal receiver, an amplifier, data storage, display and timing electronics. Frequencies in the range of 0.1 to 25 MHz are used. The signal is reflected at any interface with a difference in material impedance. This reflected wave or the transmitted wave is used to determine the location and size of the reflector by the time of transit, signal strength and spectral response. Cracks, impurities, delaminations, pores and discontinuity interfaces such as a liquid solid phase transition can all be detected and located.

Ultrasonic generators and receivers of many types have been built. The most common generators used are piezoelectrics. Piezoelectric materials when deformed generate an electric potential and, inversely, when a voltage is applied to them they deform.⁵ By cutting a piezoelectric material to the right dimensions and applying an alternating current the piezoelectric material will deform and oscillate at a characteristic frequency. This oscillation generates an ultrasonic compression wave in any material in physical contact with the generator. The same process can be used to detect an ultrasonic signal also. As an ultrasonic pressure wave passes through a transducer an oscillating electric signal is generated which can be recorded. Ultrasonic transducers are typically designed with either a single element which both generates the signal and detects the reflections or with dual elements one of which generates and the other receives.⁶ Examination using a single element transducer is commonly called the pulse/echo mode and is used to detect reflections from acoustic anomalies such as surfaces. When separate generators and receivers are used such as in through transmission testing or angle beam techniques, it is commonly referred to as pitch/catch. Piezoelectric materials have some disadvantages. They are fragile, being subject to cracking under shock. They are also heat sensitive. Once hitting their Curie temperature the materials will lose their electromechanical properties. The Curie temperature for lead zirconate titanate is 386⁰C.⁷

There are several other ultrasonic transmitters and receivers that have been used in high temperature environments. Scruby *et al*⁸ used a Q-switched Nd:YAG laser to generate ultrasonic pulses and a laser interferometer to receive signals and measure the speed of ultrasound at elevated temperatures. The Nd:YAG laser generates an ultrasound pulse either by thermoelastic or ablation effect depending on the power level used. The laser has the advantage of not having to be in contact with the material, even being able to pass through any transparent medium and pulses can be very short and intense. The disadvantage is the only way to get a strong signal is with ablation of the surface which is unacceptable here. The cost for the laser and supporting hardware, portability, low sensitivity for the received signal and safety are also concerns.

Electro-Magnetic Acoustic Transducers (EMAT) are used to generate and receive ultrasound by electrodynamic methods. An EMAT is an electromagnet or permanent magnet combined with a receiving coil carrying an alternating current⁹. The interaction of the coil and magnetic field generate a Lorentz force in nonferrous materials and a magnetostriction effect in ferrous materials. Both of these forces can generate an ultrasonic wave by deforming the material surface or inversely can detect an ultrasonic wave by the change in the magnetic field from the deflection of the surface. An EMAT is relatively inexpensive but requires amplifiers, power supplies and generate wider pulses than piezoelectric or lasers.

A method not commonly used to generate ultrasound is spark discharge.¹⁰ Spark discharge is similar to laser generation. The spark discharge can either jump to an isolated ground and generate an air pulse which in turn generates an ultrasonic pulse or the spark can jump to the grounded substrate and generate a pulse by ablation of the surface. The advantages of the spark discharge is its simplicity, low cost and ability to work in hostile environments. Disadvantages are the danger of stray high voltage sparks damaging electronic equipment. The circuit for spark generation is shown in Fig. 3.

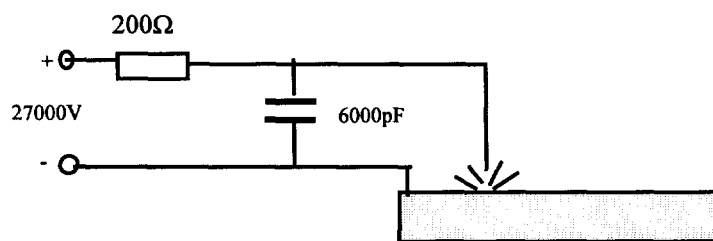


Fig. 3. Spark Generation Circuit

Once the ultrasonic wave is generated it propagates through the substrate until it reaches an interface where it undergoes reflection and mode conversion. The degree of reflection of the ultrasonic wave is a function of physical state and physical properties of the materials at the interface. A gas/metal interface will reflect almost all of a signal but at a well bonded interface of two metals much of the signal passes through the interface.

The amount of energy transmitted through an interface by an ultrasonic signal incident normal to the interface is¹¹:

$$T = 4 Z_2 Z_1 / (Z_2 + Z_1)^2$$

Where Z_1 and Z_2 are the acoustic impedances of material 1 and 2. Since all the energy is either reflected or transmitted the Reflection Coefficient (R) will be determined from this by:

$$R + T = 100\%$$

Where the angle of incidence is not normal to the interface, mode conversion can occur and the incident wave may be converted to shear waves and/or surface waves.

Ultrasound propagation is always a complex interaction of modes which is affected by the generation method, substrate material, interfaces and angle of intersection. The ultrasonic signal is a mechanical wave as compared to an electromagnetic wave. There are two primary propagation modes for ultrasonic waves. Longitudinal waves which cause atomic movement in the direction of propagation and shear waves which cause atomic movement at right angles to the direction of propagation. Shear waves cannot propagate in air or liquid. When a longitudinal ultrasonic wave is incident on an interface at an angle not normal to the surface a mode shift takes place where a portion of the wave energy is converted into a shear wave¹¹.

Two other wave types used in ultrasonic testing are Raleigh waves and Lamb waves¹². Raleigh waves propagate only along the surface of the material and are limited in depth to approximately one quarter wavelength. Raleigh waves will follow the contours of a surface and will be reflected by any surface discontinuities back along the same surface. Raleigh waves are valuable for applications where only surface defects are of interest. These wave modes are shown in Fig. 4¹³.

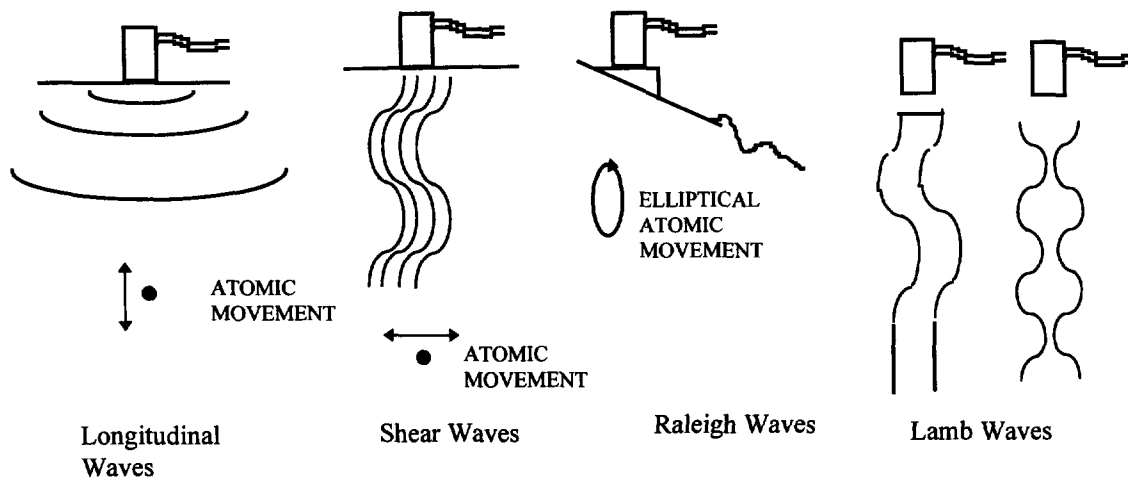


Fig. 4. Wave Modes

Lamb waves are generated in thin plates several wavelengths thick and propagate in one of two complex modes. In one mode the two surfaces of the plates oscillate in phase with each other at the wavelength of the Lamb wave. In the second mode the two surfaces oscillate 180° out of phase with each other forming an hour glass shape. The velocity of Lamb waves is dependent upon the wavelength, the thickness of the material and material type. It is used primarily for tubing and sheet inspection.

Material temperature changes the propagation rate of the ultrasonic wave¹⁴. Any compressive wave traveling through a material depends on the deformation of the atom structure within the material to propagate. Any change in the bonding of the atoms to one another will affect the ability of a compressive wave to deform the material and propagate. Heat increases the vibration of individual atoms and increases the interatomic distance. This increases the interatomic strain and lowers the density of the material causing a decrease in the propagation rate of the wave.

The propagation rate of an ultrasonic wave at any temperature is¹⁵:

$$V = f * \lambda$$

where V is material velocity, f is frequency and λ is the wavelength. This is a constant for a set temperature and material condition. In a homogenous material with cubic crystal

structure the propagation rate can be determined from the elastic modulus, density and Poisson's ratio¹⁶:

$$V_L = \left[\frac{E * (1 - \nu)}{\rho * 2 * (1 + \nu) * (1 - 2 * \nu)} \right]^{1/2} \quad \text{Eq. 1}$$

where V_L is the propagation rate of a longitudinal wave, E is Young's Modulus, ν is Poisson's ratio and ρ is density.

These variables are functions of the interatomic bonds of the material¹⁷. The forces acting on atoms in a lattice are a balance of attraction and repulsion forces. Individual atoms tend to position themselves where they are at the lowest possible energy. In Figure 5 this will be at the point d_0 at the bottom of the energy trough which is the sum of the attraction and repulsion forces. As the temperature of the lattice rises above absolute zero the vibration of the atoms will increase the repulsion forces of the lattice and the equilibrium interatomic distance of the atoms will increase. This change in interatomic spacing and interatomic force changes the value of the Young's modulus and the density.

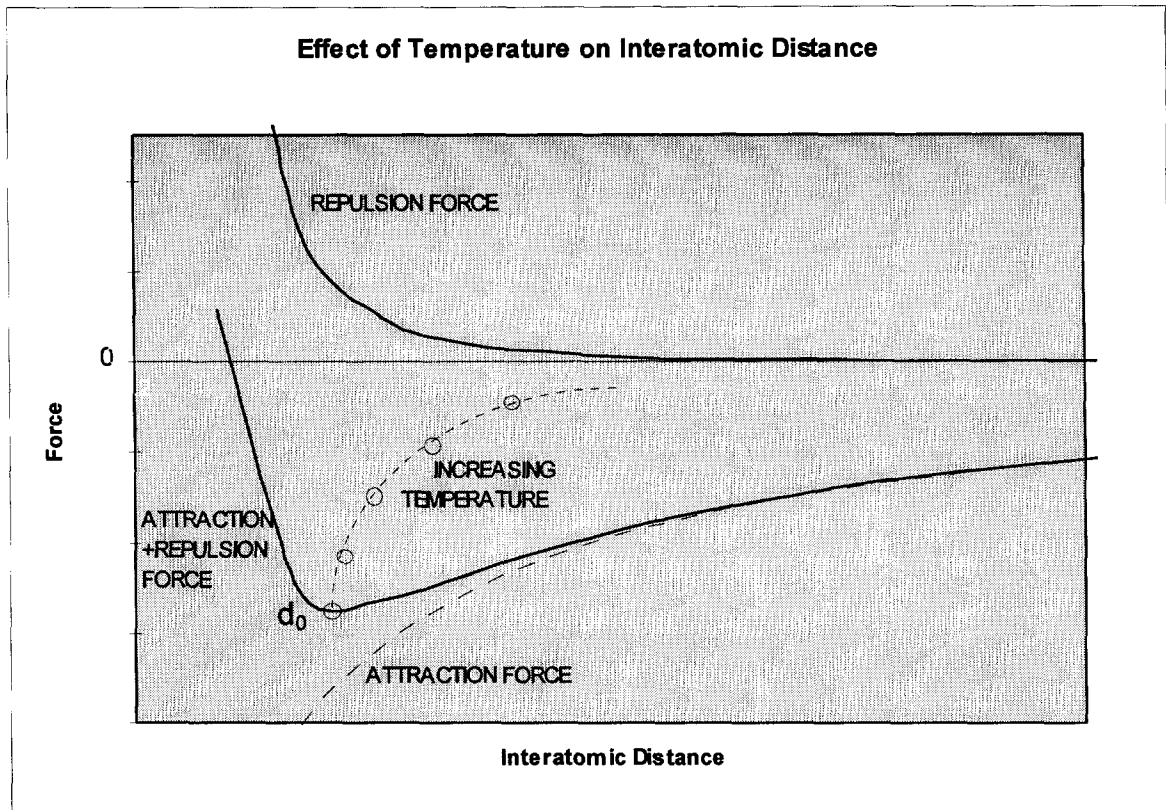


Fig. 5. Interatomic Force and Distance

The general form of the relationship of Young's modulus and temperature is ¹⁸:

$$E = E_0 - b \cdot T \exp(-T_0 / T)$$

where E_0 is the modulus at 0 degrees Kelvin, b is a constant and T_0 is a temperature constant. At elevated temperatures the exponential term approaches 1 and the equation reduces to a linear relationship. Poisson's ratio will change only slightly with temperature in steels and the change in density will be an order of magnitude smaller than the change in Young's modulus¹⁹. Therefore from Equation 1, the change in the velocity of sound in a cubic solid will be close to linear from room temperature to near the melting temperature. These equations are based on a perfect cubic structure. In less than perfectly ordered material there will be nonlinearities introduced by grain boundaries, lattice orientations and other deviations from a perfect crystal structure.

As the wave propagates through any material its energy is dissipated by beam spread, absorption and scattering²⁰. All of these cause a reduction in the amplitude of the ultrasonic signal. Beam spread in a spherical wave causes the intensity to decrease inversely with the distance from the source as the wave covers an ever increasing area.

Scattering and absorption together are commonly called attenuation. Absorption is the conversion of the mechanical energy of the wave into heat. As the atoms are displaced by the passing of the wave, work is done which results in heat. The exponential decay law is²¹:

$$P = P_i * \exp(-\alpha * d)$$

where P_i is the initial sound pressure, P is the pressure at distance d , α is the attenuation coefficient and d is the distance. The attenuation coefficient is often in units of dB/mm.

With a change of temperature the value of the attenuation coefficient also changes.

Higher temperatures increase the interatomic spacing and the attenuation of the wave will increase over a set distance.

Scattering is a function of small discontinuities such as grains that are too small to reflect detectable amounts of energy but are numerous enough to reduce the energy of the wave appreciably. The type of scattering is classified by the size of the scatterer²².

Rayleigh scattering results from discontinuities much smaller than the wavelength.

Stochastic scattering occurs with scatterers approximately the size of the wavelength. For average scatterer diameters larger than the wavelength the scattering is called diffusional.

Another factor affecting signal integrity is near zone effects. For any ultrasonic generator larger than the wavelength it generates, there is a zone at the face where constructive and destructive interference takes place. Each point of the generating surface acts as an individual generator and these individual waves interact as they propagate causing a wide variation in the intensity of the signal transversely and longitudinally along the direction of propagation. This area is called the near zone and in the propagating direction its length can be determined by²³:

$$N = \frac{D^2}{4 * \lambda} = \frac{D^2 * f}{4 * V}$$

where N is the near zone length, D is transducer diameter, λ is the wavelength, f is the transducer frequency and V is the material velocity. As the beam propagates and diverges the signal becomes progressively more coherent and homogenous. This zone beyond the near zone is the far zone where the signal exhibits a constant drop in amplitude along its propagation axis. Any discontinuities located in the near zone may or may not reflect a signal depending on its size and precise location. Wherever possible ultrasonic testing is conducted so that any target discontinuities are in the far zone.

Chapter 4

Finite Element Analysis

In order to predict the thermal gradients in the substrate a finite element model was developed. Using existing boundary conditions and known material properties an accurate prediction of the thermal gradients can be made and combined with the temperature/velocity curves to correct the time of flight values.

Finite element analysis uses the same basic equations required for static and dynamic analysis. The limitation to FEA analysis until the advent of computers was the level of complexity. Working by hand there are only a limited number of equations that can be simultaneously solved and so the number of elements that an individual problem can be divided into are limited. Electronic computation tools have increased the number of equations that can be solved simultaneously in a finite amount of time.

Any problem that can be defined by equations and boundary conditions can be solved with finite element techniques. A common type of problem is load/deflection problems. The static deflection of the end of a long thin rod is described by the equation

$$F = \frac{E * A}{L} * d$$

where F is the applied force, E is the Young's Modulus, A is the cross sectional area, L is the length and d is the deflection. It can be more generally described by

$$F_1 = -F_2 = \frac{E * A}{L} * (d_1 - d_2)$$

as illustrated in Fig. 6. This can be reduced to the matrix form

$$\begin{bmatrix} F_1 \\ F_2 \end{bmatrix} = \frac{EA}{L} \begin{bmatrix} 1 & -1 \\ -1 & 1 \end{bmatrix} \begin{bmatrix} d_1 \\ d_2 \end{bmatrix}$$

In matrix terms this becomes

$$[F] = [K] [d] \quad \text{Eq. 2}$$

where K is the stiffness matrix, F is the forcing function vector and d is the displacement vector.



Fig. 6. Finite Element

Where multiple bars are connected the boundary conditions for each bar are dictated by the adjacent bars so that the end deflection of one bar has to be equal to the end deflection of the next bar and the force on the end of one bar is equal to the force on the next bar. From summing these forces and deflections at each node together with system boundary conditions a matrix equation of the form of Equation 2 can be determined which includes each element of the system. There are many methods in linear algebra for solving this matrix equation including Gaussian direct elimination, conjugate gradient approach or Cholesky reduction.

In a thermal problem the process is equivalent but the governing equations will be different. The full general heat equation is:

$$\frac{\partial^2 T}{\partial x^2} k_x + \frac{\partial^2 T}{\partial y^2} k_y + \frac{\partial^2 T}{\partial z^2} k_z + \dot{q} = \rho c \frac{\partial T}{\partial t}$$

where T is the temperature, t is time, ρ is the density, c is the specific heat and \dot{q} is a heat source or sink in the system and is valid for constant thermal conductivity. For two dimensional steady state conduction without heat sources this will reduce to the Laplace equation²⁴:

$$\frac{\partial^2 T}{\partial x^2} + \frac{\partial^2 T}{\partial y^2} = 0$$

For a thermal analysis the temperatures at certain points are of interest. To solve for this the sample is redefined as a set of grid points. A two dimensional body broken down into nodes and elements would look like Figure 7.

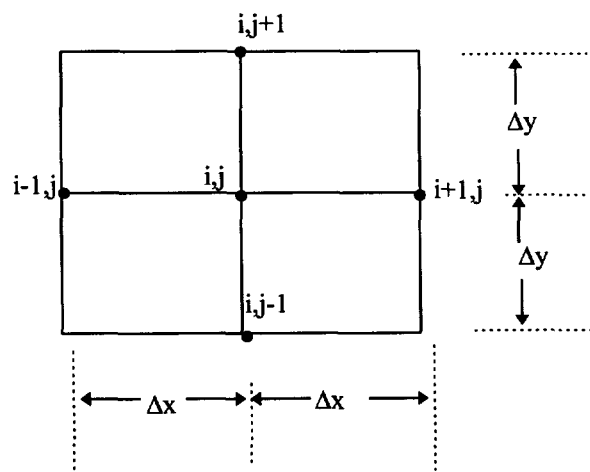


Fig. 7. Finite Difference Grid

The gradients between nodes can be described by :

$$\frac{\partial T}{\partial x} \bigg|_{i+1/2,j} \approx \frac{T_{i+1,j} - T_{i,j}}{\Delta x}$$

$$\frac{\partial T}{\partial x} \bigg|_{i-1/2,j} \approx \frac{T_{i,j} - T_{i-1,j}}{\Delta x}$$

$$\frac{\partial T}{\partial x} \bigg|_{i,j+1/2} \approx \frac{T_{i,j+1} - T_{i,j}}{\Delta y}$$

$$\frac{\partial T}{\partial x} \bigg|_{i,j-1/2} \approx \frac{T_{i,j} - T_{i,j-1}}{\Delta y}$$

The second derivative would then be:

$$\frac{\partial^2 T}{\partial x^2} \bigg|_{i,j} \approx \frac{\frac{\partial T}{\partial x} \bigg|_{i+1/2,j} - \frac{\partial T}{\partial x} \bigg|_{i-1/2,j}}{\Delta x} = \frac{T_{i+1,j} + T_{i-1,j} - 2T_{i,j}}{(\Delta x)^2}$$

$$\frac{\partial^2 T}{\partial y^2} \bigg|_{i,j} \approx \frac{\frac{\partial T}{\partial y} \bigg|_{i,j+1/2} - \frac{\partial T}{\partial y} \bigg|_{i,j-1/2}}{\Delta y} = \frac{T_{i,j+1} + T_{i,j-1} - 2T_{i,j}}{(\Delta y)^2}$$

Substituting the last two equations back into the Lagrange Equation and assuming

$\Delta x = \Delta y$:

$$T_{i+1,j} + T_{i-1,j} + T_{i,j+1} + T_{i,j-1} - 4T_{i,j} = 0$$

For each node in the model there will be a set of these equations relating the temperature gradient to the adjacent nodes. Heat generation and convection losses can also be included and then boundary conditions can be either temperatures at specified nodes or heat flow at specified areas. The equation for heat flow between nodes will be

$$q = \sum k * \Delta x * \frac{\Delta T}{\Delta y}$$

where k is the thermal conductivity.

For an exposed face with convective heat flow as in Fig. 8 there will be heat flow to the right at node i,j.

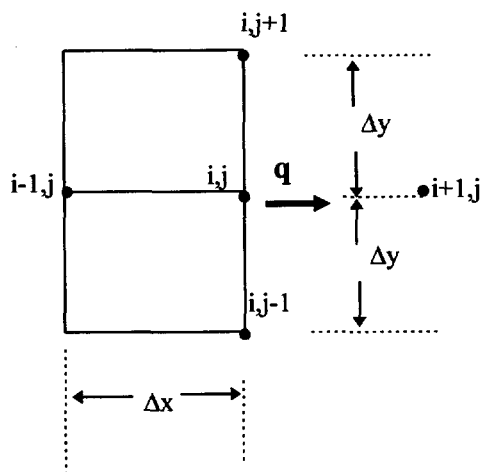


Fig. 8. Finite Element Convection Node

Summing the flow through the node i,j gives

$$-k * \Delta y * \frac{T_{i,j} - T_{i-1,j}}{\Delta x} - k * \frac{\Delta x}{2} * \frac{T_{i,j} - T_{i,j+1}}{\Delta y} - k * \frac{\Delta x}{2} * \frac{T_{i,j} - T_{i,j-1}}{\Delta y} = h * \Delta y * (T_{i,j} - T_{\infty})$$

where h is convection heat transfer coefficient. This analysis is for a flat convecting surface only but a similar analysis can be done on a corner node or a curved surface in a similar manner. For any finite element model the problem will be broken down into a series of linear equations balancing heat flow and temperature at each node. Given

adequate boundary conditions the linear equations are determinate and can be solved. In practice the number of equations can be large and complex and can be solved only with the aid of a computer.

The accuracy of the solution is a function of the size of Δx and Δy ²⁵. The smaller the element size the higher the accuracy but the number of equations and complexity of the matrix grows also. ANSYS finite element program Rev 5.3/university will accommodate approximately 8,000 nodes but requires very large amounts of memory for the solutions.

While the computational power of these programs is their primary strength the user interface makes the setup of the problems very easy. Very complex shapes can be laid out and viewed, constraints added and degrees of freedom assigned in a very straight forward intuitive manner with visual aids. This, as much as the computational power, has allowed for the solution of more and more complex problems.

Chapter 5

Previous Research

The determination of in-process parameters of the weld pool are critical in controlling post process material parameters. There is a large body of work on measuring and controlling welding processes with the majority of the work being done on arc welding such as GTAW and GMAW. Although research in measuring weld pool parameters is complicated by intense light and heat radiation, flux loads, rapid solidification and high pool temperatures, many techniques have been developed.

Weld pool surface parameters are the easiest to quantify and many procedures have been developed to measure them. The pool surface can be monitored by a radiation protected camera to obtain width and length measurements. Ohshima²⁶ used CCD cameras to measure weld pool width and brightness distributions. The width of the gap between plates being filled was determined with one camera to help the system make broad adjustments. A second camera determined the widths of the pool at several points. These values were used to determine the optimum values for the current waveform, torch position, speed and wire feed rate on a GMAW welder. The goal was to optimize the depth of the weld pool and control back bead width. By controlling the current waveform, the wire deposition and substrate melting could be regulated.

Heat flow can be used to accurately measure the surface parameters as well. Lukens and Morris²⁷ examined the effects of welding parameters on the cooling rate in a weld pool. They used an infrared profiler to determine the cooling rate of a GTAW weld

on a plate from molten state to room temperature at several voltages, amperages and travel rates. Varying weld parameters and taking measurements of the temperature over time they were able to make a series of charts for each weld parameter to show the cooling rate at set values.

Kozono²⁸ *et al* used a similar configuration. They attached an infrared detector to a pulsed TIG welder to measure the temperature at several points behind the weld as close as directly below the electrode. They were able to do this by timing the IR measurements to coincide with the valleys of the pulses where the current reached a base value and the radiation reached a minimum value. Their goal was to use these measurements to control the backbead width in butt welds. They correlated the pool temperatures to post weld cross sections of the back bead width and were able to control the backbead width variation to 0.5 mm using this information.

Nagarajan²⁹ *et al.* used an infrared imaging camera to look at the isotherms around the weld pool. They first used the thermal profile information to control the track of the welder along a joint. They found that the isotherms became irregular as the welder tracked away from the joint and could be used to reposition it. The second measurements were to sense the variation in substrate depth by variations in the isotherms of the weld pool. They were able to closely determine substrate dimensions using the minor axis of the primary isotherm.

All of these techniques require visual access to the topside of the substrate and the weld pool. In ESS applications that is not possible because of the flux load required to cover the arc process and pool surface. A measurement process for ESS would have to work without direct visual access to the weld pool and is much more difficult to determine than by previous techniques.

Much work has been done on indirect measurement techniques from the backside of full penetration welds. Zacksenhouse and Hardt (1983)³⁰ monitored the resonant frequency of the weld pool which is a function of the dimensions of the pool. The vibration of the molten pool was measured by photodetectors along the rear side of the

weldment. Nomura³¹ used the step function from photodetectors as the backbead goes to full penetration in a V groove butt weld to control weld depth.

More recently neural networks have come into use to control welding and specifically to control weld pool depth. Kaneko *et al*³² trained a neural network to control the power input to the weld as a function of the surface dimensions of the weld pool. The surface dimensions were correlated to the weld pool depth from post weld cross sectioning. Values for gap width, weld pool width and weld current were used as input and weld depth as output from the neural network. The resulting network was able to adjust weld parameters during operation to control penetration. Lim *et al*³³ measured temperature at three points near the weld pool as an indication of heat input and temperature gradients. These temperatures were used as input to a neural network. Partial and full penetration depths and measured pool widths were used as outputs. Partial penetration weld depths were derived from cross sections of weld beads. The resulting neural network was able to map temperature gradients to weld pool size.

All of these weld pool measurement techniques attempt to determine weld pool shape and/or penetration indirectly and are not single valued indicators. More direct measures would provide better control and research tools. Since a weld pool is a change in phase and material properties of the weldment, it is a reflector of ultrasound and time of flight measurements of reflections from the solid/liquid interface should give a more accurate measure of weld penetration. Complicating factors are attenuation of the pulse and change in ultrasound speed due to heat and refraction of reflected waves due to heat gradients. Each of these are determinate and allow development of correction factors.

Katz and Hardt³⁴ in 1983 at MIT used ultrasound to characterize a GTAW weld pool. They placed a pulse-echo transducer on one end of a rod. In the other end of the rod they generated a weld pool using a GTAW welder. A peak corresponding to the solid/liquid interface could clearly be seen in the reflected signal. The weld pools were cross sectioned and measured for weld pool depth to correlate weld pool data to time of flight data. The data showed a close correlation between reflections from machined holes

of various depths to weld pools of the same depths but no attempt was made to correct for thermal gradients in the rod.

The Idaho National Engineering Laboratory (INEL) in the mid 80's developed ultrasonic monitoring of weld defects and weld pool penetration for the Navy PAWS program. In 1983 at INEL Lott³⁵ located GTAW solid/liquid interfaces on a steel substrate using ultrasonics. The substrate was half immersed in a water bath with the piezoelectric transducer coupled through the water to the backside of the substrate. The weld pool was generated on the top of the substrate. Both refracted shear waves and longitudinal waves were used. Reflections were observed from the solid/liquid interface using both modes. The welds were cross sectioned and correlated to the time of flight. Only three welds were cross sectioned but the weld depths were very close to ultrasonically determined values.

Also at INEL Carson and Johnson³⁶ used ultrasonic signals to characterize weld quality. GTAW root passes in a V groove on steel substrate were made while an ultrasonic transducer probed the weld pool. The transducer was positioned on the top and to the side of the weld. It was attached to the weld head and moved with the welder. The signal was reflected from the backside of the substrate as seen in Fig. 9. Using longitudinal waves the data showed that defects in the weld such as porosity and lack

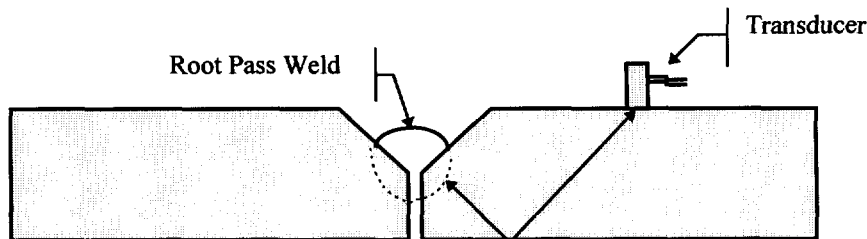


Fig. 9. Topside Ultrasonic Testing

of fusion could be detected during the process because the defects are much stronger reflectors of ultrasound than the solid/liquid interface. Carson and Johnson analyzed the observed peaks using a computer program to correct for time of flight variations and

diffraction due to gradients. Both programs use finite element methods to determine flight paths and velocities at a number of points. This data was well correlated to the resulting peaks.

In 1984 Lott et al³⁷ used the same experimental setup to measure the weld pool penetration from the backside of a solid substrate using ultrasound. This signal was compared to the results of a thermal finite element analysis model that predicted thermal gradients around the weld pool and corrected for the time of flight of the signal for the reduced speeds at elevated temperatures. A ray tracing program, the same used by Carson and Johnson above, was used to determine path length of signals not on a direct path through the weld pool. The experiment was limited by their inability to detect the weak solid/liquid signal. An approximation method was developed where the signal from a reference hole below the weld pool and the signal from the solid/air interface was used together with an assumption of the solid/air interface location and the proportional depth of the solid/liquid interface. This method worked well but was limited to three weld pool depths tested.

Similar work was done at Harwell/AEA. In 1990 Ogilvy and Temple³⁸ made a theoretical measurement of the accuracy of ultrasonic determination of position of the liquid/solid interface. They estimated the thermal gradients in the substrate by applying a delta function pulse of energy to a substrate of magnitude large enough to generate a weld pool. Then by integrating over the area of their theoretical substrate they could predict the location and magnitude of the thermal gradients. To account for the change in path length due to diffraction they used a ray tracing program using Snell's law to find the actual path length for the ultrasonic signal. They determined that the maximum correction factor required is 0.4 mm for a 0° shear wave at 0.1 seconds after the pulse. For compression waves the correction is about half that value. This is a much lower correction factor than has been found in practice.

Also at Harwell Stares *et al.*³⁹ measured the dimensions of a TIG root pass using ultrasonic waves passed through the molten pool and also from pulse echo signals bounced off the solid/liquid interface from the top side as in Fig. 10. They used a ray

tracing program to correct for diffraction. To determine the penetration of the weld pool which in this case is the width of the pool they used the difference in time between reflections from the right and left sides of the weld. They assumed no variation of the temperature within the weld pool and symmetrical distribution of the pool so there was no requirement for understanding thermal gradients to locate the solid/liquid interface. Using published values for the velocity of ultrasound through molten metal they gave a pool width of 4 mm which agreed well with destructive cross section measurements. They determined an overall error of ± 0.8 mm in the width of the weld pool.

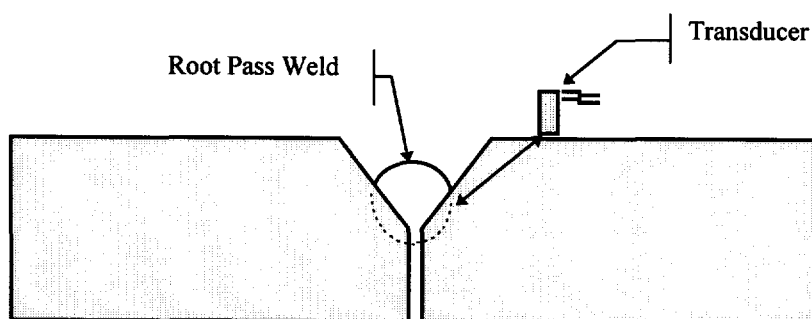


Fig. 10. Topside Ultrasonic Testing

Many finite thermal element models of weld pools have been developed and published. Heating and cooling rates in the heat affected zone around welds are of great interest in understanding cracking and weld quality. Where bearing surfaces are clad onto shafts Navy specifications require the substrate must be held below 275°C to prevent detrimental phase transformations. Wood *et al*¹ modeled ESS temperature gradients and correlated the models to data collected from embedded thermocouples. At 27 volts and 750 amps approximately 20 kilowatts are input into the shaft and heat builds up quickly even in a large shaft. ANSYS finite element modeling of a 61cm shaft with 13.3cm walls, ambient cooling and a 175°C preheat showed that 20 passes could be made with the shaft interpass temperature staying below 275°C . Comparing this to experimental thermocouple data shows correlation within 15 degrees.

The speed of ultrasound at temperature in irons and steels has been widely investigated and measured by researchers including Wadley *et al*⁴⁰ and Scruby *et al*³. Both Wadley *et al* and Scruby *et al* have used non-contact laser methods to obtain temperature vs. ultrasonic speed coefficients. Scruby developed parameters for BS4360 grade 43A and Wadley worked with AISI-1018 and AISI 304 stainless.

Wadley was determining the internal temperature map of cast ingots at the hearth using tomographic techniques. This usually requires large numbers of measurements of time of flight through the ingot along intersecting paths and combining this with velocity at temperature and ingot dimension to get a series of linear equations. Using *a priori* heat flow information they were able to reduce this to three to five measurements. They determined the velocity at temperature in the two materials using a contact piezoelectric transducer as a receiver and a Q-switched Nd:Yag laser to generate ultrasound in a test substrate. The substrate had a step cut out so the laser could generate ultrasound at either of two points along the length of the substrate with both points being inside the oven at the same temperature as in Fig. 11. The ultrasound then travels to the end of the sample outside of the oven and the time of flight is measured by the transducer. The time of flight between the isothermal steps is determined from the difference between the time of flight of the two paths. The thermal expansion of the samples was measured using a quartz rod and an LVDT outside the oven. The time of initiation of ultrasound was determined using a photodiode. Using a stepped sample and differential times has the advantage that the transducer can be used in a low temperature area and the temperature gradients between the oven and the transducer are canceled out.

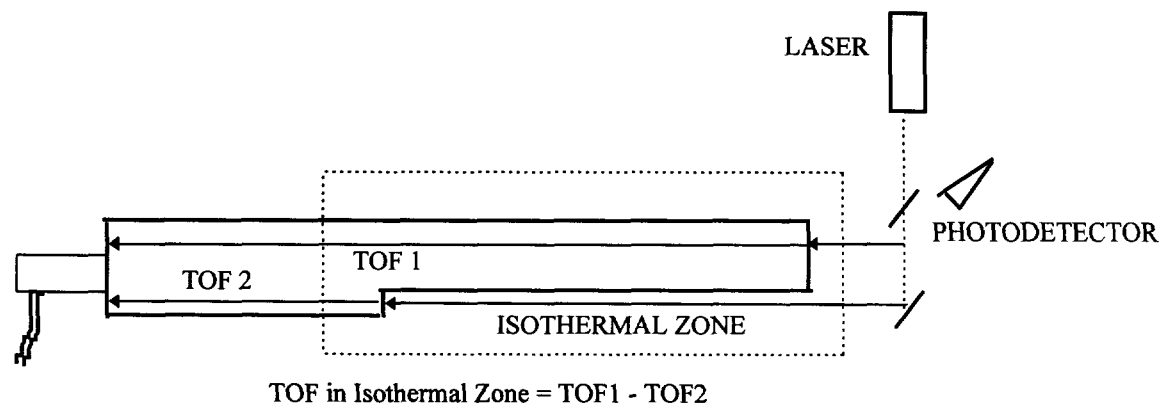


Fig. 11. Differential TOF Measurement

Scruby *et al* were able to use a non-stepped sample by utilizing a laser to generate the ultrasound pulse and a laser interferometer to detect the ultrasonic wave's deformation of the surface. This system has the advantage of having the substrate remain remote from the measuring equipment and being able to maintain the whole sample in the furnace. The disadvantage is in having to keep the surface in such a condition that it will reflect the interferometer beam while at a high temperature. Both Scruby *et al* and Wadley *et al* found the variation of sound velocity to temperature was very linear except at phase transformations.

All of these techniques can be adapted to a weld penetration measurement system for electrosag surfacing or any other system that generates a molten pool. It should be possible to combine and improve many of these techniques to more accurately determine weld pool depth.

Chapter 6

Experiment Theory

This project developed a method for in process weld pool penetration analysis using backside ultrasonic time of flight measurements. An ANSYS finite element model of thermal gradients around the weld pool, and the speed of ultrasound waves in the substrate over a range of temperatures were used to determine the location of the solid/liquid interface from time of flight data.

In measuring an ultrasonic reflection from the weld pool the wave will first travel through the waterjet cooled area of the substrate and then will encounter a significant gradient in the solid substrate approaching the pool itself. The gradients near the molten pool will be steep and at any single point dissipate quickly (short time constant) after solidification but gradient values will remain fairly constant in relation to the moving pool itself as in Fig.12. The substrate gradients farther from the pool will not be as steep.

In order to predict pool depth a way to predict the temperature and subsequently the wave speed at any point along the wave path is required. From basic material constants and known boundary conditions an ANSYS finite element model of the thermal gradients through the substrate can be constructed. This model is then correlated to thermocouple data collected during ESS operation to ensure accuracy. With a temperature/speed formula obtained from calibrated temperature tests the time of flight through each finite element can be determined.

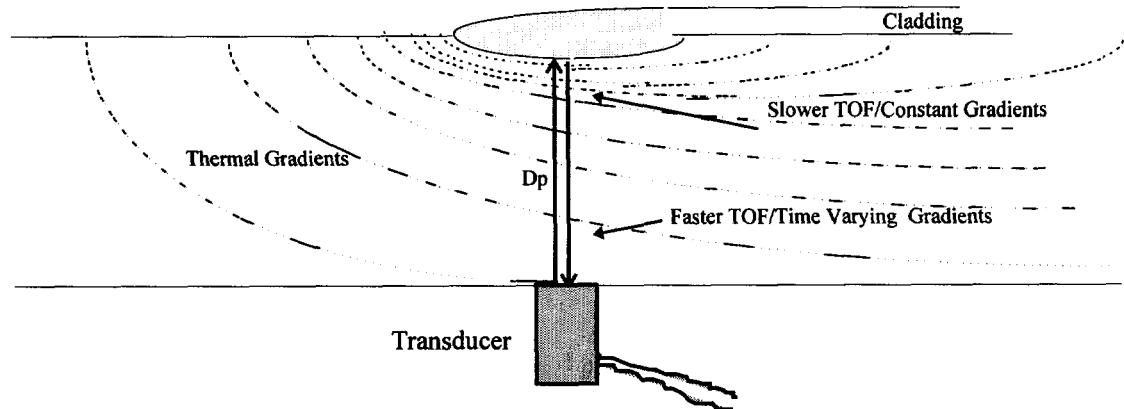


Fig 12. Time of Flight Measurements

There is not a sharp transition from solid to liquid in metal solidification. There will be a hardening or mushy zone where it is neither solid nor liquid. In this area the temperature is near the melting temperature, solid metal crystals are forming in the liquid medium and exothermic phase transformations are taking place. This will not be as sharp a reflecting surface as an air/liquid interface and will reflect the ultrasonic signal from multiple points. The thinner this zone the narrower the reflected signal will be. So a steep gradient is desired that will confine the mushy zone to a narrow space.

While the increased temperatures tend to increase the time of flight, increasing weld pool penetration tends to shorten the time of flight. In the absence of a completed ANSYS model some reasonable values were assumed for the gradients of Figure 12 to get estimates of expected transducer data. A basic time of flight equation

$$\tau_m = \int_{L_m} \frac{dL}{V(T,L)}$$

was used where V is the propagation rate or velocity of the ultrasonic wave as a function of T temperature and L the location along the path and τ is the time of flight.

First assume a 1.27 cm. thick plate and 27 equal divisions of ultrasound path with a weld pool of 1520°C, 0.104cm deep and an underside temperature of 100°C. Gradient

temperatures were estimated from thermocouple measurements during an ESS operation and an estimate made of the difference in the time of flight. To get a velocity of ultrasound in each division values from Scruby *et al* were used:

$$V(T) = 5970 + (T) * -0.88 \text{ (m/(s-}^\circ\text{C)) for } 17^\circ\text{C} < T < 800^\circ\text{C}$$

and $V(T) = 5158 + (T-800) * -0.60 \text{ (m/(s-}^\circ\text{C)) for } 800^\circ\text{C} < T < 1200^\circ\text{C}$

This gave a time of flight twice across the pool heat gradient of

$$\tau_m = 2.19 \mu\text{S}$$

As a comparison the time of flight over an ambient temperature using the same method gives a time of flight of:

$$\tau_m = 2.15 \mu\text{S}$$

This is intuitively reasonable. The increased time of flight due to the thermal gradients will be offset by the shorter flight path due to penetration by the weld pool. This is comparable to values obtained by Lott *et al*²⁰.

For development of a direct measurement system of weld pool depth it is desirable to have a deep weld pool. Stainless steels which are widely used for cladding have a melting temperature of 1410°C and have known material properties. For this experiment a higher melting temperature is desired and the material properties are not of primary concern. Using a lower melting point substrate such as cast iron would provide a deeper weld pool but ultrasonic waves do not permeate white and gray cast iron very well due to its high damping coefficient. Ductile iron also has a low melting temperature and much the same composition but has its graphite in nodules. Cast iron holds graphite in a thin flat flake configuration which alters the damping capability of the material. Ductile iron has a much lower damping coefficient ($8.316 * 10^{-4}$) than the white or gray cast iron

$(68.67 * 10^{-4})^{41}$ and a low melting point of 1140°C. AISI 1005 is a very low carbon steel with a melting temperature of 1520°C which is higher than most steels. 1005 combined with ductile iron should produce a deep weld pool with low attenuation.

The configuration for the substrate is an important factor. The high temperatures around the pool will cause an increase in attenuation of the ultrasonic signal. A thinner substrate will decrease the overall attenuation but will reduce the material available for absorbing heat. In a thinner substrate more heat will tend to build up and the weld pool will be deeper which is good for our experimental purposes but there is a concern with the pool melting all the way through the substrate which would destroy the transducer and cause a range of problems. Experimentation showed that a substrate thickness using ductile iron of 12.7mm worked well with a good safety margin against meltthrough.

There is a lot of published data on ultrasonic velocity in ferrous materials at temperature. Unfortunately even with the same composition the properties can vary significantly with different processing methods. It was decided to measure the temperature vs. time of flight coefficient for 65-45-12 ductile iron that was on hand. Because equipment required for noncontact methods such as pulsing lasers and interferometers were not available, a parallel method to Scruby was used except a pulse/echo transducer was used to generate and receive the ultrasonic pulses instead of laser generation of pulses.

With temperature versus time of flight data and a finite element estimation of temperature gradients it is possible to determine the actual weld pool penetration. The ultrasound path is broken down into a number of blocks determined by the finite element model. Each block is assigned a temperature value by its location in relation to the model. A velocity is then assigned to the block by the temperature/velocity curves for this substrate. These two values will remain fixed. The variable in the equation will be the size of the elements. The total time of flight (TOF) through each element is

$$TOF_{elem} = V(T) * L_{elem}$$

And the total time of flight will be the sum of each of the elements

$$TOF = \sum V(T) * \sum L_{elem}$$

Since all of the elements are the same size this will reduce to

$$\text{TOF} = \sum V(T) * L_{\text{elem}} * n$$

where n is the number of elements. The TOF will be the measured value for this experiment and the solution is obtained by solving for L, the corrected path length as shown in Figure 13.

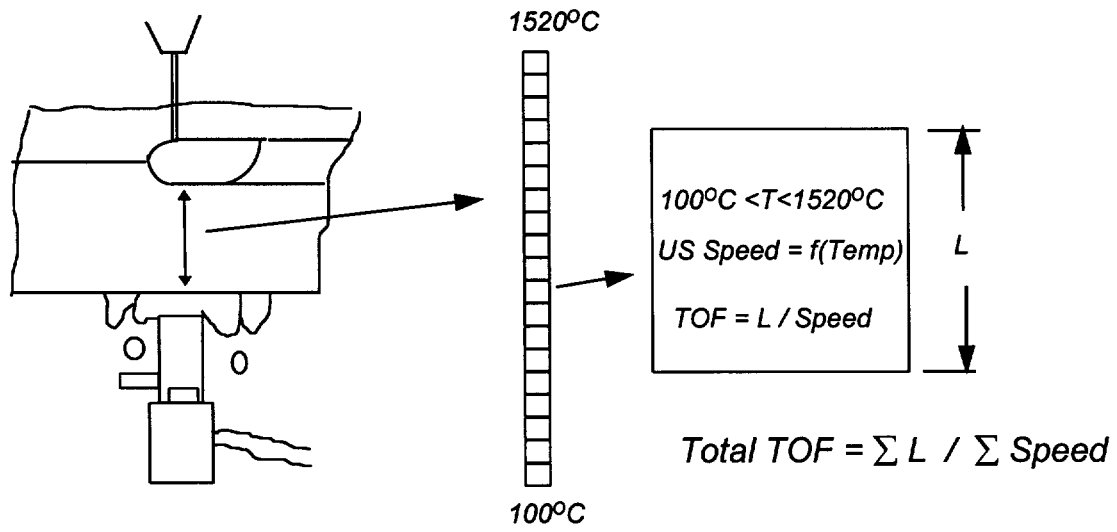


Fig 13. Determination of Weld Pool Depth

Chapter 7

Experiment Procedure

The goal of this experiment is to accurately determine the solid liquid interface of an Electroslag Surfacing molten pool using ultrasonic methods. The experiment will consist of time of flight measurements to an inprocess weld pool, a finite element model of the thermal gradients in the substrate and velocity of ultrasound at a range of temperatures. The thermal gradients and the time of flight of the ultrasound will be used to correct the time of flight measurements and the flight path to determine the actual location of a reflecting interface.

In order to correlate the finite element model, thermocouple data is needed to determine the actual thermal gradients at several points and a substrate configuration must be selected. Too thick a substrate will limit the signal strength due to heat attenuation. Too thin a substrate will have the danger of meltthrough which would damage the transducer. As a first estimate substrates were prepared 5.08 cm wide, 1.27 cm thick and 20 cm long. This thickness was adequate to prevent meltthrough but after several cladding experiments it was determined that a thicker substrate was required to separate in time the liquid/solid interface peak from the bottom side peak and prevent them from overlapping.

Each of the peaks in the signal has a steep leading edge and the trailing edge of the peak decays more slowly. Where the peaks are close together the first peak may be still decaying when the leading edge of the next peak is initiated and if the second peak is small it will be lost in the tail of the first peak. In order to separate the signals the physical sources of the signals must be moved farther apart. In this case a 2cm thick

substrate was used instead of the 1.27 cm thick. This provided only a small increase in attenuation and moved the first peak so the solid/liquid peak would appear against a background of only noise. Thermocouple data was taken from the 12.7 mm substrate. Finite element models were run for both the 12.7 and 20.3 mm thicknesses. Time of flight data was taken from the 20.3 mm model.

To determine substrate temperatures during cladding K type thermocouples were spot welded onto a 12.7mm thick substrate, five each on top, bottom and in drilled holes in the middle 25 mm apart as in Fig 14. In order to measure substrate temperature rather than hole air temperature the middle thermocouples had to be welded into the bottom of the holes. The thermocouples were pushed into horizontally drilled holes 2mm in diameter. In order to weld the thermocouple in the hole to substrate, the bare wire had to be held by the weld clamp for a good electrical connection. The thermocouple was twisted together at the ends and pushed into the hole with the insulation on the wires and the insulation was cut back from the thermocouple wire at a point outside of the hole. The exposed wire could then be used as a clamping point and the thermocouple welded into the bottom of the hole. The thermocouple data was collected using Labtech data acquisition software once per second.

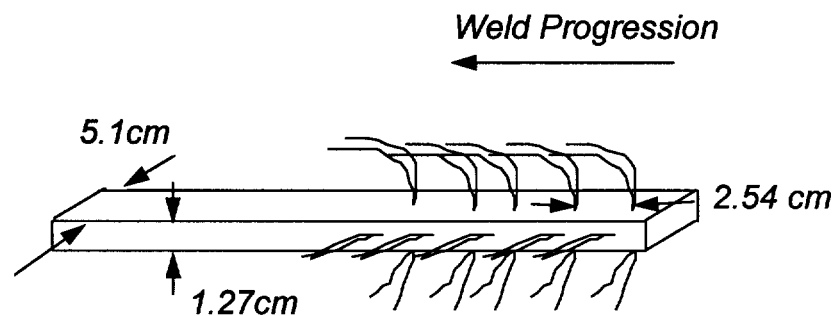


Fig. 14. Measurement of Thermal Gradients

Substrates were prepared from bulk 65-45-12 ductile iron. The substrate is rough cut with a bandsaw and milled to near size. A milled finish was originally used but the surface was rough enough to diffract the signal as the transducer moved along the substrate. A final size was obtained by grinding the top and bottom faces to a polished finish. A 46 grit wheel was used in a Thompson Surface Grinder. The ground surface produced a much more stable reflected signal.

The 4MHz transducer had to be coupled to the sample. It would be possible to slide the transducer over a lubricated surface but the transducer would be subject to overheating and abrasion of the transducer surface. A water couple between the transducer and substrate was selected as shown in Fig 15.

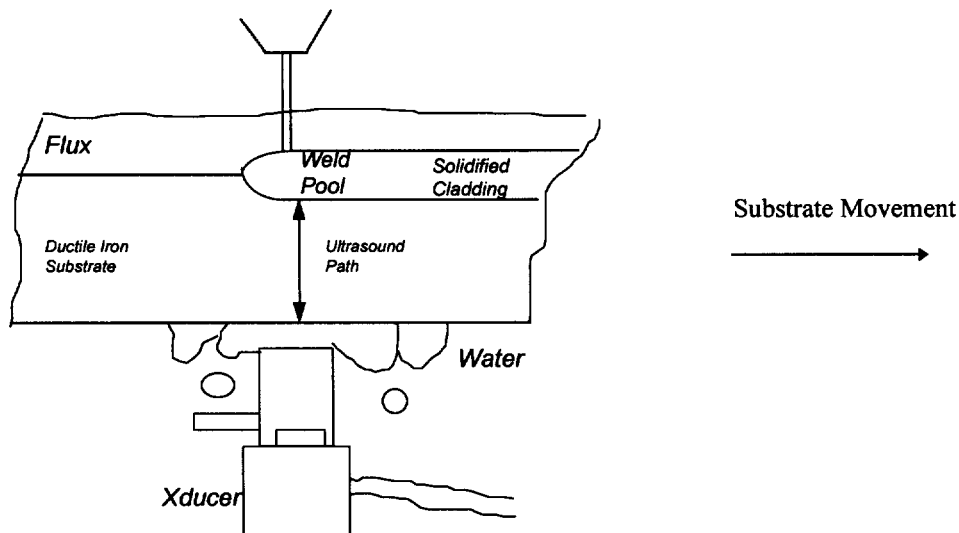


Fig. 15. Transducer, Weld Head and Substrate Orientation

The water couple acts as a good ultrasound medium, the sample bottom is cooled reducing the chance of meltthrough, weld heat is dissipated, and the water flow protects the transducer from overheating which would destroy it. Also the water couple provides a known boundary condition of 100°C for the finite element program whereas the bottomside temperature would be difficult to predict without it.

Several couples were designed and tested before finding an optimum design that minimized attenuation and multiple reflections. The water coupler is a 41mm length of 15mm dia. plastic pipe with a collar around the base which admits water. Multiple holes drilled in the inner pipe allowing water to flow freely from the collar with a minimum of turbulence as shown in Fig. 16. The column is 41 mm tall and is mounted with approximately 5mm clearance between the substrate and column. Water flow rate is 4 liters per minute giving a fountain in free flow about 12mm above the column. It was found that the ultrasonic signal reflected from the bottom of the substrate would reflect again from the top edge of the coupler causing a spurious signal. By tapering the top of

the couple to an edge the reflection was reduced to a negligible value although a peak is still seen in the data. No effort was made to focus the ultrasonic signal through the couple. Although this was possible to do, the signals were strong enough that it was not necessary.

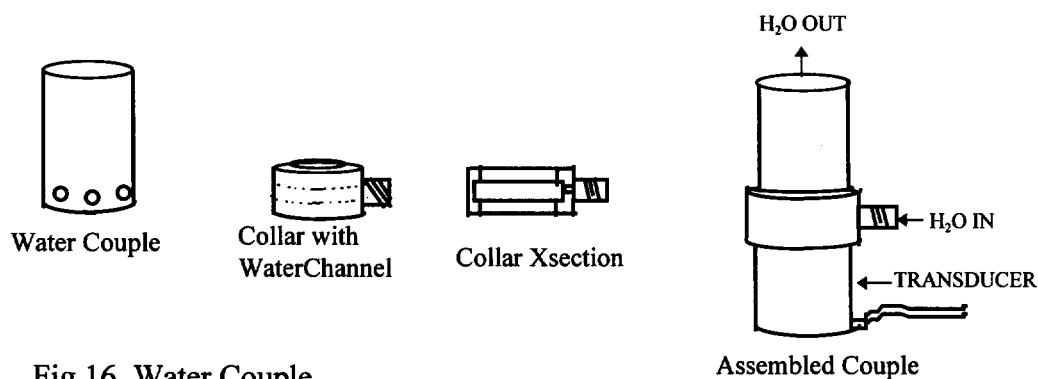


Fig 16. Water Couple

The transducer must remain fixed in relation to the weld pool and weld head as the pool progresses and a path for the ultrasound has to be maintained. To find the optimum position in relation to the weld pool for the transducer, an experiment was performed that moved the transducer in relation to the weld head. The strongest signal occurs in the area of 6mm behind the weld. This agrees with observations by Fenn⁴² that the weld pool is deepest 3 mm behind a GTAW weld and makes intuitive sense since this would be the area of full development of the weld pool before solidification occurs.

All weld data collection was done with the same parameters. The substrate was moved at 178 mm per minute with a 19mm clearance between the head and substrate. Blue Max flux was used. The 1005 strip used is 30mm by 0.5mm. The weld power supply is a Linde VI-1200 CV/DC Power Supply run at 27v and 650 amps. The transducer is a Krautkramer model MSEB4 4 MHz 3.5x10.

The reflected signals are digitized by the USD10 ultrasonic tester. The tester has an effective digitization rate of 240MHz.⁴³ There is the capability to store 10 waveforms in internal memory but 100 waveforms were required for each experiment. The USD10 also has RS232 remote capability. All machine functions can be implemented from

external control including the downloading of collected waveforms. The data is downloaded at 9600 baud. A Basic language program was written to iteratively poll the USD10 to collect data and download it to be stored on hard disk. This program was capable of collecting a waveform every 2.5 seconds. When reference holes were machined into the substrate it was possible for the hole to pass over the transducer in the 2.5 second window without being recorded. It was also desirable to have a higher resolution for the data. The second data collection program was rewritten in C++ and assembly language with ROM-BIOS interrupt instructions [Appendix]. After optimization the program was able to collect waveforms in less than 1.5 seconds. For every data point digitized two bytes are generated by the USD10 for a number between 0 and 99 which is the percentage of full deflection on the USD10 screen. 220 points are digitized for each waveform. At 8 bits per byte this would require 0.37 seconds to transfer but for each digit two extra separator bytes are generated which doubles this time to 0.72 seconds. The rest of the collection time is taken up by transfer protocols and wait states. The program used here is probably the fastest technique possible. The best way to increase the rate would be to upgrade the USD10 to a unit with a higher baud rate.

The ANSYS Finite element model is a three dimensional half symmetry model of the ductile iron substrate 25.4 mm wide, 127 mm long and 12.7 mm deep. Elements are 2mm by 3 mm by 1mm. The data of interest in the model is primarily in the depth where the gradients are the steepest between the weld pool and the cooling jet on the bottom and this was selected to have a finer scale of 1mm. There is also a limit on the number of elements in the program. This element size optimized the maximum number of elements with the finest detail in the direction of interest. A patch of nodes on the top surface 30mm by 20.3 mm were selected and constrained to 1520°C to simulate the weld pool and are shown in Fig. 17. A similar patch on the bottom was constrained to 100°C to simulate the water coupling.

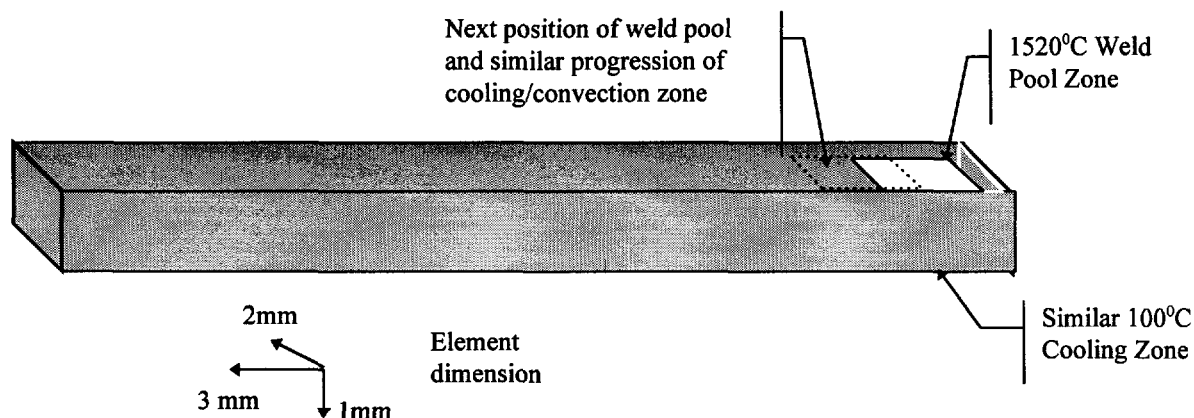


Fig. 17. FEA Model

These selected elements and nodes were moved 3 mm each 1 second step which is the rate of movement of the substrate between the weld head and transducer. The element size in this direction is 3 mm so that each 1 second step will move exactly 1 element. The material parameters used are listed in the Appendix with the code and ANSYS/Research Rev 5.3 was used for analysis on a Pentium workstation.

Convection values associated with the water couple are difficult to evaluate because of the complexity of the water flow but a good estimate of its magnitude can be calculated by making some basic assumptions. A flat plate analysis is assumed with a length of 3.5 cm and a 50 cm/sec flow of 30°C water. The Reynolds number calculated from these values is ~2200 which is well below the critical value but it is reasonable to assume a turbulent flow after passing through so many passages, turns and narrow tubes in a short distance and impacting against a flat surface. The water will spread and travel some short distance. Using the calculations for the Nusselt number of⁴⁴:

$$Nu_L = \frac{h * L}{k} = Pr^{1/3} * (0.037 * Re_L^{0.8} - 850)$$

where Nu_L is the Nusselt number, Pr is the Prandtl number, Re_L is the Reynold's number, L is the length of the flow along a surface, h is the convective film coefficient and k is the thermal conductivity. Given a value of 13.25 for the Prandtl number⁴⁵, 0.02 m for the

length, a Reynold's number of 500,000 for turbulent flow and thermal conductivity of 0.566^{45} will give a convective heat transfer coefficient of about $32000 \text{ W/m}^2\text{-C}$.

The time of flight versus temperature data was collected using a stepped ductile iron bar fitted with thermocouples and placed in an oven with one end protruding. A cooling collar and a transducer are attached to the protruding end. Time of flight at temperature was measured with the ductile iron substrate at temperature and measuring the difference in the time of flight between an ultrasonic signal reflected from the end of the sample and from a step cut into the sample. This provided a test point for the transducer below the Curie temperature and only the section between the end and the step has to be held at temperature. The configuration is illustrated in Fig. 18.

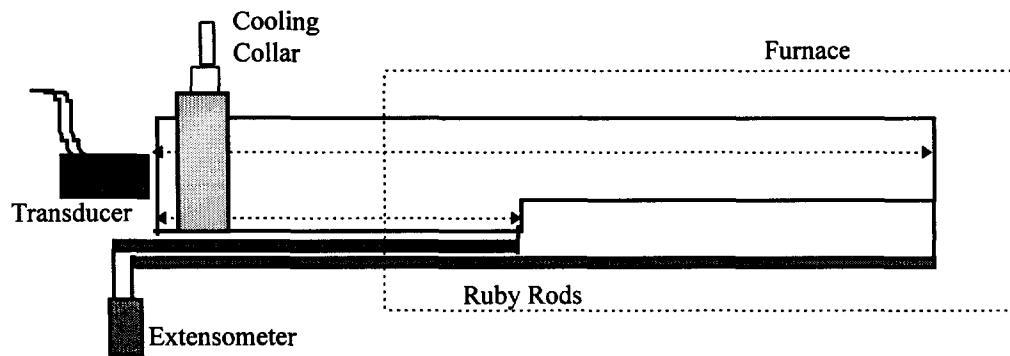


Fig 18. Configuration for Measuring Time of Flight at Temperature

Two substrates were used. The first was 9 inches between the step and end. Above 800°C the attenuation was so high that it was not possible to determine the time of flight using this configuration. A second substrate was made with 4.5 inches between the step and the end which worked well for higher temperatures.

To prevent oxidation or nitriding of the substrate the furnace was flooded with argon. The argon was also used to control variations in temperature along the substrate by introducing the cool gas at higher temperature sections. Three thermocouples were welded onto the first substrate and two on the second. The temperature was held to $\pm 5^{\circ}\text{C}$ along the length of the sample and soaked for 15 minutes at the target temperature before measurements were made.

To determine linear expansion two ruby rods were butted against the end and step also shown in Fig 18. Ruby has a low coefficient of expansion at 9.06×10^{-6} and a high melting point. An MTS extensometer Model 632-12B-20 was connected between the two ruby rods which was connected to a Capacitec Model 4100-SL amplifier. The extensometer was calibrated on a Pratt and Whitney Model M-1471 Supermicrometer. The extensometer gave a reading for the thermal expansion between the end and the step.

Chapter 8

Experiment Results

These experiments determined the time of flight of ultrasound at different temperatures, predicted thermal gradients during welding and then combined this data with time of flight measurements to the solid/liquid interface to measure penetration during cladding. This section will describe the results of these experiments and compare them with the results of destructive testing.

8.1. Time of Flight Vs Temperature

As the ultrasound wave passes through the substrate during cladding it will pass through temperature gradients that reduce its propagation velocity. A measurement of the speed of ultrasound at temperature will give a correction factor for the time of flight through the substrate. The ultrasonic speed varies with temperature because the bonds between the atoms change as the temperature changes. Atoms vibrate at a higher rate, interatomic distances increase and cubic structures change.

This experiment determines how the propagation rate changes across a range of temperatures between 0 and 1100°C. The three controlled variables in this experiment are temperature, elongation and time of flight. The hardware for this experiment consists of a 1200°C furnace, a thermocouple furnace control system, an inert gas bath and cooling system, a data collection system, an ultrasonic test system and an elongation measurement system. The procedure for the experiment was to bring the substrate up to temperature, record temperature and elongation and, holding the transducer to the end of the substrate, to measure the time of flight through the substrate.

It was difficult to hold the substrate at the same temperature along its length. The first furnace used was a 151 cm long three zone tube furnace. The element diameter was 15 cm with an alumina center tube 10.16 cm in diameter. One end of the substrate protrudes from the oven and is cooled by a water collar to provide a low temperature test point for the piezoelectric transducer. Heavy gauge K type thermocouples spot welded at three points along the isothermal area of the substrate were wired to the furnace controls for temperature control.

The substrate heats unevenly due to uneven exposure to the source which is characteristic of infrared heating. More heating is needed at the cooled protruding end to compensate for conduction and the middle section is subsequently exposed to more furnace elements and absorbs more heat. The original furnace was used in several configurations, vertical, horizontal, at angles with convection baffles and IR heating shields to heat the substrate evenly. There was no configuration that would provide a stable, even heating of the substrate. The control unit used was an on/off type instead of a proportional control. This meant there was a heating and cooling cycling of the individual elements which further complicated the heating regimen. A smaller three zone furnace 76 cm long with a quartz center tube 7.6 cm diameter tapered to a port tube at one end was used to improve local temperature control. This oven did not improve the heating results for the substrate but was easier to use overall and was utilized for the rest of the experiment. Either localized heating or cooling was required to achieve an even temperature across the substrate.

To prevent decomposition and phase changes in the substrate an inert gas bath (argon) was introduced at temperatures above 300°C. The smaller furnace and closed tube reduced the amount of gas required and improved the sealing of the chamber. The argon gas turned out to be a good localized cooling source. A 5 mm stainless steel tube was insulated with a glass cloth. Argon gas was introduced to the chamber through the tube and ported at the mid section of the substrate. Increasing or decreasing the gas flow increased and decreased cooling respectively. This was very effective in holding the substrate at an even temperature.

As the substrate heats it expands, increasing the path length and the time of flight of ultrasound. This expansion was measured with an extensometer which operates outside the furnace. To couple the extensometer to the substrate hot zone, a link with a low coefficient of thermal expansion (CTE) was needed. Invar was considered but it has a low CTE over a narrow temperature range. Ruby was finally selected with a CTE of 9.06×10^{-6} over a wide temperature range²⁵.

Coupling the extensometer securely to the substrate was difficult. Ruby rods approximately 50 cm long were used to connect between the substrate faces and the extensometer. The best technique would be to butt the rod directly to the faces with the extensometer at the other end of the tube furnace from the transducer. This provides a direct connection from the measured surface to the extensometer with little source of error. But the substrate had to be removed often from the oven and having the extensometer and rods attached to the substrate as a single unit next to the transducer was much more practical. This required mounting brackets at the substrate faces to butt the rods against. The preferred mounting method would be a bolt through the substrate but on the first substrate there was nowhere to drill a hole that would not become a reflector so a hook was glued onto the rod with a high temperature cement. The rod was spring loaded to hold the hook against the step with tension. At the end of both substrates brackets were fit to the surface using bolts to increase contact pressure without passing through the substrate. A slit was cut into the second substrate instead of a step which allowed a hole to be drilled behind it. This hole was behind or 'in the shadow' of the slit and did not constitute a reflecting surface. An end bracket was fit to the end. See Figure 19.

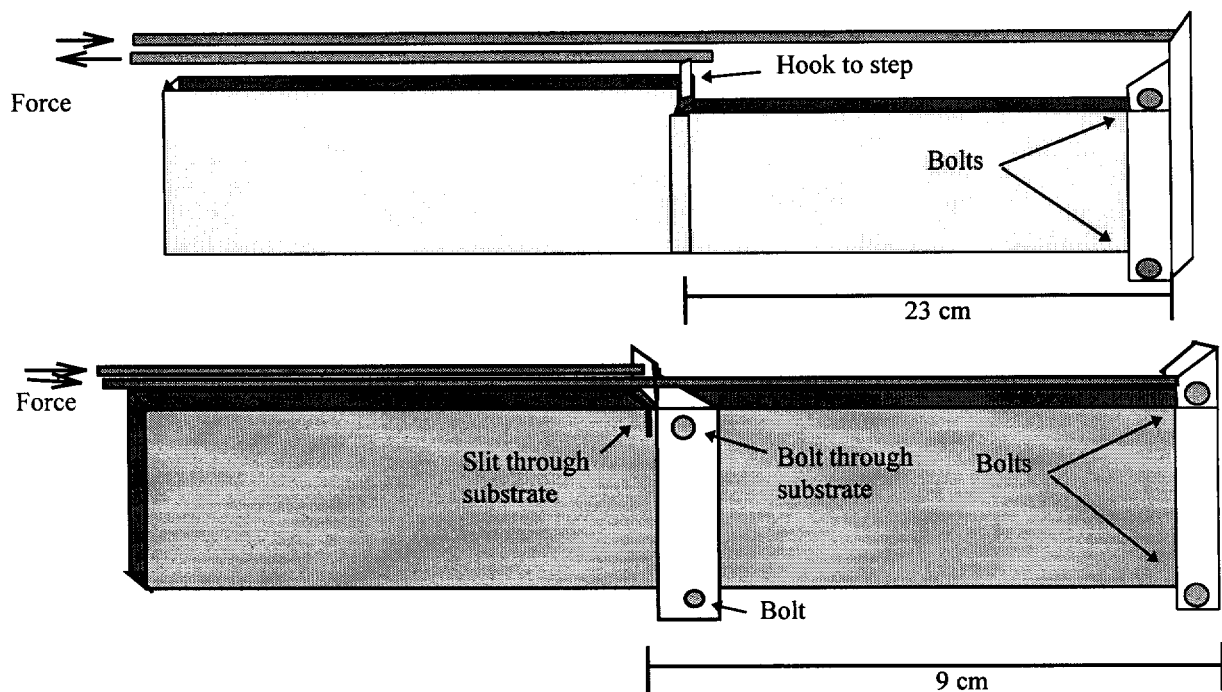


Fig. 19. Extensometer Link

With a method in place to hold the substrate at temperature for a period of time and an elongation measurement system, it was possible to make ultrasonic measurements of time of flight. A Basic language program running on a Pentium workstation was used to collect data. Temperature and elongation was input by the operator from equipment displays. Ultrasonic data was downloaded by an RS232 connection from the USD10 tester. The timescale for the USD10 was adjusted to collect two profiles at each measurement. One for the reflection from the step and one for the reflection from the end. A typical peak is shown in Figure 20. This data is full wave rectified with all negative values being made positive.

The peak is a modulated sine wave composed of a series of smaller peaks marked by circles. To determine time of flight a method is required to find the time between the first and second group curve peak.

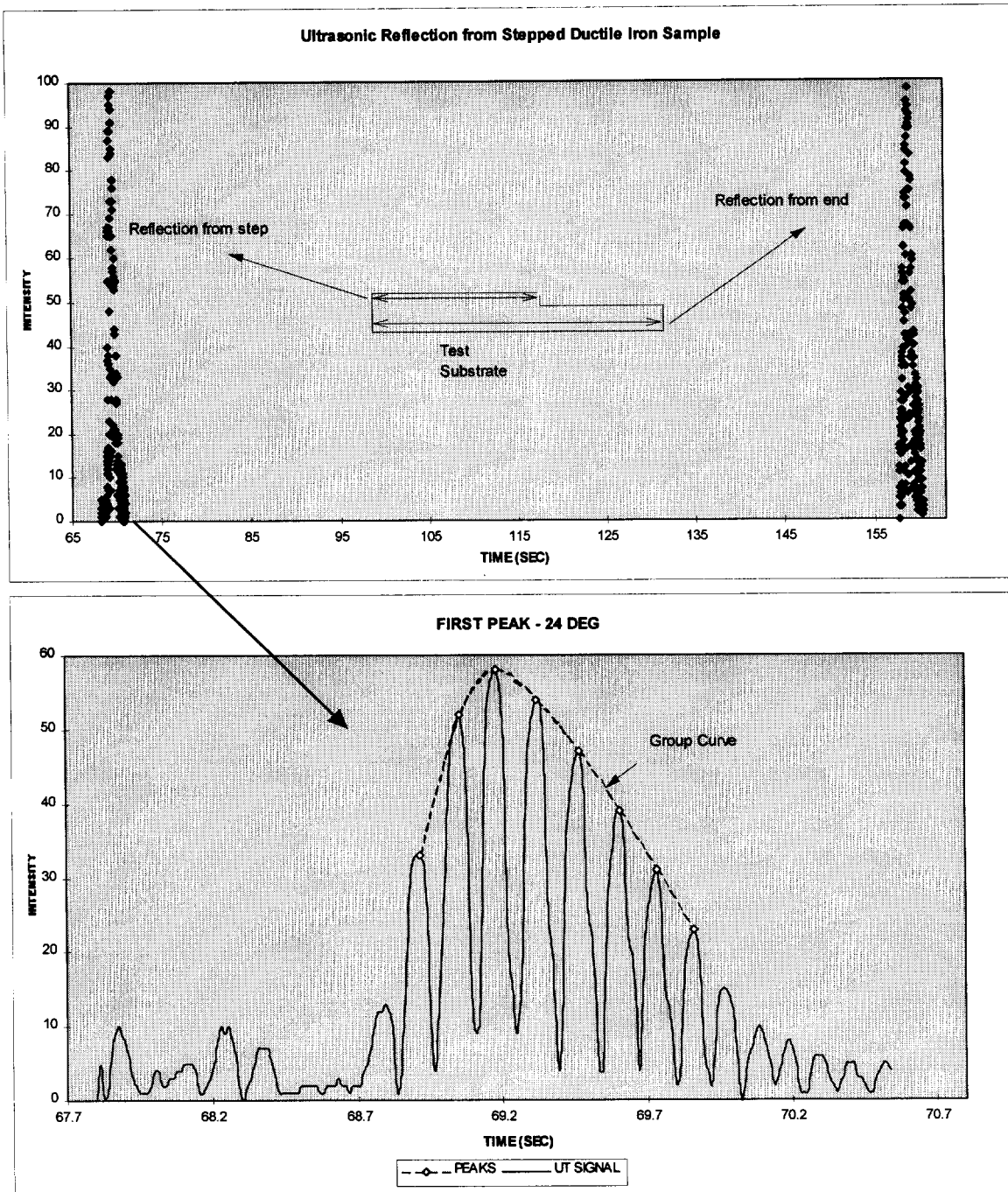


Fig. 20. Peak Analysis

The group peak value is determined by applying the method of weighted least squares to the individual peaks. All calculations were done in Excel Visual Basic macros. The macros are listed in the Appendix. During each data collection, which is nominally twice

at each temperature, the temperature, elongation value, the first peak and second peak data are recorded.

Above 800⁰C it was not possible to discern the reflection peak from the end of the 23 cm substrate due to attenuation although the reflection from the step was still discernible. Because the reflection intensity measurement is very sensitive to the coupling between the transducer and the substrate, attenuation measurements could not be accurately made for this experiment. Scruby *et al*⁴⁷ measured attenuation in mild steels and found a marked increase in attenuation above 800⁰C going from 0.4 dB/cm to 1.5dB/cm at 1000⁰C. Ductile iron undergoes a phase transformation at approximately 800⁰C changing from a body centered cubic structure to a face centered cubic structure as the temperature increases which will affect the interatomic bonds and the ability of the material to propagate the signal without losses.

In order to circumvent the high attenuation, a spark gap generator was built and tested to determine if ultrasound could be generated at the hot end of the substrate. If it is generated at the end in the furnace it has to travel the substrate length only once which reduces attenuation by half. The transducer is electrically insulated so the testing system is protected from the high voltage. The disadvantage is that the ultrasonic tester cannot be used since it can only be triggered internally. A digitizing oscilloscope was used to collect data and was triggered by the electromagnetic noise from the discharge. Unfortunately it was too difficult to maintain an appropriate spark gap over a range of temperatures making it unreliable. It was decided at this point to use a second shorter substrate with lower attenuation.

The elongation and the time of flight are shown in Figure 21. The values for both substrates are shown and since the substrates and flight paths are different lengths on the two substrates the values are discontinuous. Three time of flight outliers are circled. The last at 1050⁰C is the result of high attenuation causing a misidentification of the peak. No data was taken above this value because of the risk of melting the substrate.

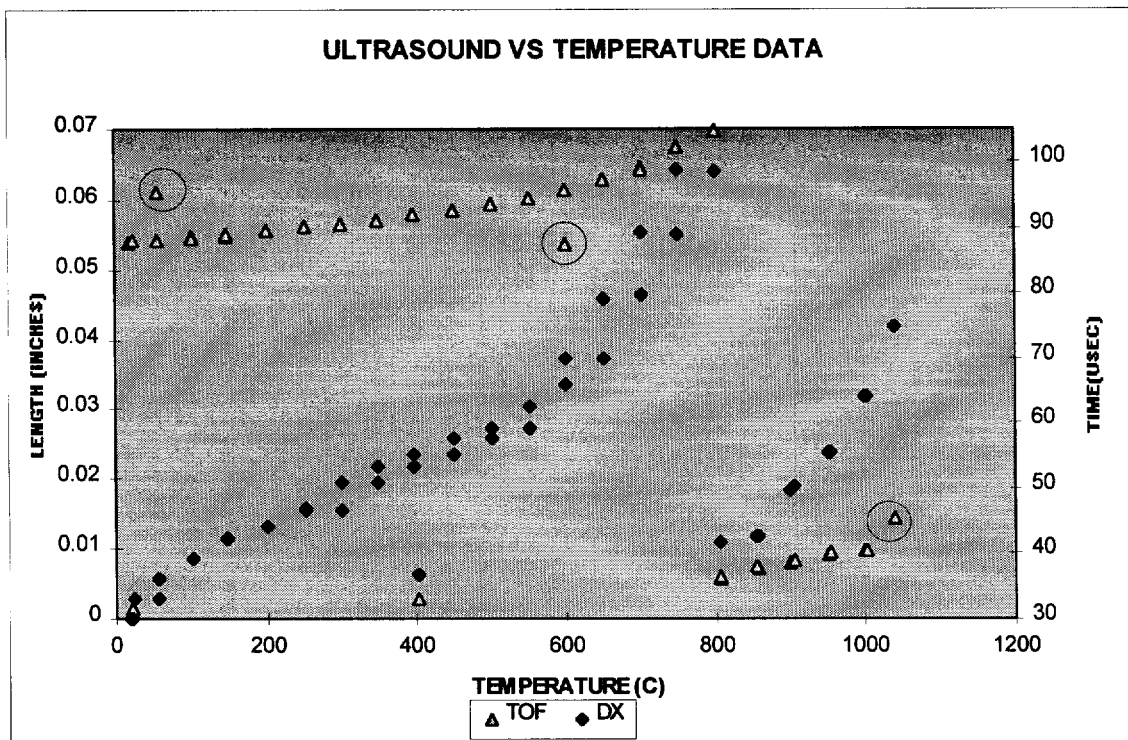


Fig. 21. Elongation and Time of Flight in Ductile Iron

Figure 22 shows the speed of ultrasound at temperature. This value is calculated by adding the room temperature path length to the elongation value at each temperature and dividing the result by the time of flight at temperature. The two separate curves correspond to the two substrates. This curve is dependent only on the material and not length. The fact that there are two discontinuous curves indicate a serious problem with the substrate material. The data was first reexamined for discrepancies and errors and values recalculated. All data was in order and calculations done correctly. The only other explanation was a material difference in the substrates.

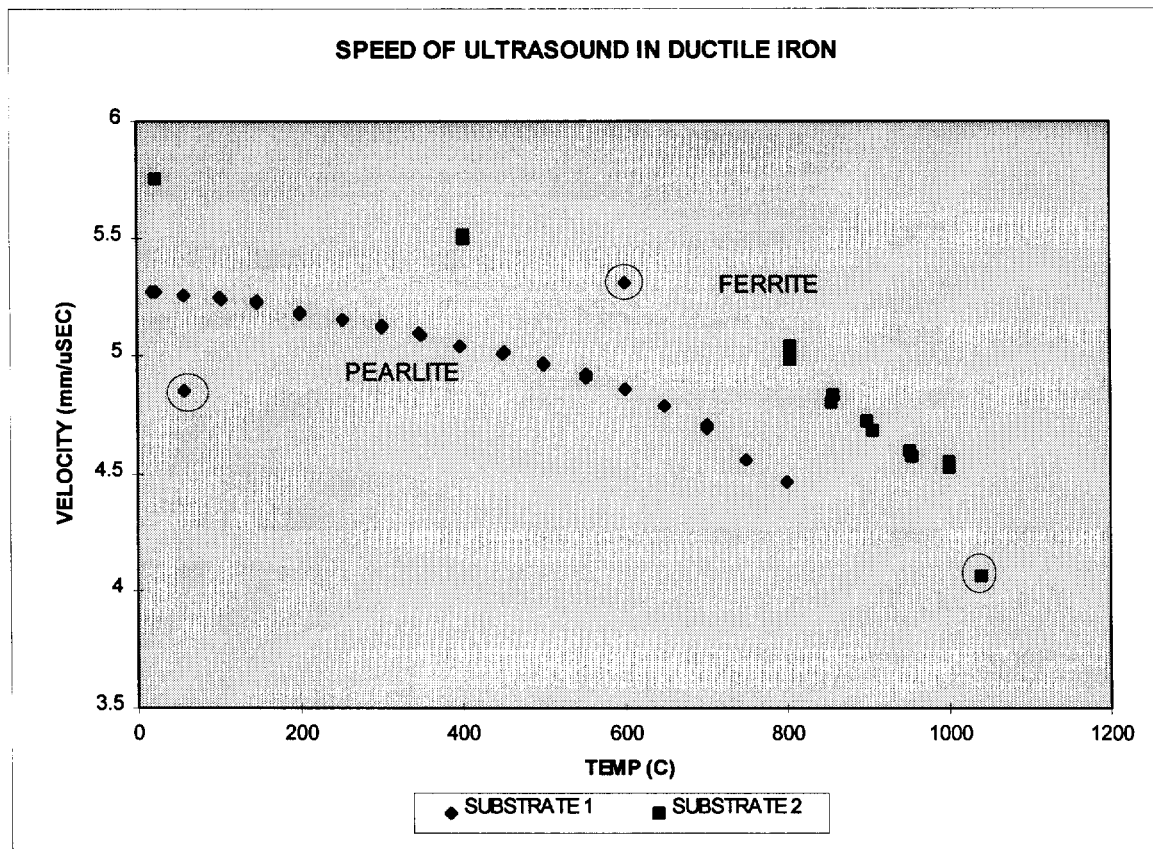


Fig. 22. Speed of Ultrasound at Temperature in Ductile Iron

Samples were taken of both substrates, mounted, polished, etched and photographed as in Figure 23. Comparing these samples to published pictures from the ASM Handbook⁴⁸ it was obvious that the low temperature substrate had undergone nitriding. Nitriding transforms the graphite into flakes rather than nodules and results in pearlite formation instead of the ferrite of nodular iron. This has a significant effect on the speed of ultrasound.

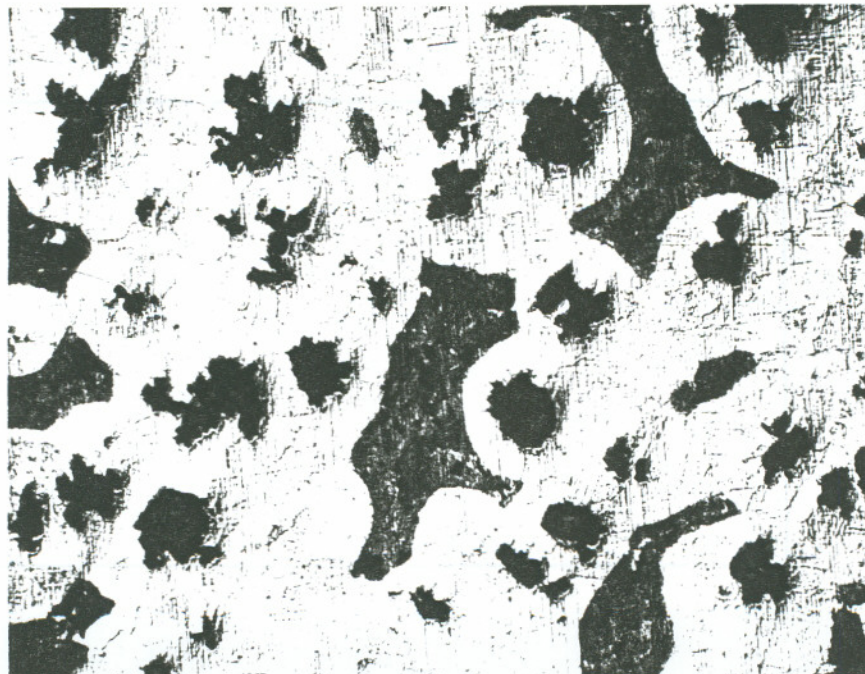


Fig. 23. Photo of Nitrided Ductile Iron Substrate

Data at 240, 400, and 800^oC which were taken from both substrates show a close agreement of the curvature of the two data sets. Dropping the outliers and offsetting the experimental data for the nitrided substrate gives a smooth curve shown in Figure 24. These values will be used in calculations.

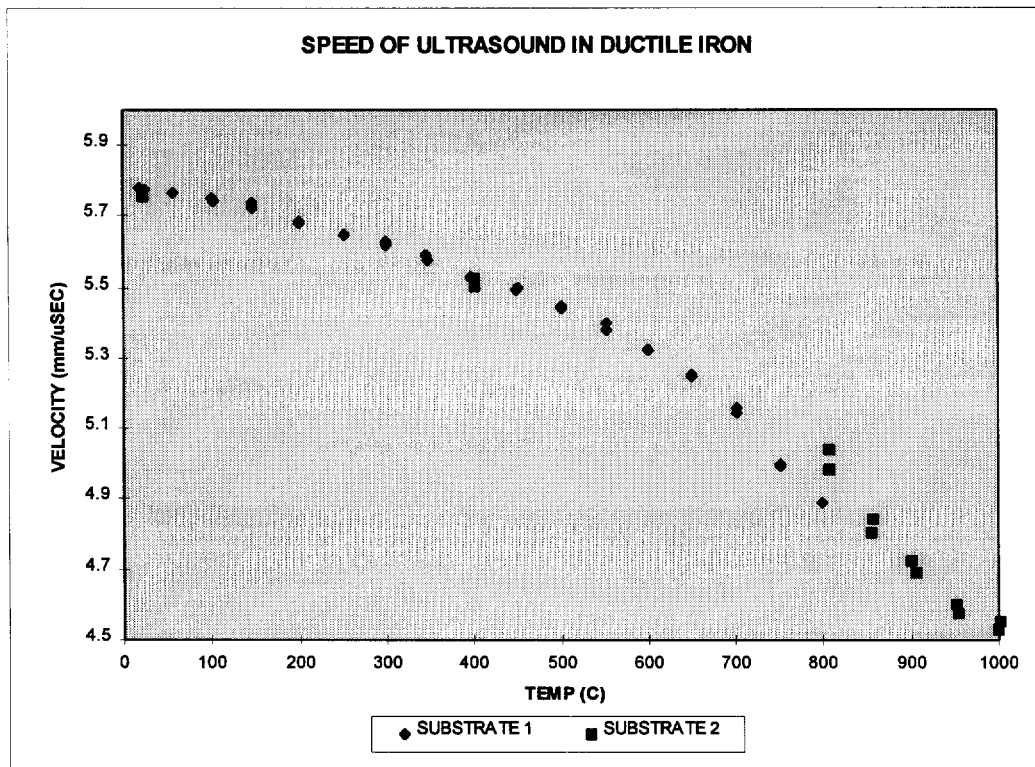


Fig. 24. Adjusted Time of Flight vs. Temperature

An exponential equation was determined by iteration to give a best fit curve to the data.

The equation derived is:

$$V = 5.85 - 0.155 * \exp (T - 445)$$

and the plot for this data is shown in Figure 25.

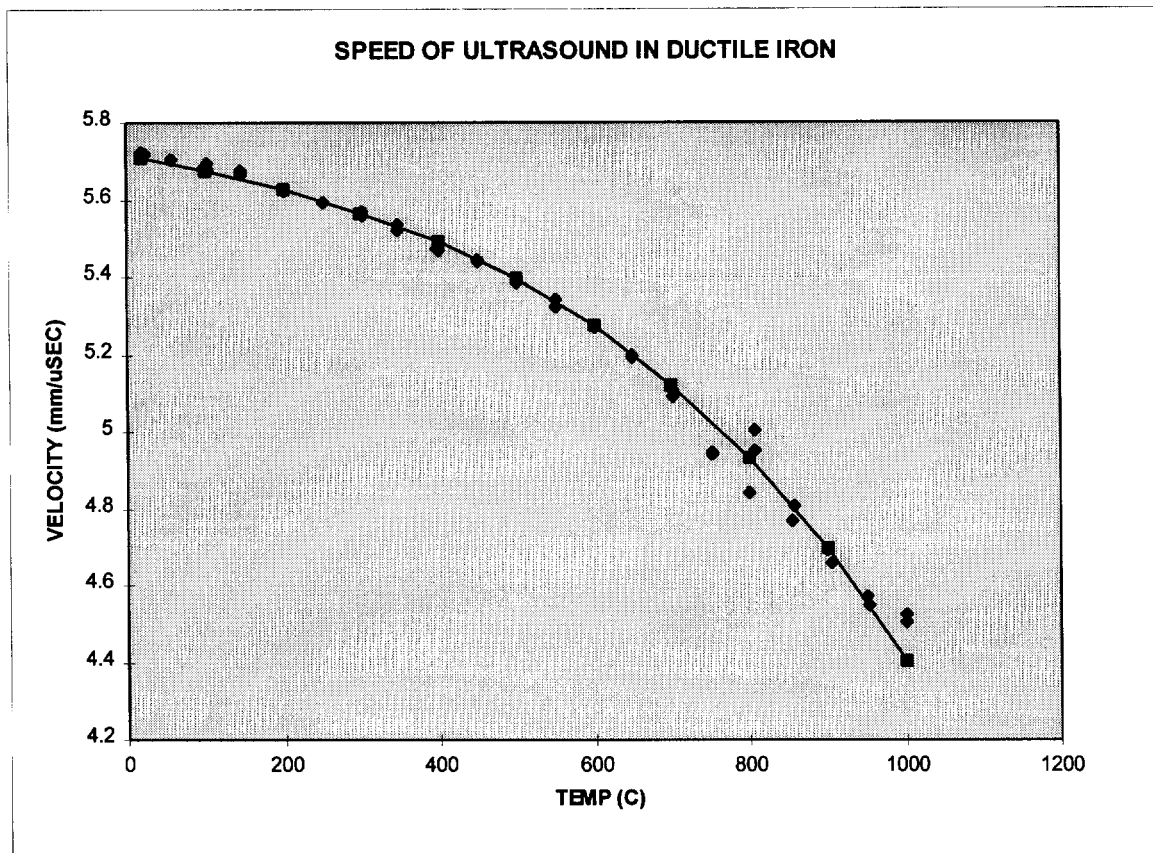


Fig. 25. Curve Fit to Ultrasound Data

8.2. Thermocouple Measurements

In order to correlate the finite element model of the cladding process temperature was measured at 15 points in the substrate. Thermocouple data was collected from a 12.7 mm thick substrate with thermocouples welded in place along top, bottom and middle centerlines. 1005 steel was clad on a ductile iron substrate and temperature values recorded at one second intervals from each thermocouple. The results are shown in Figure 26, Figure 27 and Figure 28.

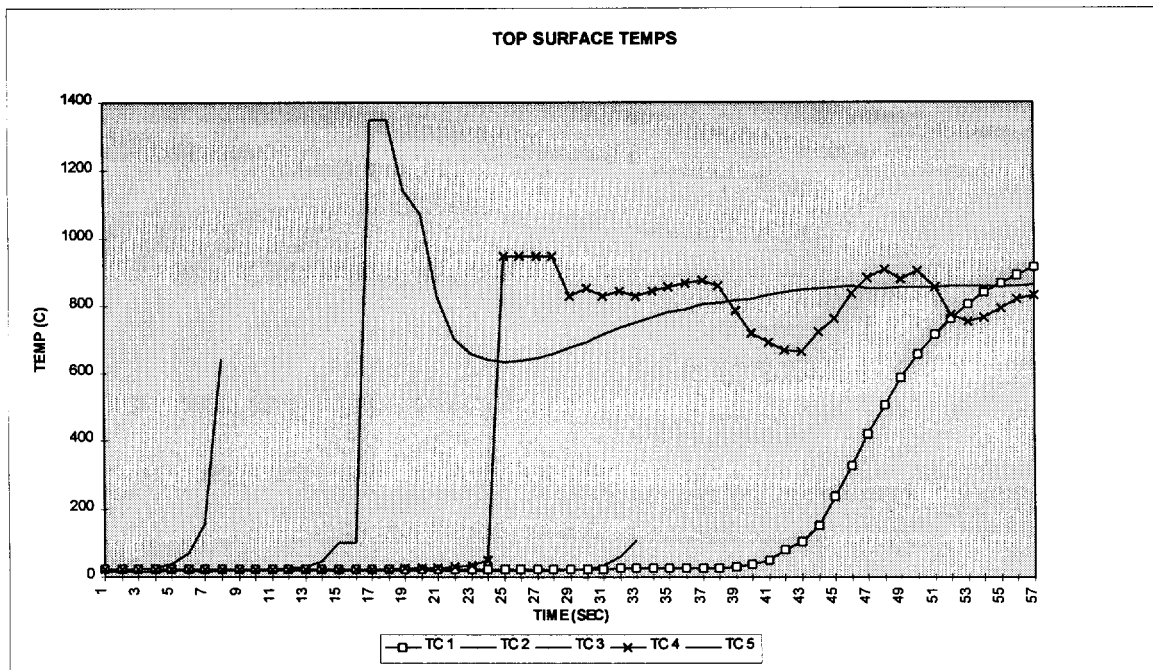


Fig. 26. Thermocouple Data from Top of Substrate

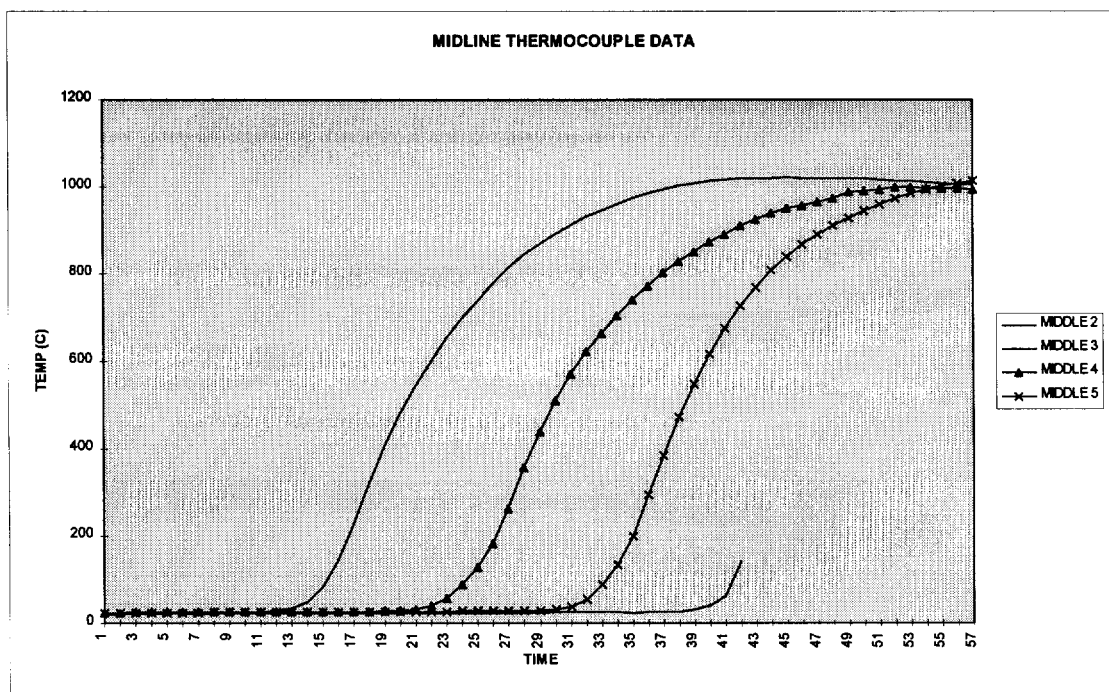


Fig. 27. Thermocouple Data from Middle of Substrate

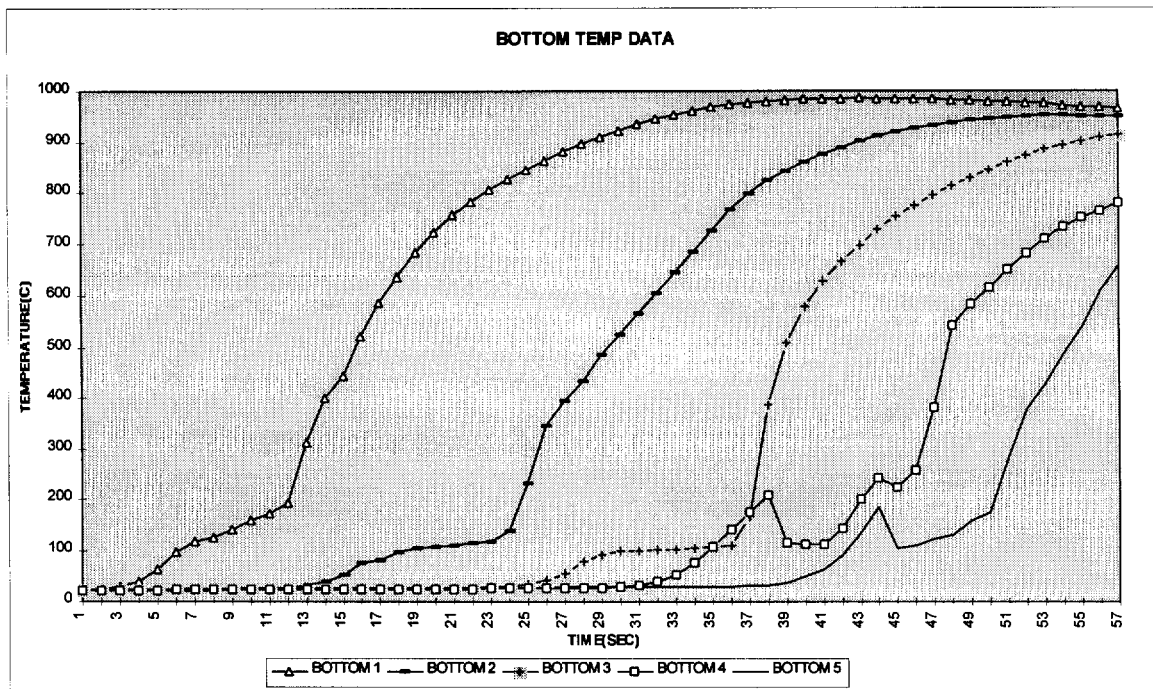


Fig. 28. Thermocouple Data from Bottom of Substrate

The midline temperatures from the first thermocouple were lost due to a programming error. The thermocouples on the topside are quickly damaged as the weld pool contacts them producing a discontinuous profile. But the data does give an indication of the rise in temperature in front of the weld pool. The increase in temperature is steep with the pool damaging the thermocouple within three seconds of the initial temperature rise. The welder was turned off at approximately 42 seconds before the fifth thermocouple could be damaged.

Response from the thermocouple values from the bottom of the substrate was according to expectation. The temperature stays at 100°C until the water jet passes and then the heat rises sharply to approximately 1000°C. Some anomalies are seen in the 4th and 5th positions which is probably attributable to the uneven coverage of the water along the bottom surface allowing certain spots to go uncovered for short periods.

Figure 29 shows data from three thermocouples, top, middle and bottom, at position 37.5 cm from the starting end. The midline temperature rises almost simultaneously with the top temperature which is intuitively correct. The top temperature begins rising 3 seconds ahead of the weld pool which corresponds to 9 mm of weld head

travel. At that point the midline thermocouple is at a radial distance of 11 mm from the weld pool leading edge making the temperature rise very similar for both positions.

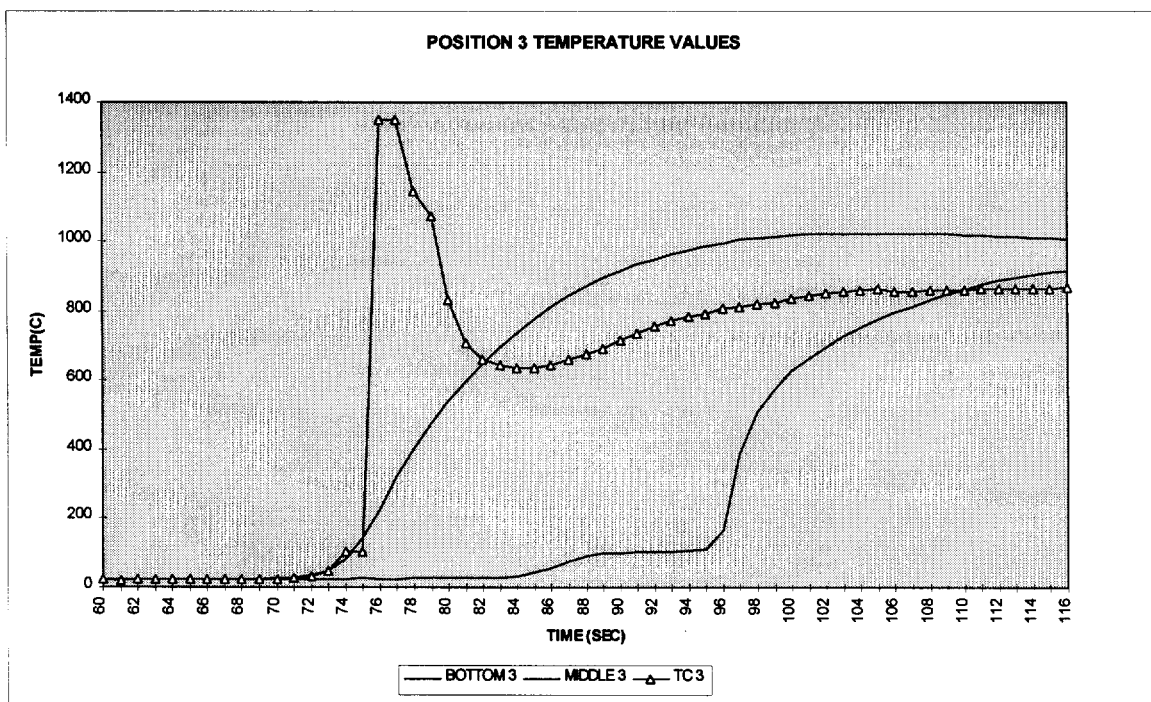


Fig. 29. Thermocouples Data at 37.5 mm.

8.3. Finite Element Model

A finite element model was built to determine temperature gradients within the substrate. The predicted gradients together with ultrasonic velocity at temperature were used as a correction factor to the time of flight during cladding. There are several assumptions, approximations and estimations that have to be made to simplify this problem enough to use numerical methods. There are radiative heat flows which are very complex primarily in the pool itself and in the solidification area. There is some conductive heat flow to the fixture, there is natural convective heat transfer from all the surfaces and there is the forced convective transfer from the water jet which flows unevenly over the bottom surface. The melting temperature of the flux is higher than the admetal or substrate and superheating of the pool can occur. There are endothermic and exothermic processes in the flux, the metal and the cooling water. The flux load on the top of the substrate forms an insulating layer. Most of these factors are too complex to

model altogether or are beyond the scope of this project so reasonable estimates of their behavior were made to pose a tractable problem.

The finite element simulation was done on a Pentium 100MHz computer with 64 megabytes of RAM running ANSYS/Research Revision 5.3. A half symmetry 3D Model was used with $2 \times 3 \times 1 \text{ mm}^3$ elements with the highest resolution in the vertical direction between the weld pool and bottom of the substrate where the water cooling and ultrasonic coupling impinge as in Figure 30.

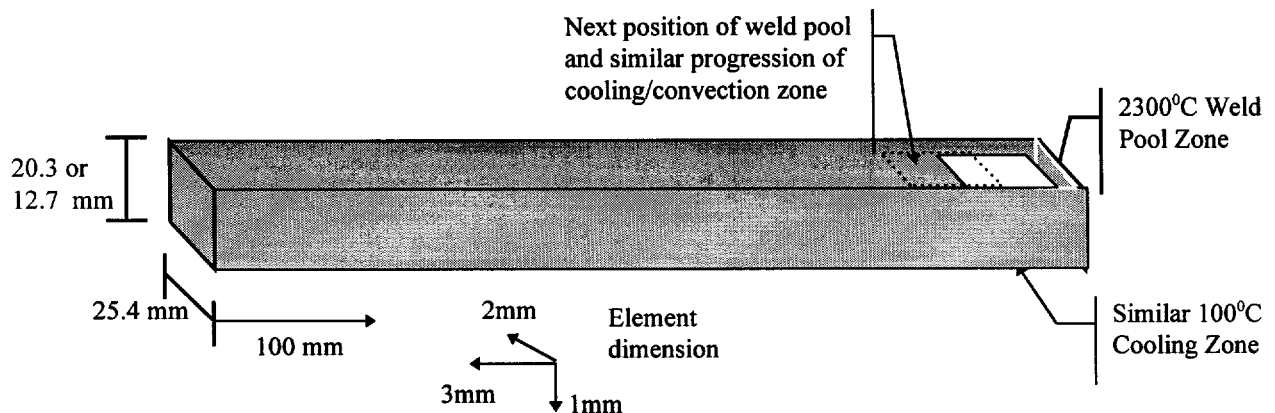


Fig. 30. Domain of the FEA Model

Originally a weld pool temperature of 1520°C was assigned to the surface nodes in the weld pool patch. The resultant gradients were not in agreement with the thermocouple data. Many different configurations were analyzed before representative results could be obtained. The factors being optimized were rate of temperature rise and peak temperature for the midline nodes. In the final configuration the first layer and the second layer of nodes below it in the weld pool zone were assigned a temperature of 2300°C to simulate the weld pool. This can be justified by the fact that the melting temperature of the slag is 2300°C and superheating of the weld pool does occur. The water couple of the transducer which cools the bottom was moved forward 15 mm relative to the top heating area. This more accurately reflects the actual application than having a mirror image top to bottom for heating and cooling. The bead behind the weld pool was assigned a convective film coefficient of $1000 \text{ W/m}^2\text{-}^{\circ}\text{C}$ to account for radiative heat transfer. The cooling was of less concern than other aspects of the model since the

only values from the model used are those along the flight path 6 mm behind the leading edge of the weld pool. More complex models were run with more complex convective cooling values and more nodes but they generally would not converge in a reasonable amount of time. As laid out, the simulation required 50 hours to converge.

A good test of accuracy for the model is its correlation to the thermocouple measurements taken from the 12.7 mm substrate. Since the top thermocouple data shows only the onset of heating and the bottom thermocouples are affected by the impinging cooling water, the main concern are the middle thermocouple data and to some degree the top. Figure 31 shows midline finite element nodes overlaid on the middle thermocouple data.

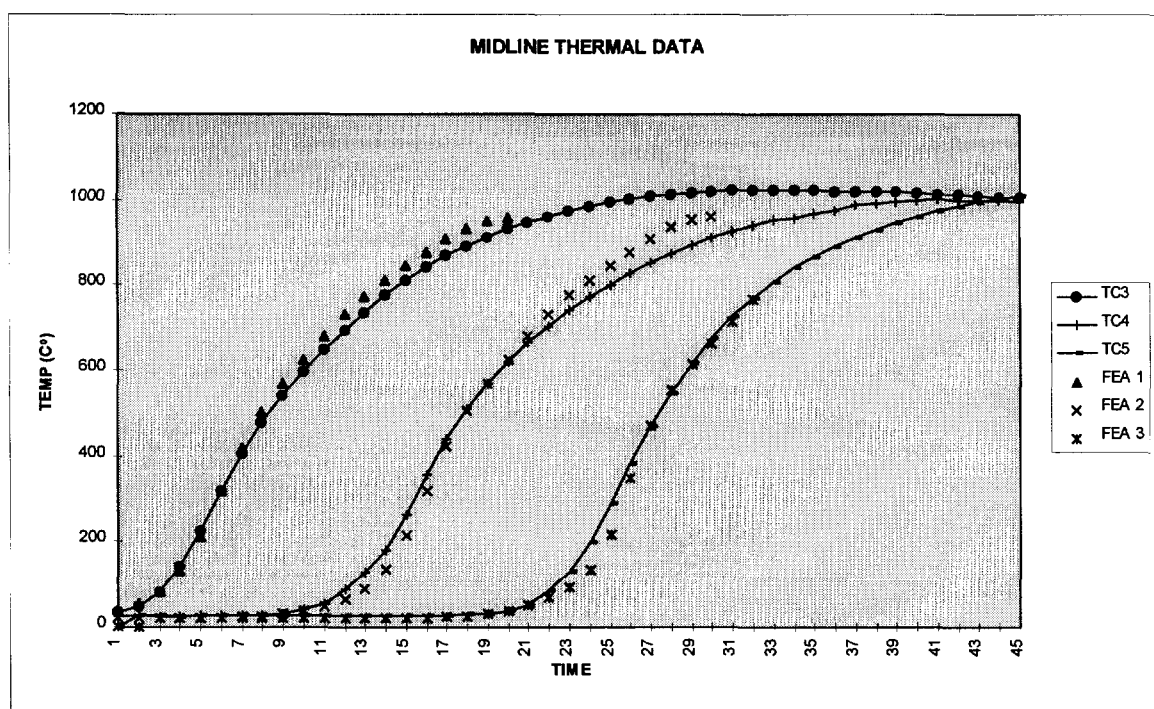


Fig. 31. Finite Element Model Thermal Data Compared with Thermocouple Data

The thermocouple placement within the hole i.e. whether it is welded to the top or bottom of the hole has an effect on the rise time and shape of these measured thermal profiles and causes some variation between the curves. The finite element data correlates very well to this thermocouple data. The rise times for the FEA data is a little steeper and overshoots a small amount especially on the second curve. Further refinement could be

done by adjusting the weld pool temperature and weld pool depth but this should be more than adequate for this research.

The top nodes and top thermocouple data are shown in Figure 32. This data also correlates very closely and shows agreement with the known data at the surface. Rise time is very short and steep with less than 7 seconds from initial rise to peak temperatures. The complete FEA model appears to accurately reflect the temperature gradients during welding and can be used to determine velocity and time of flight along the flight path.

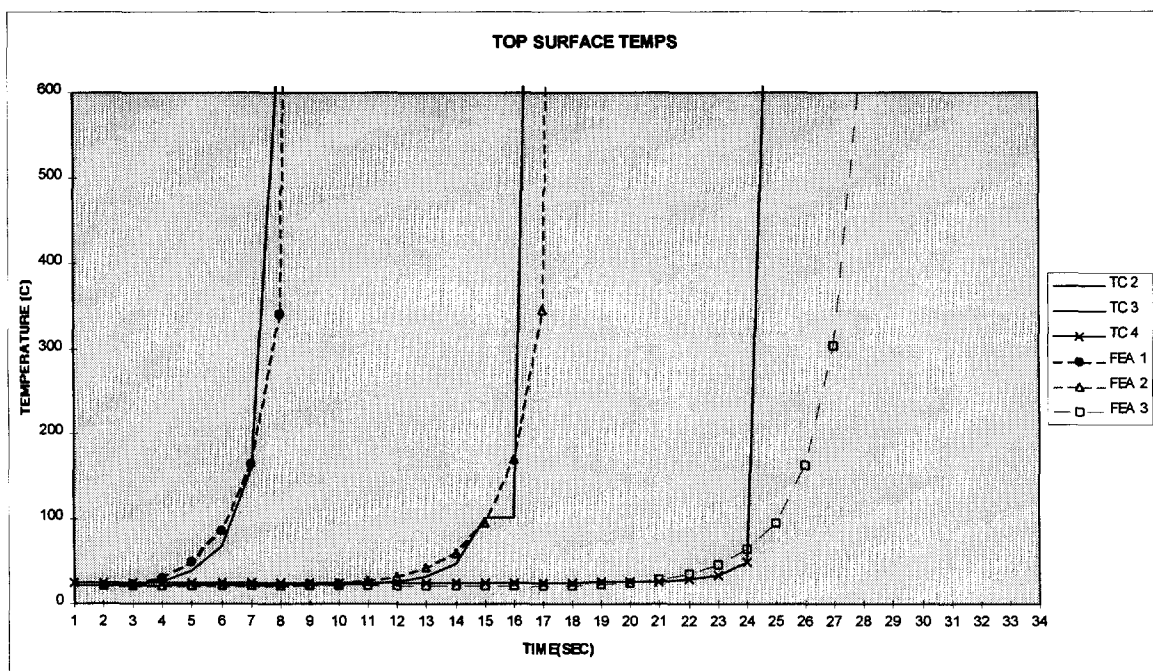


Fig. 32. FEA Model versus Thermocouple Data for Top of Substrate

One of the surprising results of the finite element analysis is that the temperature gradients stabilize within 10 seconds and remain constant thereafter. This allows a single analysis and one correction factor at any time in the cladding process. The first 10 seconds of the cladding process do not provide a discernible solid/liquid interface so no analysis can be done during this time anyway.

From the close correlation of this model to measured data, an assumption was made that increasing substrate thickness and using the same parameters will have the same level of accuracy. This assumption is necessary since a 20.3 mm thick substrate was used for the final time of flight data. The temperature gradient in the 20.3mm substrate

from the finite element analysis at 10 seconds is shown in Figure 33 together with a plot of a curve fit to the data. The equation fit by iteration is:

$$T = 80 + 23.8 * \exp (X / 4.87)$$

where T is the temperature and X is the distance along the flight path. It is evident that temperature variation with depth is exponential in nature.

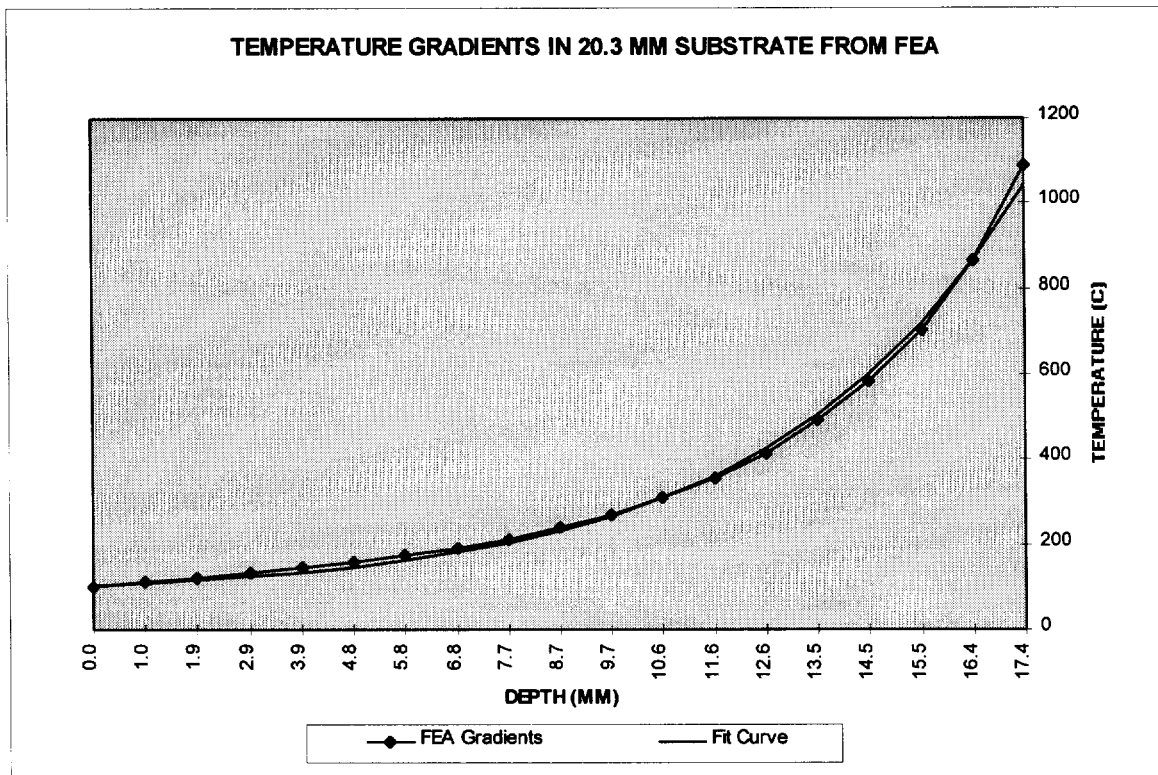


Fig. 33. Comparison of FEA Temperature Gradients and Fit Curve

8.4. Ultrasonic Test on Weld Pool

Adjusting data collection parameters is critical in measuring time of flight during cladding. The large heat input to the substrate requires adjustments to amplification, window width and window location. The time window has to be narrow enough to maximize the accuracy of the reading and wide enough to account for shifts in the display. As the water supply used for bottom side cooling heats during cladding, the time of flight through the water couple increases which shifts the whole display to the right. If there is any inclination to the substrate as it moves between the transducer and weld head during cladding, the distance between the transducer and the peaks shift again. This also occurs as the substrate warps during cladding. Heat in the substrate increases attenuation

which requires higher amplification. Target peaks are of different intensities so different target peaks require different amplification. These parameters cannot be adjusted during data acquisition and so must be set before data acquisition begins. Values were determined by trial and error before each run.

Figure 34 shows the paths for all peaks seen in this data. The shortest path from the transducer and back is path 1 to the backside of the substrate. This peak was the reference for all subsequent peaks since all other paths overlapped this path. The second shortest path would be the reflection from the backside to the top of the couple to the backside and to the transducer. This path is through water with a sonic velocity of 1.5 mm/sec⁴⁹. With a couple/substrate gap of approximately 3mm and a path length twice that of approximately 6 mm this will correspond to a time of flight of 4 μsec. The next shortest path will be to the solid/liquid interface. With a 20.3 mm thick substrate and assuming a 2 mm cladding penetration gives a path length of $2 * (20.3 - 2)$ or 36.6 mm and a travel time of 8.1 μsec at 4.5 mm/μsec. The last two peaks will be from the liquid/liquid interface at the top of the weld pool and liquid/air interface at the top of the liquid flux. Values for sonic velocity through liquid metals of 3.6 mm/μsec will be used for both of these calculations⁵⁰. The locations of each peak is tabulated in Table 2 and illustrated in Figure 35.

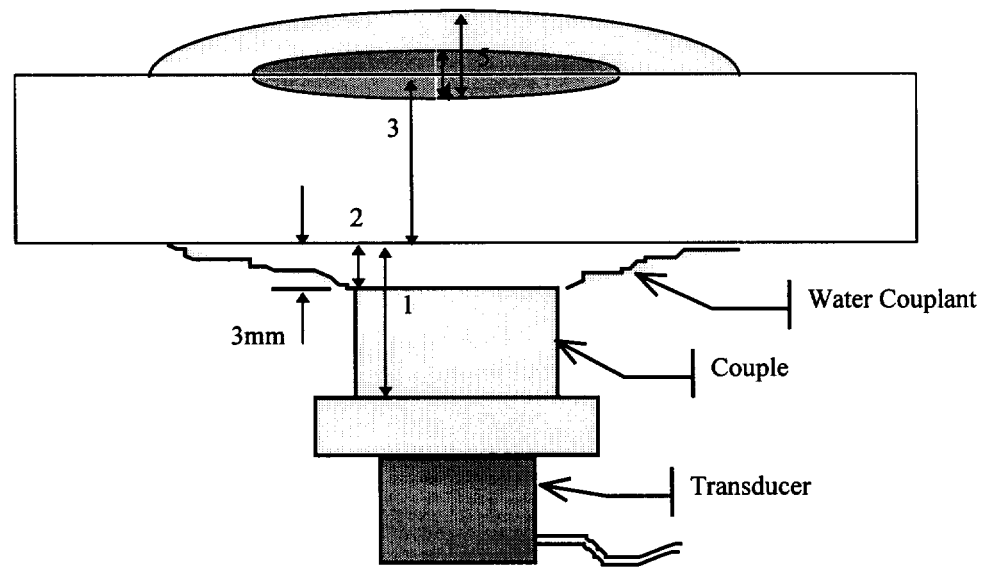


Fig. 34. Ultrasonic Paths During Cladding

Peak	Velocity	PathLngth	TOF	POS
1	1.5	x	0.00	1.00
2	1.5	6	4.00	5.00
3	4.5	36.6	8.13	9.13
4	3.6	4	1.11	11.24
5	3.6	6	1.67	11.80

Table 1. Example Values

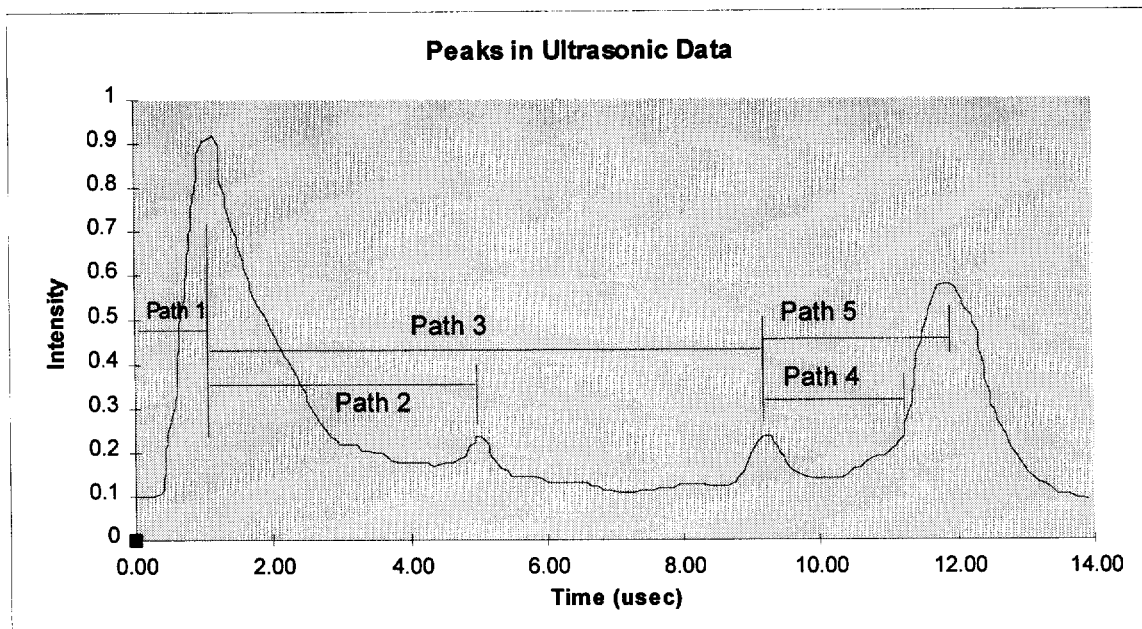


Fig. 35. Ultrasonic Reflection Peaks

The peak in Figure 35 at approximately 5 μ sec. is the reflection from the top of the couple. To ensure path 2 originates at the top to the couple, a fine copper mesh was rolled up and placed inside the water couple so it contacted the substrate and lined the couple. This allowed a free path for the ultrasound and the water flow could pass through the mesh but any signal to the top edge of the couple is dispersed passing through the mesh. The signal disappeared with the mesh in place indicating that the peak originates at the couple.

It was initially thought that the reflection from the top of the weld was the liquid/solid interface but the liquid/solid interface peak was actually a much smaller peak and to measure it accurately the signal amplification had to be increased drastically and also a thicker substrate was needed to separate the peaks from each other.

The peak for the solid/liquid interface is shown in Figure 36. The identification of this peak is confirmed by the fact that when power is turned off to the welder the peak disappears as the pool solidifies and the solid/liquid interface becomes the solid/air interface.

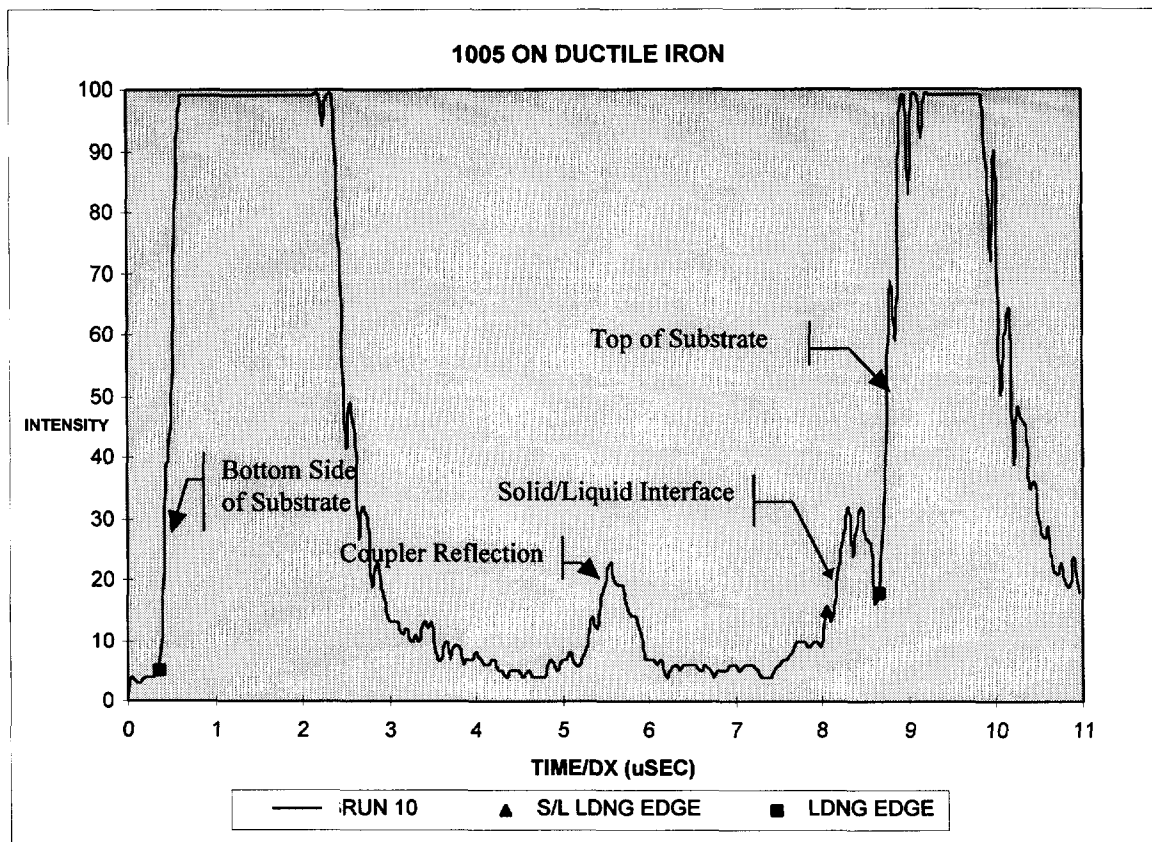


Fig. 36. Ultrasonic Data Peaks

Determining peak values can be done either by the maximum value of the peak as was done with the time of flight versus velocity measurements or by the location of the leading edge. The maximum value method is adequate for peaks that are of the same order of magnitude in intensity. For this application where the peaks are several orders of magnitude different in intensity the leading edge provides a more accurate measure. The penetration is determined by the difference between the initiation of the bottomsideside peak and the initiation of the solid/liquid interface peak. Two techniques were used to identify the three leading edges. The bottom side peak is located by the slope of the leading edge in software since its shape was so consistent. The leading edges of the solid/liquid interface and the topside were located manually because of variation in the signal shape. This method produced a consistent value for the time of initiation of the peak. A software solution could be developed to compensate for this variation but the manual method is more time efficient and practical for this application. The three reflection peaks, the

backside, the solid/liquid interface and the topside will be the reference points of interest. The results will be discussed in a later section.

8.5. Destructive Testing

Two samples of cladding were destructively tested to determine the correlation of recorded ultrasonic data to cladding structure. Both samples were cut in half longitudinally to expose the centerline of the bead. The surfaces were polished to 1 μ m and etched using 10% nital to contrast the microstructure of the material. The samples were examined and photographed under 40X metallurgical microscope and digitally photographed without magnification.

There are three distinct zones of interest, the substrate of ductile iron characterized by nodular graphite, the cladding with little graphite structure and a mixed zone. The mixed zone is a result of the melting of the substrate and mixing with the melted cladding forming an intermediate mixture. This structure is shown in Figure 37, a micrograph of the mixed zone. At the bottom, nodules of graphite from the ductile iron substrate are visible and, above that, a graphite enriched structure is visible where graphite has mixed with the 1005 steel to form white iron. The thickness of this mixed zone varies from 1 to 3 mm. The top interface is very uneven and the bottom is smooth. The zone is thinner at the beginning and ending of welding and thicker during continuous welding.

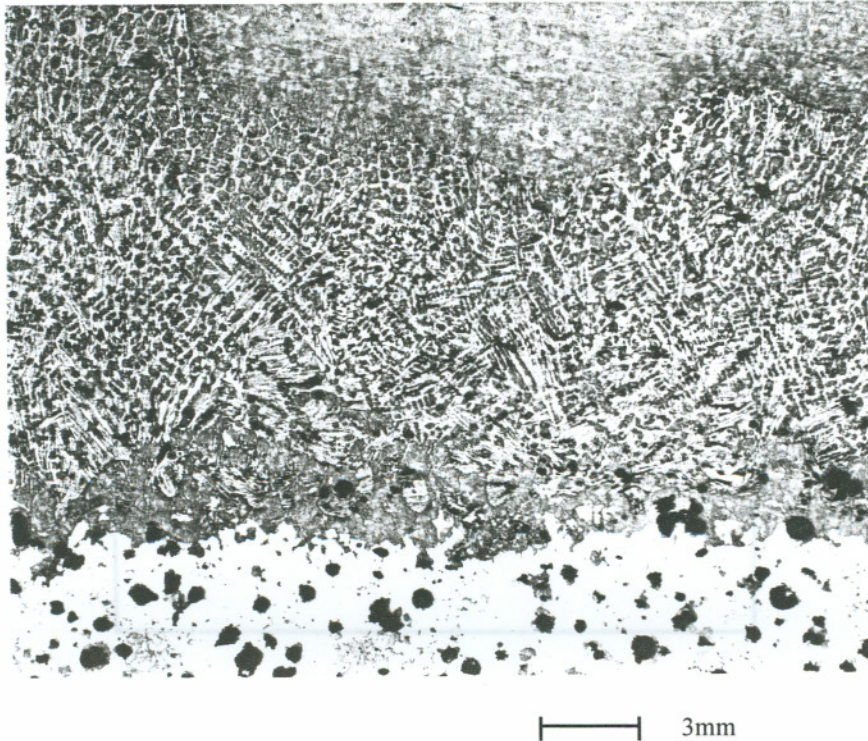


Fig. 37. White Iron Interface Between Cladding and Substrate 40X

Figure 38 shows an image of the substrate cross section showing a larger area. Several inclusions and cracks can be seen in the cladding especially at the end where the welder was shut down. Measurements to determine distance from the backside to two points were made using Optimas software. The two points are the ductile iron/white iron and the white iron/1005 interface. Measurements were made every 3 mm along the length of the cladding. These measurements are shown in Figure 39.

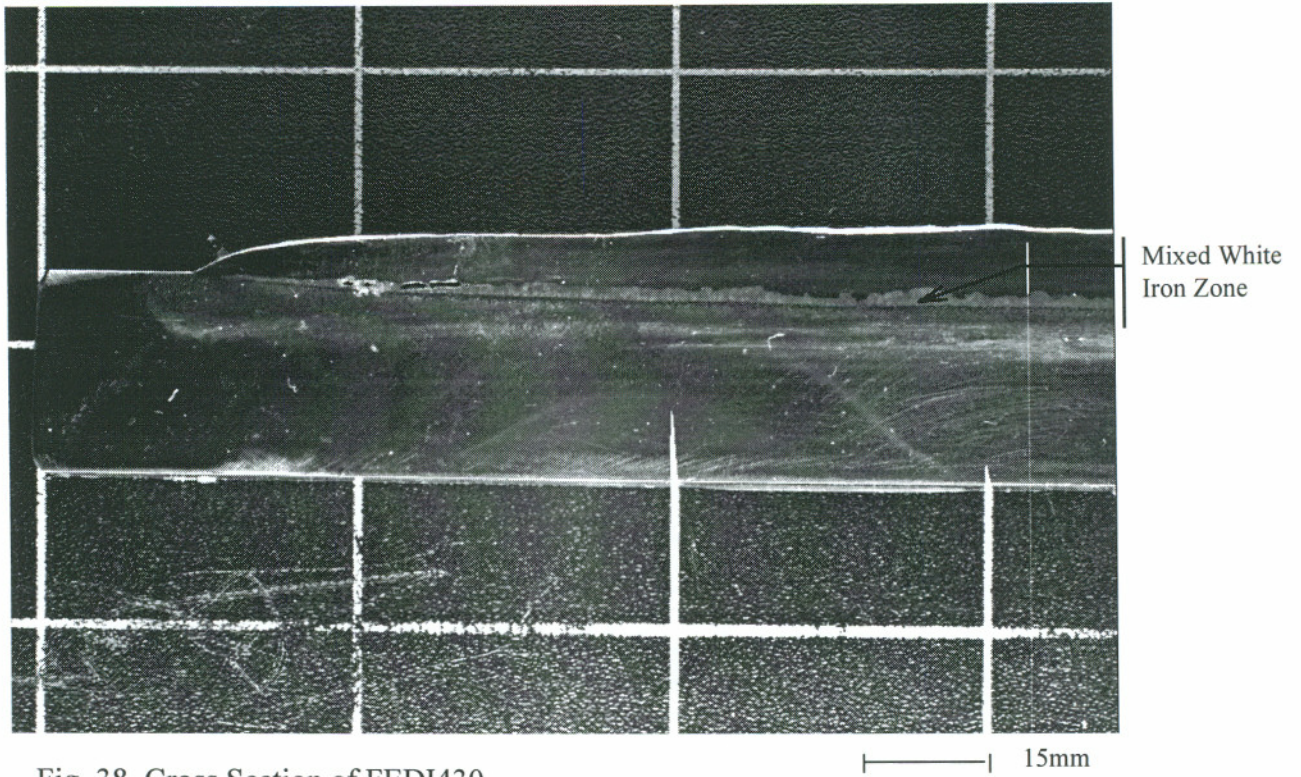


Fig. 38. Cross Section of FED1430

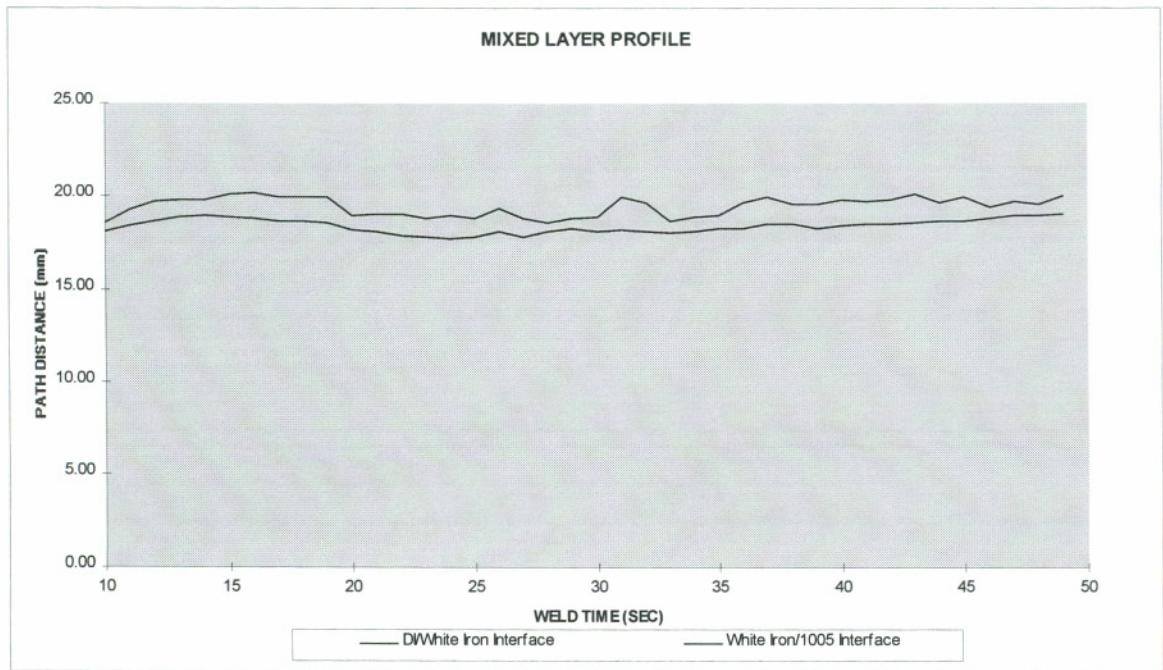


Fig. 39. White Iron Mixed Zone Profile

8.6. Calculation of Liquid/Solid Interface

With an understanding of the temperature gradients along the flight path and the velocity of ultrasound at temperature it is possible to determine a correction factor to the measurements of reflector location. These corrected interface location values will then be compared to values of the actual interface location derived from destructive testing.

Equations for a best fit curve to the data for velocity versus temperature and for temperature gradients along flight path have already been determined. They are :

$$T = 80 + 23.8 * \exp (X / 4.87)$$

$$V = 5.87 - 0.155 * \exp (T / 445)$$

Combining these values results in:

$$V = 5.87 - 0.155 * \exp ((80 + 23.8 * \exp (X / 4.87)) / 445)$$

where X is the distance from the bottom face of the substrate and V is the velocity of ultrasound. The flight path is broken down into 36 discrete elements along the flight path of the ultrasound and a velocity is assigned to each element by its location. Making each element an identical size and dividing the size by the velocity in the element gives the time of flight through the element. The sum of the time of flights through the elements gives the total time of flight as illustrated in Figure 40.

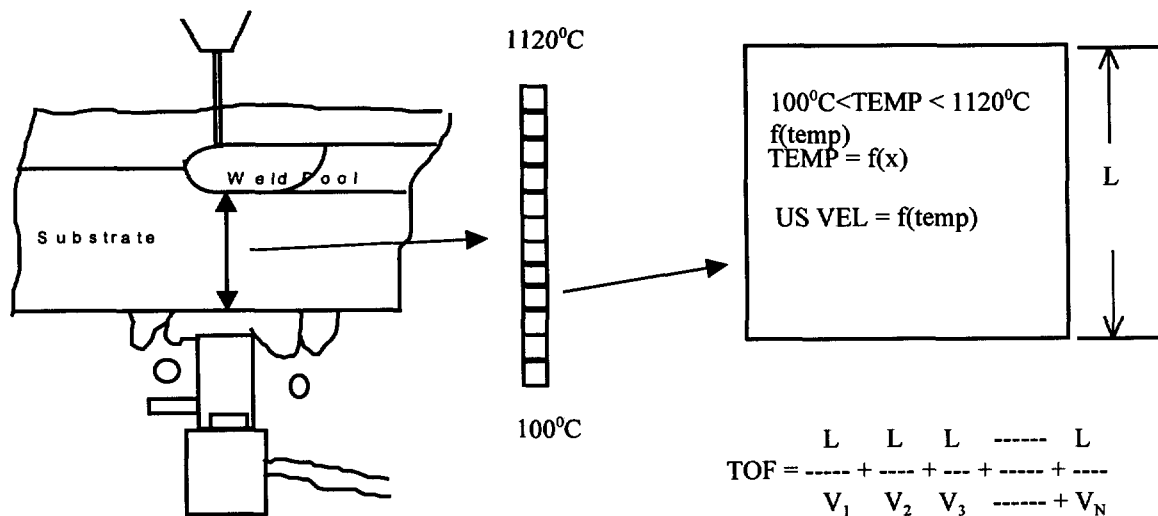


Fig. 40. Calculation of Reflector Position

The size of each element was adjusted so the sum of the element time of flight equals the time of flight measured during cladding. The distance to the reflector is then the sum of the element lengths and no prior knowledge of this value is required to determine it. The results of this calculation are shown in Figure 41 compared with the measured distances to the mixed zone between the cladding and substrate. Also shown is calculated distance to the interface without a correction factor for the temperature gradients i.e. at a constant velocity through the substrate.

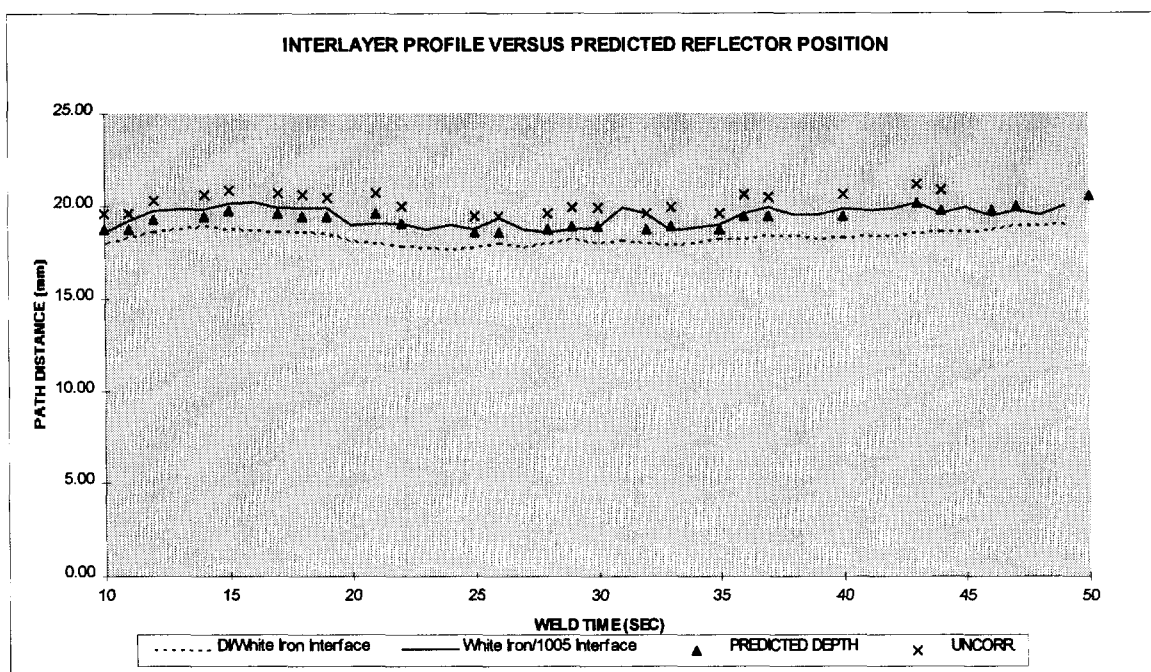


Fig. 41. Reflector Position in Relation to Mixed Zone Boundaries

The correction factor moves the interface point an average of 0.98 mm. There is a close correlation between the top of the optically measured position of the mixed zone and the predicted position of the reflecting interface. This data suggests that there is a solid/liquid interface at the top of the mixed zone of white iron that solidifies before the rest of the weld pool. This would make intuitive sense since this material in the middle zone will have a solidification temperature between that of 1005 steel and ductile iron. It will solidify first and after further cooling the 1005 steel will begin to solidify.

8.7. Refraction:

Initially the temperature gradients along the flight path were assumed to be flat enough that refraction could be ignored. But some of the isotherms are quite steep and will have an effect on beam direction and flight path that need to be considered.

The refraction of a beam is determined by Snell's law:

$$\frac{\sin \alpha_R}{\sin \alpha_i} = \frac{V_R}{V_i}$$

where V_i and V_R are the incident and refracted sound velocities and the angles are the incident and refracted angles as shown in Figure 42.

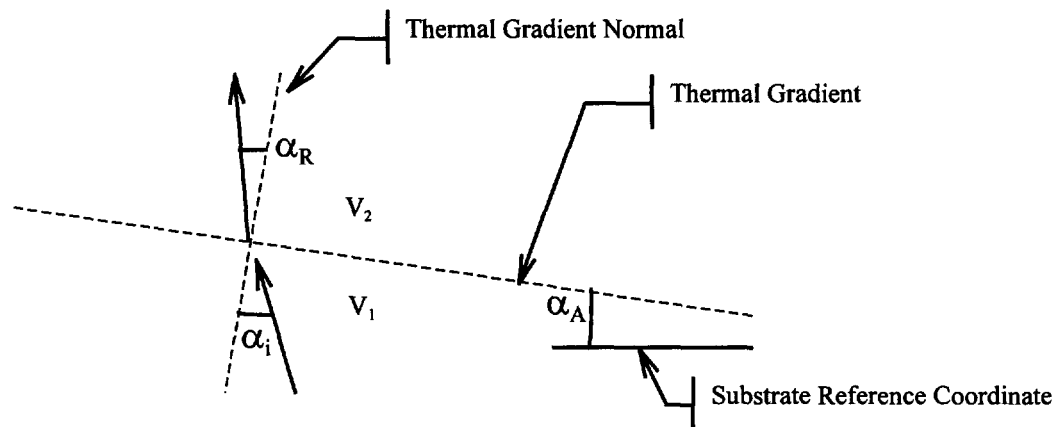


Fig. 42. Snell's Law

To determine the flight path deviation in this substrate due to temperature gradients an element approach was again used. Using 18 elements along the flight path through the thermal gradients, the velocity at equilibrium in each element has already been determined. To find the gradient angles the temperature profiles at 3 mm to each side of the flight path are taken from the finite element model. After fitting a line to each profile, isotherms and their inclination to the substrate can be calculated and plotted as in Figure 43.

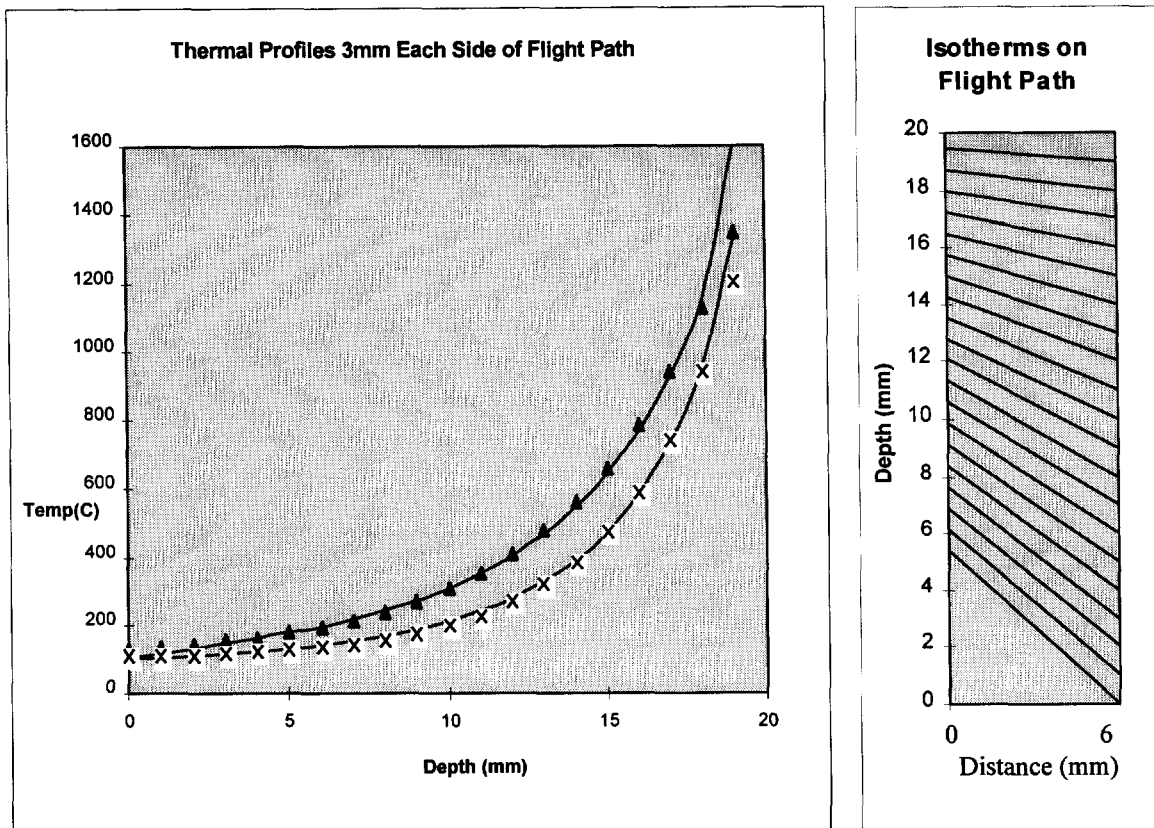


Fig. 43. Thermal Profiles and Gradients from Finite Element Analysis

From this data the refraction at each element boundary can be determined and a flight path calculated. The bottom side of the substrate is used as the reference angle.

As the beam refracts and spreads during propagation only a portion of the beam energy returns to the transducer. The flight path of interest here is the path that returns to the transducer. Using a value of 0° for the initial path angle of the ultrasound results in a flight path that returns to the bottom side 3 mm behind the transducer. By using an initial angle of 5° the flight path will reflect off a point 1 mm to the left of the uncorrected flight path at the top of its travel and will return to the transducer as illustrated by Figure 44.

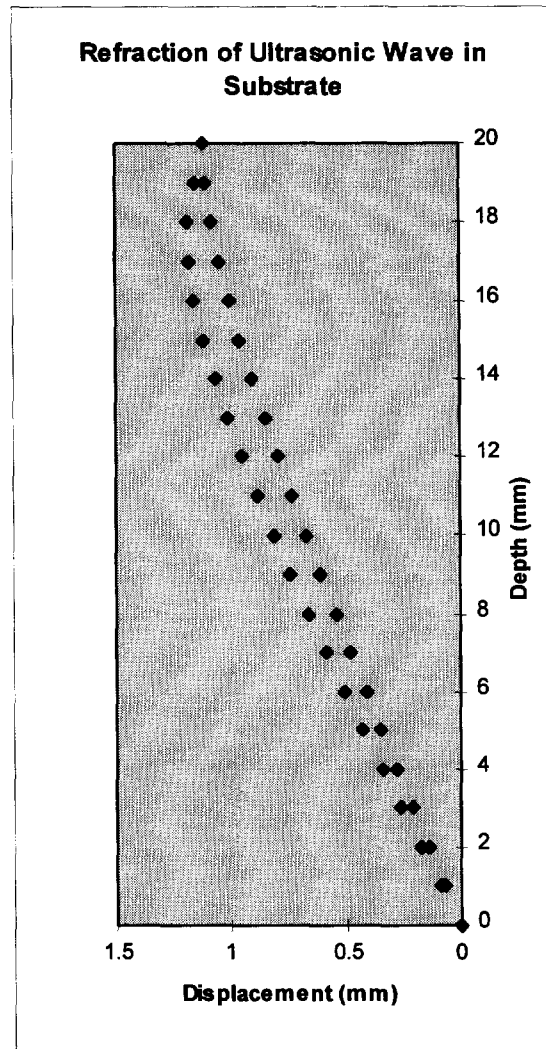


Fig. 44. Ultrasonic Flight Path Due to Thermal Gradients

The total length of the flight path is 40.08 mm which is an increase of 0.2%. This is an order of magnitude less than the correction factor for the change in velocity due to temperature and would move the calculated location of the reflecting interface down 0.04 mm. This is a small enough effect that it was not included in the calculations.

8.8. Frequency Response at Temperature

The transducer produces an ultrasonic wave of characteristic frequency as determined by the size and shape of the piezoelectric element. This frequency is centered around 4 MHz in this application. The velocity of the wave is a function of frequency and if frequency components of the wave are lost it will affect the measurement of time of flight. To determine if temperature has an affect on the frequency of the signal, an

acetylene torch was used to heat a ductile iron substrate to a red hot surface temperature. A transducer water coupled to the backside of the substrate recorded a signal reflected from the topside of the heated substrate. A fast fourier transform (FFT) was applied to the signal to determine the principle frequency components of the signal. This was compared to an FFT of a signal through a room temperature substrate. The real and complex results are graphed in Figures 45 and 46.

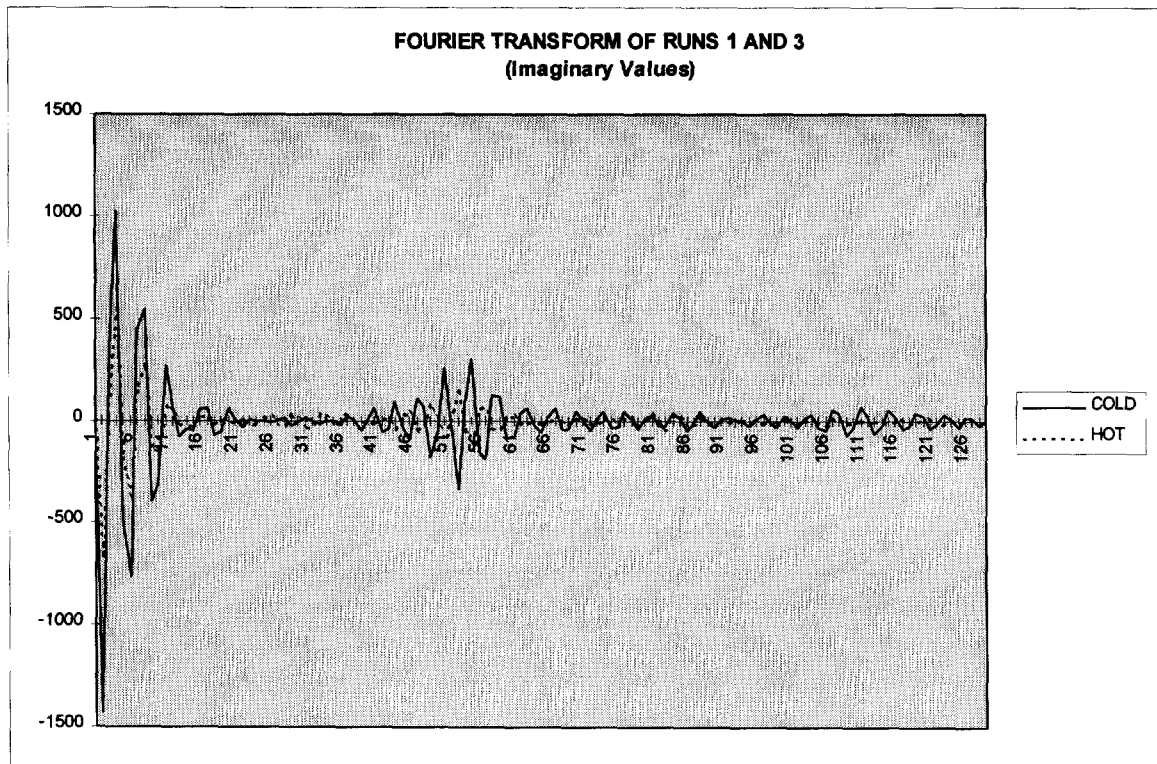


Fig. 45. Imaginary Portion of Fourier Transform

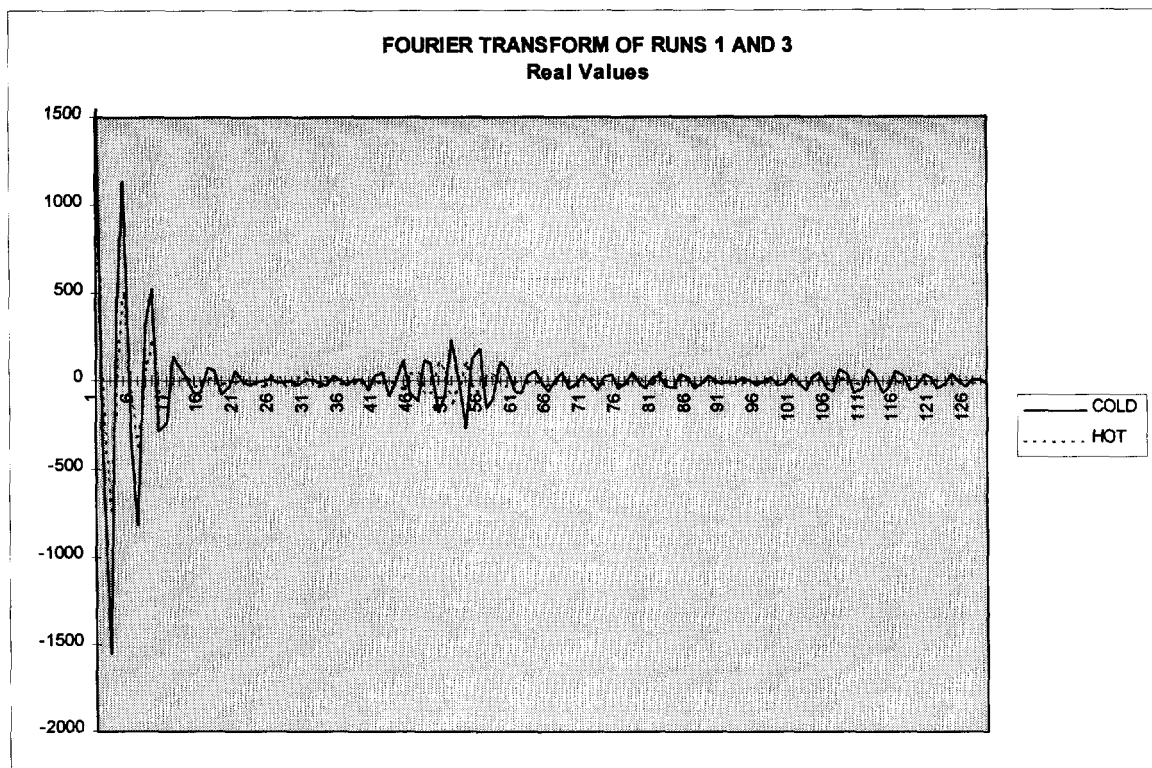


Fig. 46. Real Portion of Fourier Transform

The principle components are close to identical for both the high temperature and room temperature measurements. This indicates that there is no change in the frequency components of the signal at high temperature and that the time of flight signal will not be affected by frequency shifts or signal component loss at temperature.

Chapter 9

Conclusion

The thermal gradient correction system worked accurately and as expected.

In the original hypothesis it was assumed that the time to reach equilibrium thermal gradients was longer and would require continuously varying correction factors over the first 60 seconds of operation. The finite element model predicted that the thermal gradients in the substrate reach equilibrium in a short time meaning that a single correction factor could be applied to all measurements which simplified the application. The finite element analysis was shown to be accurate by its agreement with thermocouple data.

The measurement of the time of flight versus temperature resulted in a transformation of one of the two substrates which altered the velocity of the ultrasound. The remaining substrate had adequate redundancy to determine the velocity over a range of speeds.

The thermal gradient correction factor to the ultrasound velocity provided a 5% correction to the solid/liquid interface location expected if the substrate were at room temperature. The locations of time of flight predicted reflector points correlated to the top of a mixed zone where the melted substrate diluted the cladding to form white iron. The close correlation of the corrected time of flight measurements to the top of the white iron mixed zone indicate the measurements are very accurate although the exact location of the reflector is very difficult to determine.

This is a very accurate method for determining the penetration depth of the weld but adapting it to a real time system would require modifications. A new finite element

model for different materials would be required but the material properties and dimensions could be modified for this model with a minimum time investment to develop the new analysis. It is possible that the FEA model could be extrapolated to other thicknesses to determine the temperature gradients without doing an actual analysis. This would require more study to understand the model's flexibility and adaptability.

Water coupling is not a practical method to use in welding because it quenches the metal but an oil couplant would prevent quenching and still maintain a safe temperature for the transducer. This would change the bottomside temperature profile and would also have to be included in a new finite element model.

This penetration measurement method is based on working from the bottom side but it should be possible to collect data from the top side, reflecting the ultrasound off the bottomside. The difficulty would then become defining the reflector source of the signal which would probably be the edge of the molten pool and would not be as valuable in determining penetration.

The biggest problem for wider industrial application of this technique would be the need for a smooth surface. When a milled surface was used on the substrate there was a great deal of distortion of the signal which affected the data significantly. Often an adequately smooth surface is not available in welding applications.

Laboratory applications of this technique would be very practical. Determining penetration of welds under a range of conditions and parameters could be done without cross sectioning samples. Real time defect generation could be simultaneously studied according to previous research³⁹.

Chapter 10

Future Work

Possible avenues for future work would be to move the transducer to several positions behind the weld head and determine the distance to the solid/liquid interface at each point. This would provide a clearer picture of how the interface progresses during solidification.

Another approach would be to develop a high speed positioning system to collect time of flight data at several locations. By mapping the points correctly and collecting the data in a very short period of time synthetic aperture methods can be used to reconstruct the shape of the weld pool. This would probably require a laser generation system and an interferometer detector in order to generate ultrasound and collect data at as small a point as possible.

Chapter 11

APPENDIX

11.1. Vision Based Electroslag Surfacing Bead Following and Overlap System

Introduction

The Electroslag Surfacing System (ESS) was developed to provide economical deposition of large volumes of weld metal onto surfaces. This technology is being used by industry in a range of applications. Typical surfaces include propulsion shaft and rudder shaft bearing surfaces. For extended cladding such as surfacing a shaft or lining tanks where long spiral beads are applied to a substrate, the process must be controlled by an experienced technician to provide appropriate bead overlap. An automatic system to position the weld head for a preset overlap with the last pass bead would reduce cost of production and improve quality.

A range of methods have been developed for positioning a welder in relation to a seam or gap. Detecting parameter changes as the arc moves out of the weld gap is widely used and contact methods can be used in some situations. Digital imaging has been limited by the arc flash around the weld and varying light and cleanliness conditions in industrial settings. Several researchers have worked to develop more robust techniques for determining position from images during welding. Nagarajan *et al* used an infrared (IR) camera to measure the heat gradients around weld pools³⁰. By determining the isotherms around the weld pool, pool position in relation to a gap being filled could be determined. As the weld moved away from the gap the isotherms that were normally even and ellipsoid became uneven and lopsided with a characteristic shape in the direction of deviation. With continuous monitoring of the isotherms, tracking of the weld could be

maintained.

More often CCD (Charge Couple Device) video camera visible light images are used to determine reference points on the substrate in relation to the welder. Neural networks have found many applications in digitally extracting information. Suga⁵¹ *et al* used digitized images that were processed using a longitudinal log filter to enhance edges of the image. This produced a binary or high contrast black/white image with edges as black pixels. The high intensity light from the weld left noise in the images even after filtering. A neural network further processed the image by extracting line position and controlling weld position through noise reduction, and recognizing offset and change in direction of the reference line. The system was found to be very effective in tracking the weld line in welding experiments.

Another approach is to use an illumination line usually of coherent light which can be filtered to eliminate the broad band illumination from the arc. Kaneko *et al*⁵² used a laser line to illuminate a weld line between a pipe and a plate. The line laser projected light onto the pipe and plate while the camera observed the line from an oblique angle. From the camera view the light on the surfaces form two lines at an angle with the weld joint where the end of the two lines meet. From the position of the join line in the field of view, the welding torch was positioned using a fuzzy logic system.

Electroslag surfacing is different from most arc welding processes in the sense that there is not a seam or gap for joining two pieces. In this application there is a flat or curved surface for the first pass and then for subsequent passes there is a bead edge which is the reference point for the next bead. Inadequate overlap will require more material and more machining and too much overlap can trap contaminants at the bead edge. Applying cladding to a large area can require several hours and needs an experienced technician to control the overlap. In electroslag surfacing the process is arcless depending on IR heating to melt flux and admetal. Without the arc flash digital images are more easily utilized and provide a versatile tool for automation. There is a disadvantage that flux is required in electroslag surfacing to eliminate oxygen which would oxidize the molten metal and cause arcing. The flux makes it impossible to view the process area directly.

Weld head placement in the ESS system in a continuous spiral application requires finding the edge of the bead clad on the last pass. This bead will have the next pass bead butted against it and if overlapped correctly will form a smooth surface. By offsetting a viewing camera to a flux free area ahead of the cladding process it can be used to locate the bead edge and position the weld head.

Bead overlap is critical for a high quality clad surface. Different voltage, current and shaft rotation speeds produce different bead profiles which require different overlaps between beads. If the shape of beads produced by different parameters were known, the overlap between beads could be adjusted to improve the finished overlay. It is possible to measure bead shape of the existing bead using the line laser illumination and digitizing camera during welding. The difficulty is that the new bead cannot be profiled until it is clad. It is possible to determine parameters while cladding. If the bead shape resulting from any set of weld parameters was known it would be possible to determine an optimum weld overlap and position the weld head appropriately.

This could be done by cladding a number of reference beads under a range of parameters then digitize those bead profiles and train a neural network with the parameters as input and the profiles as an output. Neural Networks (NNs) are pattern classifiers that correlate output parameters to input parameters. They are very good at dealing with non-linear, hidden and multivalued problems. The trained neural network could then predict the bead profile from parameter data only. The current parameters and the parameters for the existing bead stored in memory can be input to the neural net, the two bead profiles predicted, an overlap calculated and the head positioned appropriately. This also has the advantage that little computer time is taken away from bead tracking because using a neural network after training is computationally very efficient.

In this application propulsion shafts from US Navy ships were clad with 625 stainless steel as a bearing material. In the past bearing surfaces were machined collars that were interference or shrunk fit to the propulsion shaft. Inspection for seawater corrosion between the shaft and sleeve required the replacement of the sleeve which is very expensive. Electroslag surfacing can produce a bearing surface without an interface which is susceptible to seawater corrosion. To clad on a surface of a large shaft, a long

spiral is the preferred technique. The first part of this appendix will describe a vision based feedback control head positioning system for semi-autonomous operation of the Electroslag Surfacing system. The second part will describe a neural network for predicting the profile of the bead from weld parameters and determining optimum overlap for the control system.

Background

Neural network development is a result of both biomedical research and mathematics. Neurological research has shown how groups of nerve cells interact and learn to function as a whole⁵³. Learning in the brain can be accounted for by the mechanism of the creation of new synaptic connections between neurons and the modification of the existing synaptic connections. Neural networks reflect the structure and functioning of these neurons and were inspired by them⁵⁴. A neural network is usually implemented using electronic components but they can also be simulated by software. What differentiates neural networks from other circuits is their ability to learn and modify themselves. This is implemented through a process called a learning algorithm which modifies the synaptic weights in a network as a function of the network environment⁵⁵.

Neural networks as a field began with the work of McCulloch and Pitts at the University of Chicago in 1943. McCulloch was a psychiatrist and neuroanatomist and Pitts was a mathematician. Their 1943 paper described a logical calculus of neural networks and was very influential in von Neumann's work with computing and computer theory⁵⁶. Hebb in 1949 began describing learning systems and that the connections between synapses in the brain were changing as learning occurred⁵⁷. In his postulate of learning he stated that the synapse connection between two neurons was strengthened by the repeated activation of one neuron by the other across the synapse. The field progressed through the 50's and 60's, building on this work with the development of learning systems and elements. The momentum of this development ground to a halt with the publication of an analysis in 1969 by Minsky and Papert⁵⁸ which showed that there are strict limitations to the capabilities of single layer perceptrons and that there was no reason to believe multiple level perceptrons were able to perform any better. This

combined with the lack of personal computers caused a serious lag in research and applications. In the 1980's a range of learning algorithms were developed including Boltzmann learning and reinforcement learning which extended the capabilities of neural networks immensely⁵⁹. In 1986 Rumelhart, Hinton and Williams⁶⁰ published their back-propagation algorithm which has become the most widely used training method for multilayer networks. This is the method that is used in this application.

The multilayer neural network is a collection of individual neurons which takes one or more inputs from source nodes or other neurons, sums the inputs and passes this

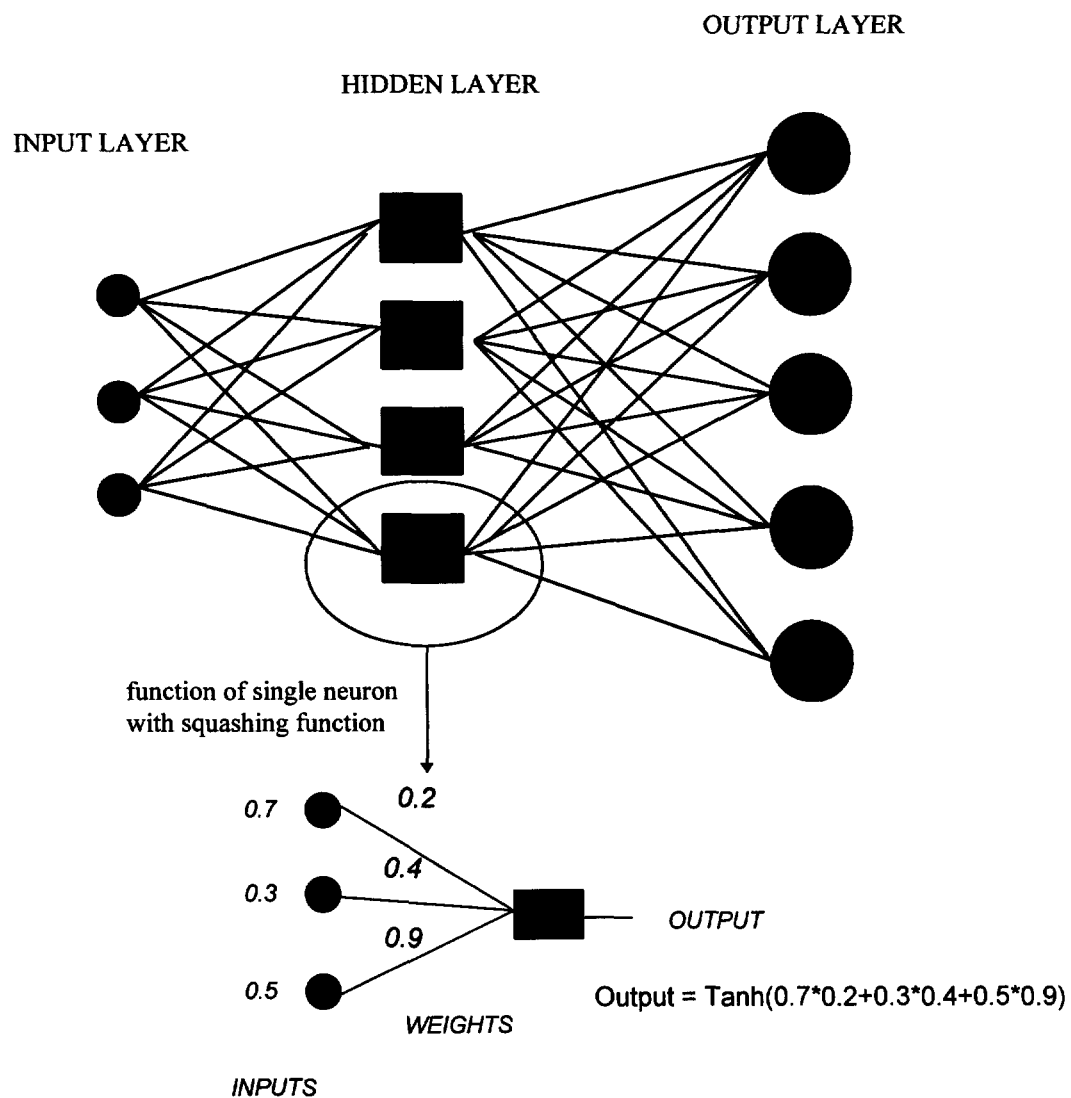


Fig. A1. Fully Connected Neural Network

sum through an activation function. A typical fully connected multilayer feedforward network will have three layers as shown in Fig A1. An input layer of source neurons, a layer of hidden neurons, and a layer of output neurons. There are a huge number of variations on this layout. More layers can be added, the number of neurons within each layer can be modified and the layers can be less than fully connected to each other. There are also many different types of neural networks than this but this discussion will be limited to Multilayer Feed-forward Networks (MFFN). This structure in itself would be the mathematical equivalent of a single layer network except for the activation function.

The activation function is a non-linear function which is smooth or continuously differentiable. Two commonly used functions are the sigmoid:

$$y_j(n) = \frac{1}{1 + \exp(-v_j(n))}$$

and the hyperbolic tangent:

$$y_j(n) = \frac{1 - \exp(-v_j(n))}{1 + \exp(-v_j(n))}$$

The value of the hyperbolic tangent function is shown in Fig A2.

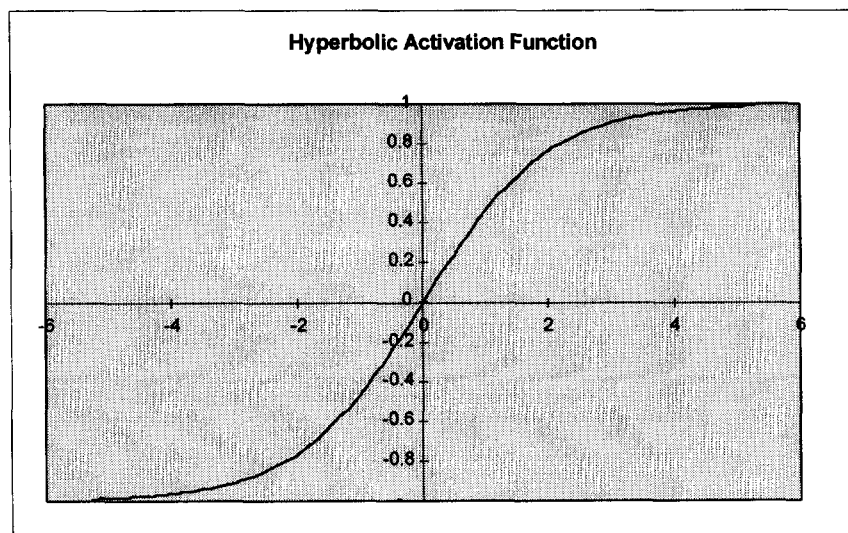


Fig A2. Hyperbolic Tangent

The activation or squashing function serves to limit the output of a neuron between maximum and minimum values set for all the neurons in the network. This keeps the working values within the network bounded.

Once the neural network is built either in software or hardware it has to be trained to set the weights between neurons. This is typically done by taking as large a number of examples as possible which consist of a set of inputs and a set of outputs. The inputs are a set of characteristic values which will be free variables in the application. The outputs are the situational results of the inputs. The outputs must be a direct result of the input values. At times this is the question to be answered i.e. there are a collected set of inputs and it is unclear whether there is a direct correlation for any or all of the inputs to the output values. The weights assigned to the neurons and degree of convergence of the training will be an indication of their correlation.

An example of this training would be the prediction of crop output from weather conditions in a certain area. This would be easy to implement because all of the data is readily available. Possible input values would be amount of rainfall, days of overcast, average high temperature, average low temperature, sunspot activity and water table level. Output values could be bushels of grain. The data can be collected for each growing season for as many years as good data is available. Each set of numbers is presented to the neural network. The network starts with the weights set to a random value. As the inputs of the example set is computed the network predicts results with the present value of the weights. The output of the network is compared to the example answer and an error value is determined. The training algorithm then backpropagates the error value to reset the weights to values which will produce a value closer to the correct answer. Then another example set is presented and the process repeats with a new example each time. The result after the appropriate number of training sessions is a set of weights controlling the interconnection between neurons. When a different set of values that the network has not been trained on of rainfall, temperature etc. is input, the network will predict that year's grain crop in bushels. The accuracy of the result will be a function of the correlation between the input and output training data.

This process can be thought of as curve fitting to a multidimensional set of data. While there may be noise in the input data, the network will try to find a graph surface which will fit to the data. A high level of accuracy is not desirable for most curve fitting to allow for noise in the data⁶¹. The training algorithm must also be set for a certain level of accuracy to prevent overtraining. Oppositely, if the input data does not correlate to the results, such as using the number of potholes in China etc. as inputs, the algorithm will not be able to converge and find a surface of any accuracy to the data.

Experience, background knowledge and some trial and error are required to successfully apply a neural network to a given situation. Neural networks are finding a wide range of applications. One of the hot spots for neural networks is in financial planning in world bond markets. In applications such as stock ranking neural networks will far outperform the current best practice of arbitrage pricing models⁶².

Bead Tracking Experiment:

To position the weld head correctly it is necessary to locate the existing bead, determine the correct overlap and position the weld head to lay down the next bead. With a CCD camera it is possible to offset the camera from the cladding process and compensate for lag time to determine reference points and position the weld head. The camera must be offset from the welder due to the flux load but it must not be located so far away as to increase the lag time excessively. After experimenting with several positions for the camera, lighting and software settings, an optimum configuration was determined. The camera was oriented approximately 45° ahead of the weld head, 90cm from and normal to the shaft surface.

Optimas image processing software was used to process the captured images. Optimas contains a function to locate a change in brightness along a reference line and report this location as a relative datum point. The only point of interest in the images is the edge of the bead to be overlapped so the image can be framed to show only this area. By using lighting that originates near the shaft at an oblique angle to the camera view, the bead edge will be in high contrast to the rest of the bead as shown in Figure A3. This contrast is easily detected by Optimas. The reference line in Optimas is positioned across the bead in the captured image. A datum point is established at the intersection of the

bead edge and the reference line. Movement of the weld head relative to the bead along the shaft will move the relief profile left or right in the image and consequently the datum point location. To make a spiral on the shaft a constant weld head progression or speed along the shaft is required and ideally the shaft speed and datum point value remains constant.

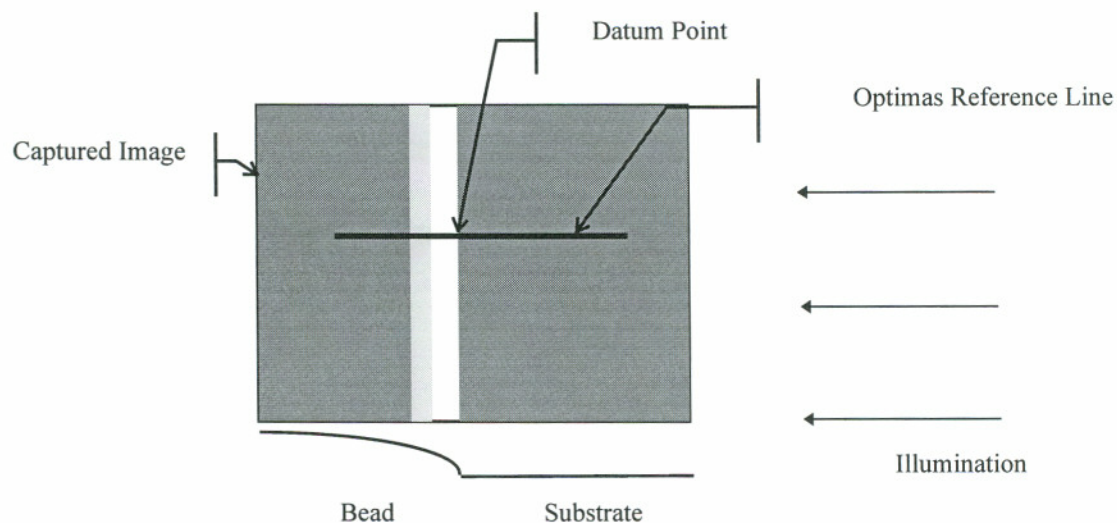


Fig. A3. Captured Image of Bead

The ESS welding head and camera are all mounted to a fixture on a moving beam over the shaft. The beam moves along the shaft length and its speed is controlled by a 0 to 6 volt signal to the motor controller which results in a speed of 0-1.68 cm per minute. A control value is output through the parallel port of the computer to an Analog Device 7528 8-bit digital to analog converter which controls the motor speed. A speed equal to a constant spiral for the given shaft is used as a default value. For a two foot diameter shaft this is 2.583 volts which produces a speed of 0.353 cm/min. or 3.11 cm per shaft rotation which is a nominal bead width. Shaft rotation is held constant at 15.24 cm/min. or approximately 29 deg./min. on a 40.6 cm. diameter shaft. Data flow is shown in Fig. A4.

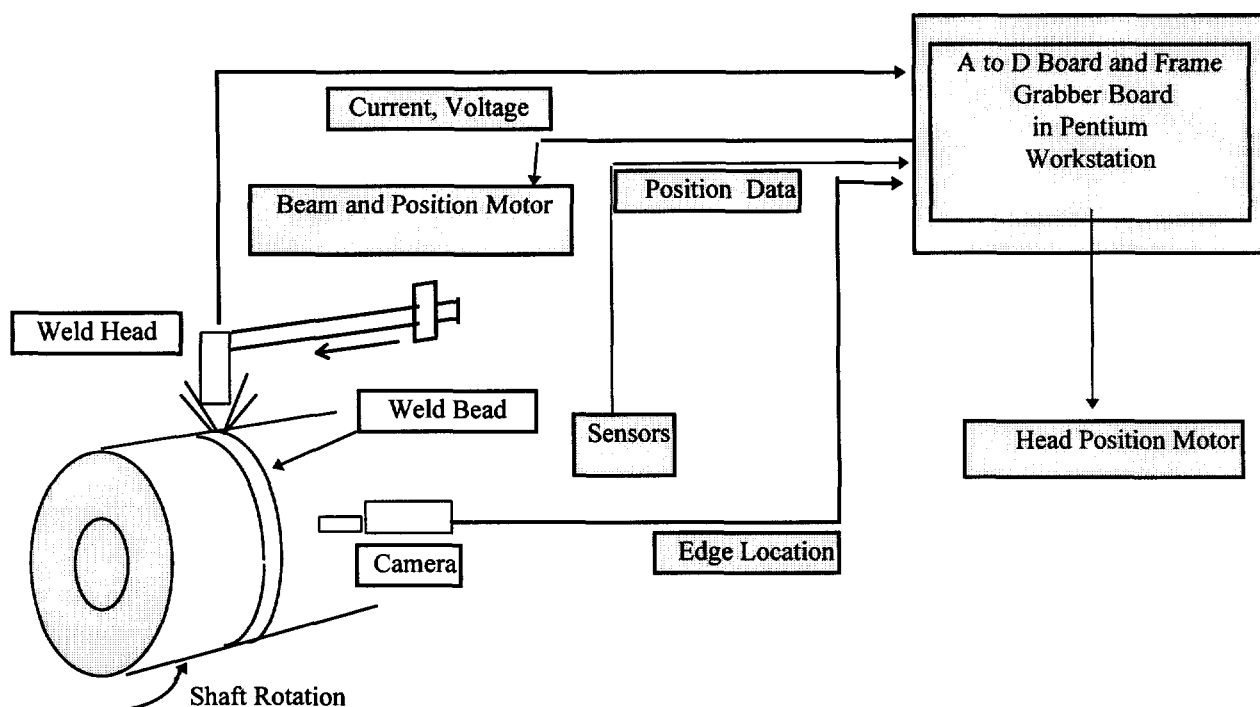


Fig. A4. Data Flow

By tying the weld head location to a datum point in the image the weld head speed can be adjusted to maintain a constant bead overlap. Datum points too far to the right will generate a higher head speed, and too far to the left will generate a lower head speed.

Bead Profile Determination Experiment:

Since bead shape varies with weld parameters and different shapes require different overlap values, a method is needed to adjust overlap with changing weld parameters. A trained neural network can use welding parameters as input and will provide bead profiles for the existing bead and the new bead. Training the neural network requires data on bead shape resulting from set weld parameters. From these parameters an optimum bead overlap can be set for the weld head controller. During the cladding process parameters stored in memory for the existing weld bead can be input into the neural network, which will output the existing weld bead parameter and the new weld bead parameters. With this data a bead to bead center distance and overlap can be

calculated for the current conditions. This is done entirely in software and is illustrated in Figure A5.

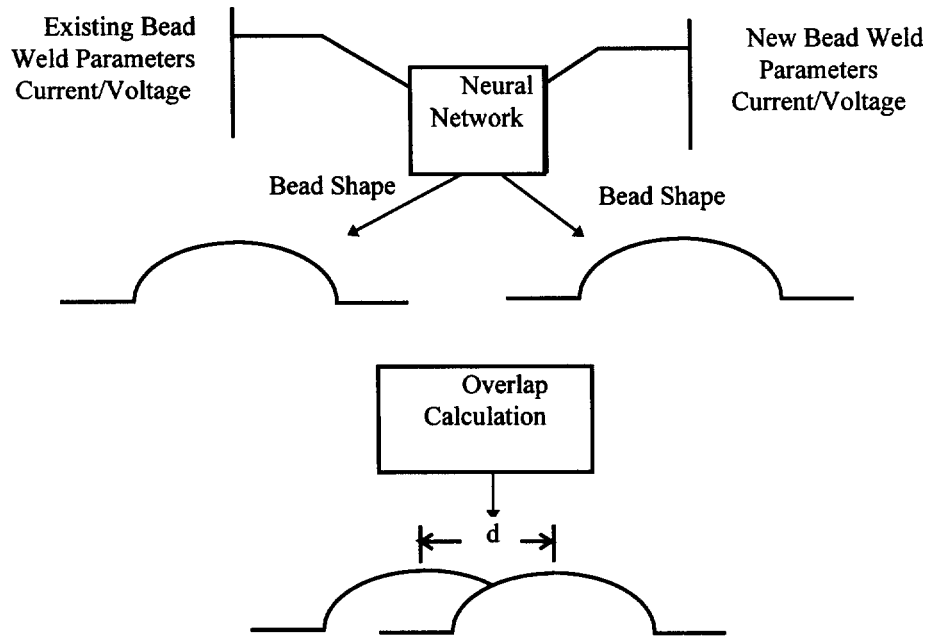


Fig. A5. Bead Overlap Determination

To determine bead profile a similar technique to edge location is used but instead of finding one horizontal datum point, thirty vertical profile points are determined. The cladding surface was illuminated by a 5mW laser commonly used in construction. The line is produced by a rotating mirror deflecting the laser beam through a plane perpendicular to the original axis. The laser is mounted on the horizontal beam together with a CCD camera. The laser produces a single line on the shaft surface. When viewed at an angle, any vertical relief on the shaft shows as a deflection of the line as shown in Figure A6.

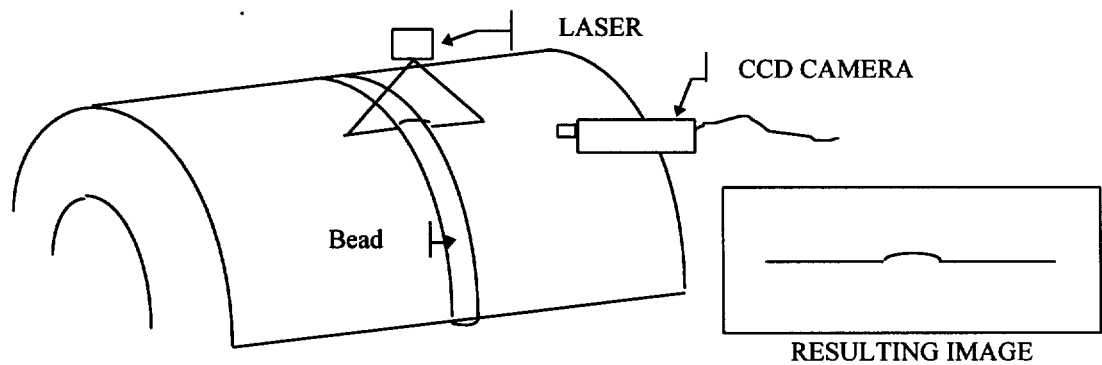


Fig A6. Vision System

The contours of the line can be measured to determine the bead profile. With the Optimas software a reference line is set vertically on the captured image of the bead and line laser illumination. Again a datum point is established by the change in illumination at the line laser point. By moving the reference line across the image a series of datum points is established that correspond to the relief of the bead as shown in Figure A7. A correction factor is applied to the datum points to determine actual vertical relief from the datum point data.

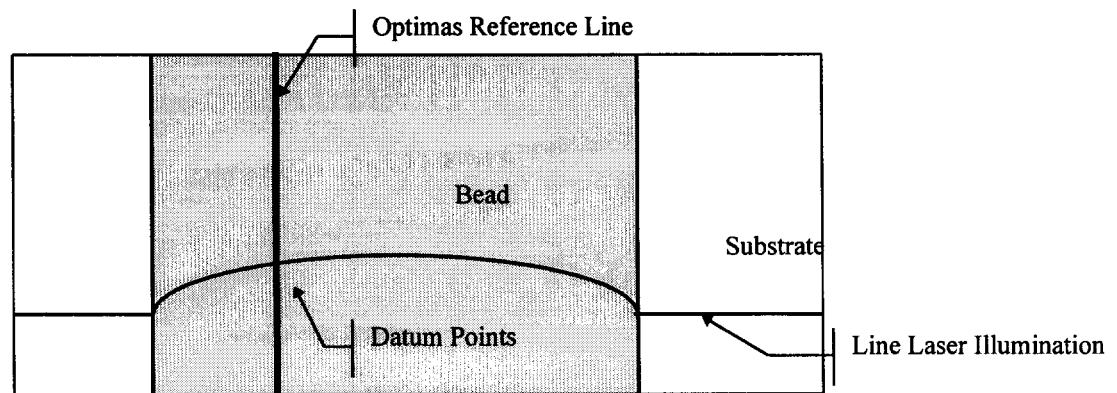


Fig. A7. Captured Image of Laser Illuminated Profile

To establish a training set for the neural network several beads were clad at set parameters. Four parameters were selected for an experiment matrix as shown in Table A1. Originally the matrix contained 72 parameter settings but only 48 settings produced acceptable welds. The 48 beads were 20 cm long and clad to a 40 cm diameter shaft. 30 datum points at 3 locations on each bead were profiled using the procedure described

above and averaged. This provided 4 parameter values and 30 profile values from each bead which served as the training sets for the neural network. There are many configurations of NNs available. In this analysis a Multilayer Feed Forward Network was used.

Table AI. Experimental Parameters:

	Min.	Max.	Units
Weld Voltage	24	30	Volts
Weld Current	500	900	Amps
Offset (Dx from TDC)	1.3	5.1	cms
Rotation Speed	13	28	cm/min.

The hardware and software used in this experiment were a Dell XPS P100 Pentium computer with 32 Mb Ram, a Coreco TCX frame grabber board, a Sony CCD/IRIS color digitizing camera, a DAS16F data acquisition board, Labtech data acquisition software, a 5mW line laser and Optimas 5.0 image analysis software

Weld Head Positioning Results:

The cycle time for the weld edge location and head speed adjustment was crucial to being able to make a real time control system. This system was able to record images and process them every 5-6 seconds. The time required for calculations to translate datum points to head speed voltage was negligible. The Optimas macro code is included at the end of this appendix.

Originally the code was written to translate datum points to a master grid of locations on the shaft that were time shifted to the location of the head. The angular, longitudinal and time shifts became quite complex. It was found that it was more effective to establish an optimum value for the datum point which would correspond to an optimum overlap. Any deviation from this optimum value resulted in a head speed change to correct the overlap. The value of the head speed seemed to not be critical. Both linear and logarithmic change in head speed with deviation maintained a reasonable

tracking with the bead. In order to damp out any oscillations, three sequential datum values were averaged. The system at startup generally does not have a bead to follow so the head speed is set to a default value until one shaft rotation gives a bead to follow.

During operation there were problems with the software crashing, locking up the system and requiring the computer to be rebooted. This problem could probably be eliminated with a later revision of software or by adding more memory to the computer. In this application the mean time between failures seemed to be about 45 minutes of operation. The actual cause of the crash was not addressed.

Correct lighting for bead identification was important for the software to be able to locate an edge. The threshold in the Optimas software could generally be set to adapt to any current conditions. The overhead lights in the work area were turned off for better contrast. Stray surface reflections sometimes cause erroneous identification of the edge but data averaging and maximum/minimum bracketing of the values generally removed or limited the effect of outliers.

Figure A8 shows a graph of head position versus rotation. To develop a baseline for system performance, a spiral was drawn on the shaft with ink to serve as a template. This is shown in the first curve. The second curve is the head position using the vision system to follow the template line and shows very good agreement. The head position value is taken from a linear position transducer mounted on the beam. The third curve shows the head position following the edge of an existing weld bead. The existing weld is not an even spiral and the graph reflects the edge accurately. The change in head speed can be seen at -100° to compensate for the deviation in the bead spiral.

The head positioning system performed as well making production runs as in tests. Spirals were even and consistent giving a smooth overlay.

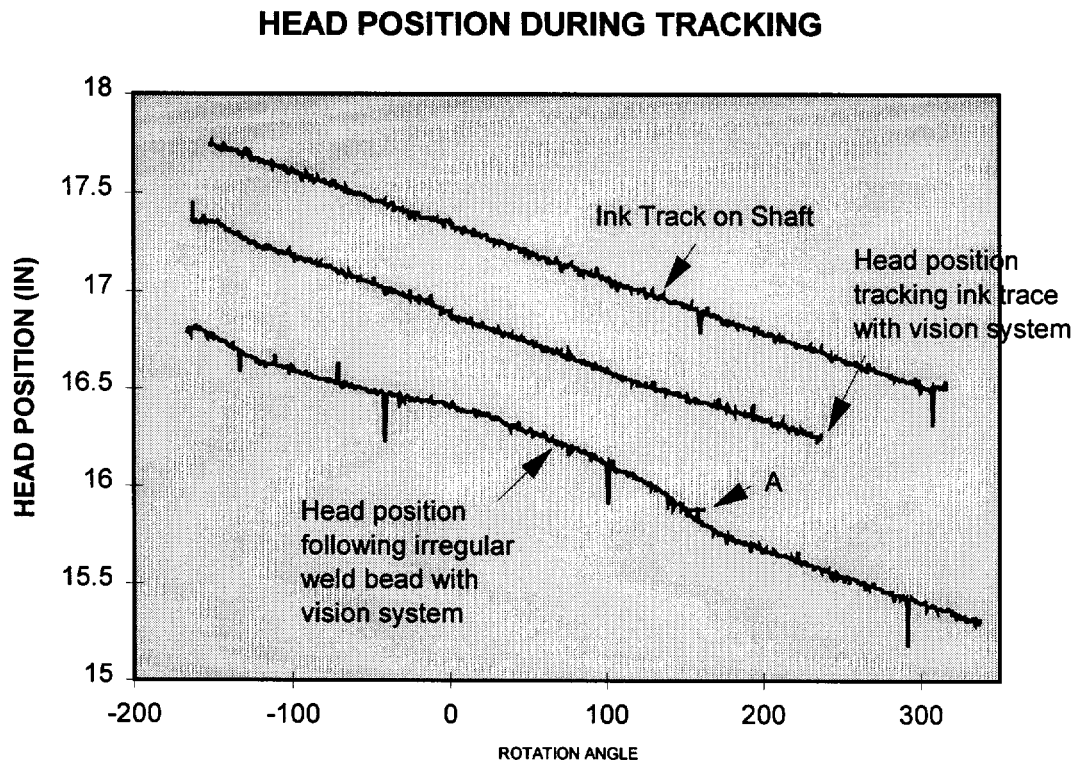


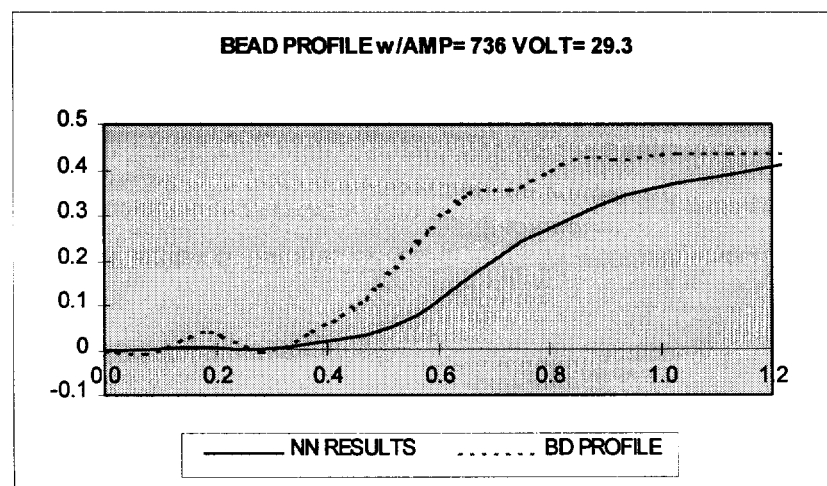
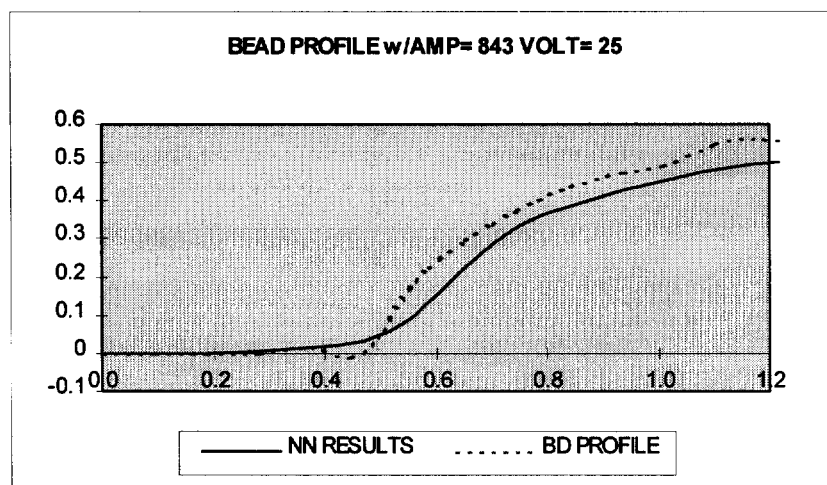
Fig. A8. Head tracking position.

Neural Network Bead Profiler Results:

There is not a good formula for the best configuration of a neural network to solve any specific problem. Neural network solutions are usually the result of experimentation with a number of configurations. In this study it was found that the strongest correlation between weld parameters and bead profile was for voltage and current. The correlation was determined by the connection weights between nodes after training. The node connections for offset and rotation speed were weak which meant that regardless of the value of these parameters they would have only a small effect on the results. The correlation between the voltage and current and the output values was strong. Symmetry of the beads allowed analysis of only one half of the bead so ultimately only 14 outputs were required.

The architecture selected after trial and error was two input nodes, eight hidden nodes and 14 output nodes all of which were fully connected. The settings on the power

supply for voltage and current are coarse and the actual values vary widely during welding. The data utilized was from measured values of voltage and current averaged over 10 samples at 5 samples/second. A combination annealing conjugate gradient descent learning method was used and the network was trained for 55 hours. Several examples of measured profiles compared to predicted profiles for those parameters are shown in Figure A9. Because the neural network is a curve fitting application that generalizes from the data given, the sharp edge of the bead tends to be averaged away after training but the shape height and width are preserved very well.



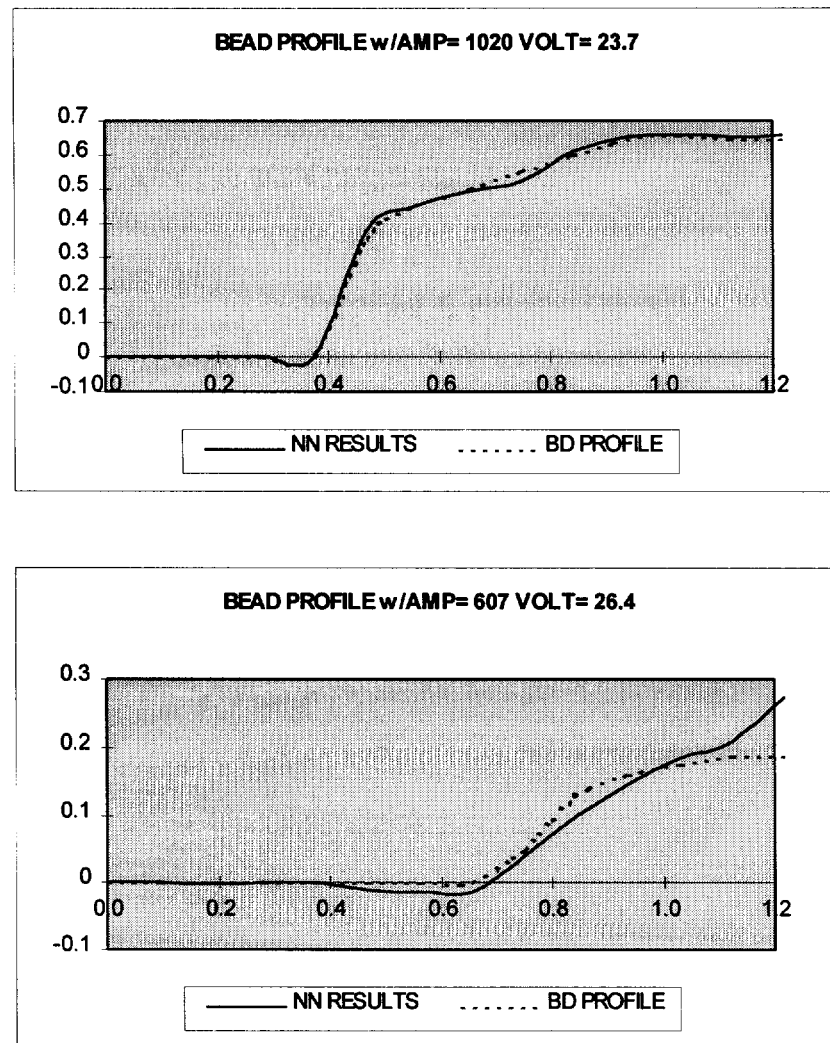


Fig. A9. Measured Bead Profiles vs. Profiles Predicted by Neural Network.
(Dimensions in inches.)

With the trained neural net, an accurate prediction can be made of the bead profile at any voltage and current and with bead profile predictions a center to center overlap with an optimum fill level can be calculated. The goal was to have an 80% fill level between profile peaks giving a smooth surface with minimal undulation. The center to center distance was calculated by determining the volume of weldment that becomes fill as the two predicted bead profile centers are moved closer together. This center to center value is input to the weld head position program to give the appropriate overlap.

The trained neural network was integrated into the bead tracking system to operate in real time. It worked well without slowing the cycle time of the system significantly. Ultimately the corrections that it provided were very small in the cladding done in this experiment. While the current and voltage varied over a wide range of values, the mean values were stable enough and the averaging effect of the cladding process made a stable bead shape. No overlap adjustment was necessary after the initial setting. In a production system with longer weld times than these development runs the process might be more useful.

Conclusion:

The bead tracking system is very effective in guiding the weld head and produces an excellent bead overlap. It is simple to implement, low cost, generally unaffected by noise and should be capable of working in a factory environment. This technique is directly applicable to submerged arc and strip cladding and should be applicable to arc welding processes as well with shielding from arc flash.

The bead profile prediction system worked as designed but provides a higher level of control and adjustment than was required for this application. This system would be more valuable together with a bead tracking system in applications where a range of power settings are used.

11.2. SOFTWARE CODE

Optimas5 Macro to Set Up Measurement Parameters

```
integer Ln_Marker1_Index_A;
ActivateMeasurementSet("Area Particle Shape 2");
DataCollection (1);
ActivateMeasurementSet("Line 1-Marker Analysis");
LineCNVFactors[0..6] = 0.0 : 1.0 : -1.0 : 120.0 : 0.0 : 3.0;
LinkMeasurementSet(1, "[Book1]Sheet1", 1, 1, FALSE);
DataCollection (0);
DataCollectionType = 1;
SetExport (Ln_Marker1_Index_A, 1, TRUE);
//SetExport (mLn_Marker1_Index_A, 1, TRUE);
ViewBox (Ln_Marker1_Index_A);
PositionWindow ("Ln_Marker1_Index_A", 441, 42, 321, 201);
integer i=0;
```

Macro to Control Weld Head Position in Optimas5

```
nData= 170;
ports=0x378;
integer i=0;
integer edge = 88;
integer avgi = edge;
integer M1=edge;
integer M2=edge;
integer M3=edge;
boolean test;
integer cnt0 = 0;
while (i < 1)
{
Acquire( );
Freeze( );
CreateLine (10. : 13. :: 10.0 : 3);
MultipleMode = TRUE;
test = Extract();
//MacroMessage("Extract ",Ln_Marker1_Index_A,"nLnTally ",TotalTally,"nTst ",test);
If ((Ln_Marker1_Index_A) > 1||(Ln_Marker1_Index_A)< 150||Ln_Marker1_Index_A>
1.15*avgi||Ln_Marker1_Index_A<0.85*avgi)
{
Beep(50);
cnt0++;
}
else
{
```

```
cnt0 = 0;
m3 = m2;
m2 = m1;
m1 = Ln_Marker1_Index_A;
}
avgi = (m1 + m2 + m3)/3;
if (cnt0 <3)
{nData = 170 +3*(edge-avgi);}
else
{nData = 170;}
nValue2=PortOutWord(ports,nData);
}
```

C++ Program to Collect Data from USD10

```

#include <conio.h>
#include <iostream.h>
#include <stdio.h>
#include <time.h>
#include <windows.h>
#include <ctype.h>

DCB dcb;
extern COMSTAT ComStat;
int err=0;
int port_id = -1;

void main(){
FILE *stream;
    /* Open for read (will fail if 'data does not exist')*/
    if( (stream = fopen( "fedi430A.txt", "w" )) == NULL )
        printf( "The file 'fedi123.txt' was not opened\n" );
        struct tm *newtime;
        time_t aclock;
int rev_buf[661]={0};
char chrc,chrc1;
int c=0, p=0, x=0, n=0, i, cmnd[4] = {27,68,65,13}, cmndac[6]={27, 65,67,32,49,13};
    //ESC,A,C,3,SP,CR ESC,D,A,CR
if(port_id = OpenComm("COM1",512, 512)<0){
cout << "OpenComm didn't work!";
}
int comm_err=BuildCommDCB("COM1:9600,n,8,1", &dcb );
if(comm_err<0){
cout << "BuildComm didn't work!";
}
for (n = 0;n<100;n++) //collection iterations
    {printf("\nIteration # %i" , n);
    for(i=0;i<4;i++) //output (4)commands send data
        _outp(0x3f8,cmnd[i]);

/*_asm{
        mov     dx,0
        mov     ah,2
        int     0x14
        mov     chrc,al
    }*/
    time( &aclock ); // Get time in seconds */
    newtime = localtime( &aclock ); /* Convert time to struct tm form */
    fprintf(stream,asctime(newtime));
}
}

```

```

/*
while(chrc != 0x2a)                //0x30 (0)
{
_asm{ mov          dx,0
      mov          ah,2
      int          0x14
      mov          chrc,al
      }
}
*/
chrcl = 32;
for (c=0;c<220;)
{
_asm{
      mov          dx,0
      mov          ah,2
      int          0x14
      mov          chrc,al
}
//ninc:
if (((chrc >= '0')&&(chrc<='9'))||((chrc==32)&&(chrcl!=32)))
    {putc(chrc,stream);//cout<<"\n"<<chrc<<" "<<n;
}
if(((chrcl >= '0')&&(chrcl<='9'))&&((chrc <'0')||((chrc>'9'))/*&&(chrcl!=32)*/){c++;}
    chrcl=chrc; } //end asm end for(c)
    putc(0x0d,stream);} //end
for(n)
fclose(stream);}

```

ANSYS Code for Thermal Profiles

/FILENAM,ESS05

/TITLE, 3-D Analysis of ESS Cladding Temperature Profiles 0.5" Substrate 1.5x.05
elements

/PREP7

!*****

!VARIABLES DECLARATION

t=1

x1=0

x2=30/1000

dx=3/1000

!*****

ET,1,SOLID70

NEQIT,50

!

! Temperature table for defining the thermal properties

!

MPTEMP,1,0.0,106.67,213.34,320.01,426.68,533.35

MPTEMP,7,640.02,746.69,853.36,960.03,1066.7,1173.37

MPTEMP,13,1280.04,1386.71,1493.38

!

! Definition of material density

!

MP,DENS,1,7100

!

! Definition of material thermal conductivities

!

MPDATA,KXX,1,1,42.935,39.492,36.049,32.605,29.162,26.750

MPDATA,KXX,1,7,24.520,22.289,20.059,17.828,15.597,13.367

MPDATA,KXX,1,13,11.136,8.906,6.675

MPDATA,KYY,1,1,42.935,39.492,36.049,32.605,29.162,26.750

MPDATA,KYY,1,7,24.520,22.289,20.059,17.828,15.597,13.367

MPDATA,KYY,1,13,11.136,8.906,6.675

MPDATA,KZZ,1,1,42.935,39.492,36.049,32.605,29.162,26.750

MPDATA,KZZ,1,7,24.520,22.289,20.059,17.828,15.597,13.367

MPDATA,KZZ,1,13,11.136,8.906,6.675

!

! Definition of material specific heats

!

MPDATA,C,1,1,533,548

MPDATA,C,1,3,562,576

MPDATA,C,1,5,590,605

MPDATA,C,1,7,619,672

MPDATA,C,1,9,712,726

```

MPDATA,C,1,11,741,871
MPDATA,C,1,13,913,909
MPDATA,C,1,15,904
!
! No convection assumed in this analysis
!
! Temperature table for definition of physical properties
!
MPTEMP
STAT
MPTEMP,1,0.0,106.67,213.34,320.01,426.68,533.35
MPTEMP,7,640.02,746.69,853.36,960.03,1066.7,1173.37
MPTEMP,13,1280.04,1386.71,1493.38
!
!*****
!model definition
!*****
block,0,120/1000,0,17/1000,0,12.7/1000
block,0,120/1000,17/1000,25.4/1000,0,12.7/1000
block,0,120/1000,0,17/1000,0/1000,-4/1000
vglue,all
lselect,s,line,,5
lselect,a,line,,4
lselect,a,line,,2
lselect,a,line,,7
lselect,a,line,,14
lselect,a,line,,19
lselect,a,line,,26
lselect,a,line,,28
lesize,all,3/1000           !Length (x)
lselect,s,line,,9,12,1
lselect,a,line,,23,24,1
lselect,a,line,,37,40,1
lesize,all,1.4/1000       !hot to cold depth (z)
lselect,s,line,,1
lselect,a,line,,3
lselect,a,line,,6
lselect,a,line,,8
lselect,a,line,,41,44,1
lselect,a,line,,27
lesize,all,2/1000         !Width (y)
vmesh,all
FINISH
!/eof
!*****

```

```

/SOLU
ANTYP,TRANS,NEW
!SFA,2,,CONV,2000,21
SBCTRA
NSUBST,25
AUTOTS,ON
TRNOPT,FULL,-999
TIMINT,ON,THERM
OUTRES,ALL
TINTP,,1
SBCTRA
TIME,t
TUNIF,21
!*****
!1st RUN
!*****
TIME,1
DDELETE,ALL
!Select weld pool nodes and constrain
nsel,s,loc,x,x1,x2
nsel,r,loc,y,0,17/1000
nsel,r,loc,z,2/1000,-1/1000
D,all,TEMP,1520
ALLSEL
!Select H2O cooled nodes and constrain
nsel,s,loc,x,x1,x2
nsel,r,loc,y,0,17/1000
nsel,r,loc,z,12.7/1000,12.7/1000
D,all,TEMP,40
ALLSEL
!nsel,s,loc,x,x1,x2
!nsel,r,loc,z,12.7/1000,12.7/1000
!sf,all,conv,4000
!ALLSEL
KBC,1
AUTOTS,ON
NSUBST,25
SOLVE
SAVE
FINISH
!*****
!*****
!NEXT RUN
*do,nnn,1,30
RESUME

```

```

/SOLU
ANTYPE,,REST
t=t+1
x1=x1+dx
x2=x2+dx
TIME,t
DDELE,ALL
SFDELE,ALL,CONV
SFDELE,ALL,hflux
!Select weld pool nodes and constrain
nselect,s,loc,x,x1,x2
nselect,r,loc,y,0,17/1000
nselect,r,loc,z,.00,-0.001
D,all,TEMP,1520
ALLSEL
nselect,s,loc,x,x1,x2
nselect,r,loc,y,0,17/1000
nselect,r,loc,z,0.00,0.0015
D,all,TEMP,2400
ALLSEL
!Select H2O cooled nodes and constrain
nselect,s,loc,x,x1+.015,x2+.015
nselect,r,loc,y,0,17/1000
nselect,r,loc,z,12.7/1000,12.7/1000
D,all,TEMP,100
ALLSEL
nselect,s,loc,x,x1,x1+.015
nselect,r,loc,y,0,17/1000
nselect,r,loc,z,12.7/1000,12.7/1000
D,all,TEMP,350
!Select convection elements and constrain
ALLSEL
nselect,s,loc,x,0,x1+.015      !Topside Bead Conv
nselect,r,loc,y,0,17/1000
nselect,r,loc,z,-1/1000,-1/1000
sf,all,conv,1200
ALLSEL
KBC,1
AUTOTS,ON
NSUBST,25
SOLVE
SAVE
FINISH
*enddo
/exit

```

Excel Macro for Locating Peaks Incorporating Weighted Least Squares

```

Sub TOF() 'WEIGHTED LEAST SQUARES TO FIND PEAK CENTER AND TOF
Dim X, Y, I, N As Integer, TOP, w, SUMOLD, SUMNEW, UPRPK, LWRPK As Double
' MsgBox "start" & start
' MsgBox "finish" & finish
For K = start + 1 To finish Step 2 'INCREMENT COLUMNS
X = WS + 1 'Z
Y = WS + 1 'Z
'Cells(510, 60).Value = K
TOP = 4
For N = 1 To 2
SUMOLD = 0
SUMNEW = 0
    Do While (Cells(Y, K - 1).Value <= TOP And Cells(Y, K - 1) <> "")
        Y = Y + 1
    Loop
' MsgBox "BOTTOM VALUE " & X
' MsgBox "top " & Y
w = TOP
Do While ((Abs(SUMOLD) <= Abs(SUMNEW)))
    SUMOLD = SUMNEW
    For I = X To Y - 1
        SUMNEW = (Cells(I, K - 1).Value - w) * Cells(I, K).Value + SUMNEW
    Next I
' MsgBox "step " & w
w = w - 0.01
Cells(245, 2).Value = SUMOLD
Cells(246, 2).Value = X
Cells(247, 2).Value = Y
Cells(248, 2).Value = K
Loop
If TOP = 4 Then
LWRPK = w
ElseIf TOP = 6.6 Then
UPRPK = w
End If
TOP = 6.6
X = Y + 1
Y = Y + 1
Next N
Cells(257, K - 1).Value = UPRPK - LWRPK
Cells(258, K - 1).Value = UPRPK
Cells(259, K - 1).Value = LWRPK

```

```
Cells(258, K).Value = 50
Cells(259, K).Value = 50
Cells(260, K - 1).Value = "LWRPK"
Cells(261, K - 1).Value = "UPRPK"
Cells(262, K - 1).Value = "TOF"
Cells(260, K).Value = LWRPK
Cells(261, K).Value = URPK
Cells(262, K).Value = URPK - LWRPK
Cells((WS + K / 2 + 50), 2).Value = URPK - LWRPK
Cells((WS + K / 2 + 50), 1).Value = Cells(2, K)
Next K

End Sub
```

Chapter 12 Bibliography

-
1. Nondestructive Testing Handbook, Radiograph and Radiation Testing, Vol. 3, 2nd Ed., American Society for Nondestructive Testing, p.595, 1985
 2. Oregon Graduate Institute of Science and Technology, Electroslag Surfacing Technology Technical Reference Guide, October, p.xxv, 1995
 3. Oregon Graduate Institute of Science and Technology, Electroslag Surfacing Technology Technical Reference Guide, October, p.1.1, 1995
 4. Turpin, R.B., Electroslag Surfacing Technology Program Final Technical Report: Engineering and Operating Guide, Part I and II, p.119, October 1995
 5. Hartford Steam Boiler's Complete Ultrasonic Testing Workbook, 1st Ed., Hartford Steam Boiler Inspection and Insurance Co., p.19, 1983
 6. Hartford Steam Boiler's Complete Ultrasonic Testing Workbook, 1st Ed., Hartford Steam Boiler Inspection and Insurance Co., pp.22-27, 1983
 7. The Encyclopedia of Advanced Materials, Pergamon Press, Vol. 3, p.2019, 1994
 8. Scruby, C.B., Moss B.C., Noncontact Ultrasonic Measurements on Steel at Elevated Temperatures, *NDT&E International*, Vol. 26, No. 4, pp.177-188, 1993
 9. Krautkramer, J., Krautkramer, H., Ultrasonic Testing of Materials, Springer-Verlag, p.146, 1990
 10. Krylov, Victor. V., On the Theory of Surface Acoustic Wave Generation by Electric Spark Discharge, *J. Physics D: Applied Physics*, Vol. 25, pp.155-161, 1992
 11. Metals Handbook, Nondestructive Evaluation and Quality Control, ASM International, 9th Ed, Vol. 17, p.235, 1989
 12. Krautkramer, J., Krautkramer, H., Ultrasonic Testing of Materials, Springer-Verlag, pp.34-36, 1990
 13. Metals Handbook, Nondestructive Evaluation and Quality Control, ASM International, 9th Ed, Vol. 17, pp.233-4, 1989
 14. Krautkramer, J., Krautkramer, H., Ultrasonic Testing of Materials, Springer-Verlag, p.14, 1990
 15. Meyers, M.A., Dynamic Behavior of Materials, J. Wiley, p.12, 1994

-
16. Meyers, M.A., *Dynamic Behavior of Materials*, J. Wiley, p.37, 1994
 17. Hayden, H., Moffatt, W. G., Wulff, J., *The Structure and Property of Materials*, Vol. III, John Wiley and Sons, p.33, 1965
 18. Swalin, R.A., *Thermodynamics of Physics*, 2nd Ed., J. Wiley, p.66, 1967
 19. Boyd, D.M., *High Temperature Ultrasonic Measurements in Steel Using Electromagnetic Acoustic Transducers*, *Ph.D. Dissertation*, UC Davis, p.17, 1980
 20. Krautkramer, J., Krautkramer, H, *Ultrasonic Testing of Materials*, Springer-Verlag, p.108, 1990
 21. Krautkramer, J., Krautkramer, H, *Ultrasonic Testing of Materials*, Springer-Verlag, p.109, 1990
 22. Boyd, D.M., *High Temperature Ultrasonic Measurements in Steel Using Electromagnetic Acoustic Transducers*, *Ph.D. Dissertation*, UC Davis, p.8, 1980
 23. *Hartford Steam Boiler's Complete Ultrasonic Testing Workbook*, 1st Ed., Hartford Steam Boiler Inspection and Insurance Co., p.93, 1983
 24. Holman, J. P., *Heat Transfer* 5th Ed., McGraw-Hill, Inc., p.60, 1981
 25. Holman, J. P., *Heat Transfer* 5th Ed., McGraw-Hill, Inc., p.86, 1981
 26. Ohshima, K., *Observation and Control of Weld Pool Phenomena in Arc Welding*, *Welding International*, Vol. 4, No. 12, pp.934-938, 1990
 27. Lukens, W.E., Morris, R.A., *Infrared Temperature Sensing of Cooling Rates for Arc Welding Control*, *Welding Journal*, Vol. 61, No. 1, pp.27-33, 1982
 28. Kozono, Y., Onuma, A. Kokura, S., *Control of Backbead Width in Girth TIG Welding of Small Tubes using Surface Temperature Monitoring*, *Welding International*, Vol. 3, No. 2, pp.137-141, 1989
 29. Nagarajan, S., Chen, W.H., Chin, B.A., *Infrared Sensing for Adaptive Arc Welding*, *Welding Journal Welding Research Supplement*, November, Vol. 68, No. 11, p.462-s, 1989
 30. Zacksenhouse, M., and Hardt, D.E., *Weld Pool Impedance Identification for Size Measurement and Control*, *Journal of Dynamic Systems, Measurement and Control*, ASME, Vol.105, pp.179-184, 1983b
 31. Nomura, H., *Back Bead Width Control in One Side SAW Using Flux Copper Backing*, *Journal of Japan Welding Society*, Vol. 3, No. 3 pp.471-477, 1985
 32. Kaneko, Y., Iisaka, T., Tanaka, A., Ma, P., Yamane, S., Ohshima, K., *Sensing of the Weld Pool Depth with Neural Network and Fuzzy Control of Seam Tracking*, *Proc. of the 19th Annual Int. Conf. on Industrial Electronics, Control, and Instrumentation*, Vol. 1, pp.424-429, 1993

-
33. Lim, T.G., Cho, H.S., Estimation of Weld Pool Sizes in GMAW Process Using Neural Networks, *Proc. of the Institution of Mechanical Engineers, Part I, Journal of Systems and Control Engineering*, Vol. 207, No. 1, pp.15-26, 1993
 34. Katz, J.M., Hardt, D.E., Ultrasonic Measurement of Weld Penetration, Control of Manufacturing Processes and Robotic Systems, *ASME WAM*, pp.79-95, 1983a
 35. Lott, L.A., Ultrasonic Detection of Molten/Solid Interfaces of Weld Pools, *Materials Evaluation*, Vol. 42, pp.337- 341, March 1984
 36. Carson, N.M., Johnson, J.A., Lott, L.A., Kunerth, D.C., Ultrasonic NDT Methods for Weld Sensing, *Materials Evaluation*, Vol. 50, No. 11, pp.1338-1343, November 1992
 37. Lott, L.A., Johnson, J.A., Smartt, H.B., Real-time Ultrasonic Sensing of Arc Welding Processes, *Proceedings, 1983 Symposium on Nondestructive Evaluation Applications and Materials Processing, American Society for Metals*, pp.13-22, 1983
 38. Ogilvy, J.A., Temple, J.A.G., Theoretical Assessment of the Errors Involved in Ultrasonic Location and Sizing of Molten Weld Pools, *Ultrasonics*, Vol. 27, No. 2, pp.68-79, March, 1989
 39. Stares, I.J., Duffill, C., Ogilvy, J.A., Scruby, C.B., Online Weld Pool Monitoring and Defect Detection Using Ultrasonics, *NDT International*, Vol. 23, No.4, pp.195-200, 1990
 40. Wadley, H.N.G., Norton, S.J., Mauer, F., Droney, B., *Philosophical Transactions Royal Society of London A* 320, pp.341-361, 1986
 41. Metals Handbook, Properties and Selection: Irons, Steels and High Performance Alloys, ASM International, 10th Ed., Vol. 1, p.45, 1990
 42. Fenn, R., Monitoring and Controlling Welding by Ultrasonic Means, *British Journal of NDT*, pp.82-86, Vol. 31, No. 2, February, 1989
 43. Personal communication
 44. Holman, J. P., Heat Transfer 5th Ed., McGraw-Hill, Inc., p.202, 1981
 45. Holman, J. P., Heat Transfer 5th Ed., McGraw-Hill, Inc., p.546, 1981
 46. Encyclopedia of Materials Science and Engineering, Pergamon Press, pp.7-4963, 1986
 47. Scruby, C.B., Moss, B.C., Noncontact Ultrasonic Measurements on Steel at Elevated Temperatures, *NDT&E International*, Vol. 26, No. 4, p.182, 1993
 48. Metals Handbook, , Metallography and Microstructures, ASM International, 9th Ed, Vol. 9, p.251, Fig. 56, 1985
 49. Hartford Steam Boiler's Complete Ultrasonic Testing Workbook, 1st Ed., Hartford Steam Boiler Inspection and Insurance Co., p.38, 1983

-
50. Lott, L.A., Johnson, J.A., Smartt, H.B., Real-Time Ultrasonic Sensing of Arc Welding Processes, Proceedings, *1983 Symposium on Nondestructive Evaluation Applications and Materials Processing, American Society for Metals*, p.20, 1983
 51. Suga, Y., Naruse, M., Tokiwa, T., Application of Neural Network to Visual Sensing of Weld Line and Automatic Tracking in Robot Welding, *Welding in the World*, Vol. 34, pp.275-282, 1994
 52. Kaneko, Y., Iisaka, T., Tanaka, A., Ma, P., Yamane, S., Ohshima, K., Sensing of the Weld Pool Depth with Neural Network and Fuzzy Control of Seam Tracking, *Proc. of the 19th Annual Int. Conf. on Industrial Electronics, Control, and Instrumentation*, Vol. 1, pp.424-429, 1993
 53. Haykin, S., *Neural Networks*, Macmillan College Publishing, p.6, 1994
 54. Minsky, M.L., Papert, S.A., *Perceptrons*, MIT Press, p.7, 1969
 55. Minsky, M.L., Papert, S.A., *Perceptrons*, MIT Press, p.45, 1969
 56. Minsky, M.L., Papert, S.A., *Perceptrons*, MIT Press, p.38, 1969
 57. Minsky, M.L., Papert, S.A., *Perceptrons*, MIT Press, p.37, 1969
 58. Minsky, M.L., Papert, S.A., *Perceptrons*, MIT Press, p.38, 1969
 59. Minsky, M.L., Papert, S.A., *Perceptrons*, MIT Press, p.40, 1969
 60. Rumelhart, D.E., Hinton, G.E., Williams, R.J., Learning Representations by Back-Propagation Errors, *Nature*, Vol. 323, pp.533-536, 1986
 61. Minsky, M.L. and Papert, S.A., *Perceptrons*, MIT Press, p.177, 1969
 62. Refenes, A.N., Zaprani, A., Francis, G., Stock Performance Modeling Using Neural Networks: A Comparative Study with Regression Models, *Neural Networks* Vol.7, No. 2, pp.375-388, 1994